STUDY OF THE MISCIBILITY, CRYSTALLIZATION AND MORPHOLOGY IN POLY(PROPYLENE) BASED BLENDS AND COPOLYMERS

by

Pak-Meng Cham

Dissertation submitted to the Faculty of the

Virginia Polytechnic Institute and State University

in partial fulfillment of the requirements for the degree of

DOCTOR OF PHILOSOPHY

in

Materials Engineering Science

APPROVED:

Hervé Marand, Chairman

David A. Dillard

Ronald G. Kander

James P. Wightman

Garth L. Wilkes

October, 1996
Blacksburg, Virginia

Keys Words: Poly(propylene), Poly(1-butene), Propylene-Ethylene Copolymer, Copolymer Crystallization, Polymorphism, Morphology, Miscibility, Phase Separation

STUDY OF THE MISCIBILITY, CRYSTALLIZATION AND MORPHOLOGY IN POLY(PROPYLENE) BASED BLENDS AND COPOLYMERS

by

Pak-Meng Cham

Dr. Hervé Marand, Chairman

Materials Engineering Science Program

(ABSTRACT)

This dissertation discusses the polymorphism, crystallization and melting behavior of propylene-ethylene random copolymers. It also discusses the results of studies of the miscibility and the competitive liquid-liquid demixing and crystallization processes in blends of poly(propylene) and poly(1-butene). In the first part of this study, polymorphism of propylene-ethylene copolymers is studied by wide angle X-ray diffraction. By comparing the α and γ crystal phase contents in samples with different ethylene content as well as samples isothermally crystallized at different temperatures, it was shown that increasing ethylene content as well as increasing crystallization temperature promotes the formation of the γ-phase. Comparison of the results from fractionated samples and unfractionated samples with similar ethylene contents reveals that in propylene-ethylene copolymers with similar micro-structure, the polymorphism, crystallization and melting behavior are mainly determined by their ethylene content. The issue of co-unit inclusion and its effect on crystallization and melting behavior are also discussed.

In the second part of this dissertation, the miscibility behavior of atactic poly(propylene) (at-PP) and atactic poly(1-butene) (at-P1B) with different molecular weights is investigated by differential scanning calorimetry. The phase diagram of at-PP and at-P1B blend of molecular weight (87K/48.5K) shows a upper critical solution temperature (UCST) behavior. The UCST behavior is consistent with predictions by the group contribution method. Miscibility behavior of high molecular weight isotactic poly(propylene) (it-PP) and isotactic poly(1-butene) (it-P1B) blend is investigated by a combination of optical microscopy and scanning electron microscopy, differential scanning calorimetry and dynamic mechanical analysis. These studies reveal that for the molecular weights investigated, it-PP and it-P1B form blends that are partially miscible in the liquid state. Liquid-liquid demixing is observed by optical microscopy at temperatures above the melting temperature of the it-PP component and is also inferred from scanning electron micrographs of the freeze fracture surface of quenched blends after extraction of the it-P1B component with cyclohexane. It-PP spherulites grow through both liquid phases at relative rates that depend markedly on the crystallization temperature. The complex multiple-melting behavior of the it-PP component in the blend is explained in terms of a bimodal distribution of it-PP lamellar crystals which result from crystal growth in the phase-separated liquid. Finally, the dynamic mechanical analysis data are explained in terms of a liquid-liquid demixing process that results in a significant degree of phase mixing.

To My Parents

ACKNOWLEDGMENTS

The years as a Ph.D. student at Virginia Tech constitute some of the most memorable times in my life. I will treasure every moment I stayed here, especially the time that I shared with those who have been so crucial during this period of my life. For all my teachers and friends at Tech, I am grateful for their guidance and friendship. My gratitude to my supervisor, Dr. Hervé Marand, cannot be put into words. He always finds the time to give his students and others his help. He not only provided me with the most resourceful assistance and guidance for my research, but more importantly, he showed me ways to explore things from different angles and to solve them from new approaches. He also gave me encouragement when I needed it most.

I received both my bachelor and master degrees in Physics and knew nothing about polymers when I started my Ph.D. program. It is safe to say that my knowledge about polymer materials was built from ground zero at Virginia Tech. For this, I thank the professors for those inspirational courses and seminars that I attended throughout the years. I am also grateful for Professors Wilkes, Wightman, Dillard and Kander who kindly served as my committee members.

I would like to thank those who have contributed to this work. Special appreciation goes to Dr. Abaneshwar Prasad, who was a post-doctor fellow in our research group during my first two years in the program. From assistance on equipment operation to providing guidance in problem solving, his support was tremendous. Tom Glass spent some of his precious weekends to conduct the NMR experiments. TieHong

Lee carried many preliminary studies on the miscibility behavior of poly(propylene)/poly(1-butene) blend project. Special thanks go to Dr. Jiang Huang for his friendship, encouragement and helpful discussion and all the members of Dr. Marand's research group for providing their complete support and sharing ideas throughout the years. I should also express my greatest gratitude to all of those who gave me their encouragement and support during my writing of this dissertation. It would not be an overstatement that this dissertation could never be finished without their continuous encouragement.

This work is dedicated to my parents. I thank them for giving me a wonderful childhood and for providing me with an environment in which I was able to concentrate on my education. Their encouragement and understanding are the reasons that I have become who I am today. I would also like to thank my younger sister and brother, Cindy and Jason, for their support and confidence in me over the years.

Finally, I thank the Kimberly-Clark Corporation for their financial support on this project and Dr. Lawrence H. Sawyer, Dr. Susan E. Shawver and Dr. Peter M. Kobylivker from Kimberly-Clark for worthwhile discussions and their never-ending interest.

TABLE OF CONTENTS

List of Figures

List of Tables

1. INTRODUCTION

Isotactic poly(propylene) (it-PP) has become one of the most important commercial polymers. Since the early 1950s, when isotactic poly(propylene) was first synthesized*, this material has received increasing attention in industrial applications as well as in academic studies. The commercial interest in it-PP has been motivated by its low cost and wide range of applications. The market share of this polymer has been increasing steadily. In 1994, poly(propylene) (PP) contributed to 14% of the total plastics production in the world. Among all the commercial plastics, poly(propylene) has the highest annual growth rate. World wide production is expected to increase 5.5% annually to more than 21 million metric tons by the year 2000[3]. From the academic point of view, it-PP is one of the most interesting polymers in view of its crystallization behavior, polymorphism and morphology. It has been one of the most studied polymers from the crystallization point of view.

One of the main goals for polymer scientists is to modify the properties of the polymers to accommodate the needs for different applications. This is particularly true in the case of commodity thermoplastics such as poly(ethylene) (PE), poly(propylene) and poly(styrene) (PS). The increasing use of these materials in different areas requires a wide range of combinations in lightness, stiffness and toughness properties over a wide

* For the historical development of it-PP synthesis and the arguments about its first discovery, one can refer to the book of McMillan[1] and the paper by Pino and Moretti[2].

temperature range. Although isotactic poly(propylene) has many outstanding thermal, physical and mechanical properties, one of its disadvantages is the lack of toughness at low temperatures. At low temperatures, it-PP homopolymer becomes brittle. This has limited its applications in certain areas. It is therefore not surprising that the improvement of its toughness at low temperatures has been one of the main research areas in it-PP studies. The two most common practices for modifying the properties of it-PP along this direction are 1) producing poly(propylene) copolymers with propylene and another monomer, usually 1-butene, ethylene and dienes (EPDM, EPR rubbers); and 2) rubber modified poly(propylene) via blending poly(propylene) with one or more compatible polymers or copolymers. These two approaches not only modify the brittle-ductile behavior and improve the sample toughness at lower temperatures but also extend other physical properties to a larger range of use.

The goal of this dissertation is to address the key issues in these two approaches. The two critical issues for toughening it-PP are:

1. What is the role of ethylene comonomer in the crystallization and thermal behavior of isotactic propylene-ethylene copolymers?
2. Are poly(propylene)/poly(1-butene) blends miscible? If not, why do these blends show promising mechanical properties?[4,5]

The content of this dissertation is organized in the following way: Chapter 2 is a literature review. A brief introduction to crystallization and morphology of semi-crystalline polymers is given. This is followed by a review on poly(propylene) homopolymer including its polymorphic behavior. General properties of poly(propylene)

copolymers will also be reviewed. Crystallization theory of statistical copolymers and polymer blend miscibility theory will be discussed as well. Some of the properties of poly(1-butene), though not a point of focus in this study, will be given together with a description of the polymorphism of it-P1B at the end of chapter 2.

In chapter 3, copolymers of propylene and ethylene will be investigated. The focus will concentrate on the polymorphism, crystallization and melting behavior of this copolymer. Experimental techniques used in this study include differential scanning calorimetry (DSC), wide angle X-ray diffraction (WAXD), small angle X-ray scattering (SAXS), solution ^{13}C nuclear magnetic resonance (NMR) and intrinsic viscosity measurements.

In chapter 4, miscibility of poly(propylene)/poly(1-butene) blends will be examined. Discussion in this chapter will focus on the phase diagram of this blend, competition between phase separation and crystallization and, most importantly, the compatibility issue. Experimental techniques used in this study include DSC, optical microscopy and scanning electron microscopy (SEM). The long existing controversy over the miscibility in this polymer pair will be addressed and settled.

In chapter 5 the direction for future studies will be proposed and discussed.

Although this dissertation will focus on the academic side of the problems, the significance of these findings in industrial applications will also be proposed.

2. LITERATURE REVIEW

Some of the most important topics in polymer crystallization and polymer blend miscibility will be reviewed in the following sections. Because of their significance in the historical developments of polymer physics, it is decided to include these topics even though they are not directly related to the mainstream of this study.

2.1 Polymer Crystallization

One of the most important and fascinating topics in polymer physics is that of the crystallization behavior. Polymer materials are known for their high molecular weight chain-like structure. In the early days of wide angle X-ray diffraction studies, diffraction patterns of some natural polymers have shown that polymer materials are crystallizable. However, for polymer chains to pack in three dimensions in the crystalline state, several factors must be considered. Stereo-regularity, molecular weight, chemical defects, etc. all play determining roles in polymer crystallization. Other factors, such as pressure, nucleating agents, diluent, internal and external stress, can also affect the crystallization process. In the following, a brief discussion of polymer crystallization will be given. Owing to the complexity of the topic, this discussion is brief and by no means covers all of the important areas in this field. Review articles on this subject can be found in the literature[6-9].

Wide angle X-ray diffraction studies have further shown that polymer materials are only semi-crystalline. In contrast to those of simple crystals, the WAXD patterns of

polymer materials show broad diffraction peaks superposed on a very broad scattering peak (amorphous halo). This indicates that a significant fraction of polymer chain segments do not go into the crystal lattice even for "highly crystalline" polymers like high density poly(ethylene) (HDPE) and that the crystals are small and/or defective. Therefore, there must be regions in the polymer samples in which these amorphous polymer chain segments reside. Early studies on semi-crystalline polymers assumed a two phase model: the crystalline phase and the amorphous phase. More recent investigations have found that the two phase model cannot give satisfactory explanations for some of the experimental observations. For example, solid state NMR experiments have shown that there are two different types of relaxation time associated with the amorphous phase in isotactic poly(propylene) samples[10]. It is now generally accepted that the shorter relaxation time measured in those solid state NMR studies is associated with the mobile amorphous fraction and the second one corresponds to the "rigid amorphous" or crystal-liquid "interfacial" region. The rigid amorphous or crystal-liquid interfacial region, though not the subject in this discussion, is thought to be at the origin of some of the long term "aging" that is observed in many polymer systems above the T_g of the mobile amorphous fraction[11-13]. This interfacial region, which may be at the origin of the discrepancy between crystallinity measurements by WAXD, DSC and by density, has initiated a lot of discussion and studies in the literature. For example, in the study of interphase thickness of linear poly(ethylene), Mandelkern *et al.*[14] suggested that the difference in crystallinity obtained by density measurements and that obtained by heat of fusion measurements is directly related to the interfacial region between the crystal and the amorphous phases.

2.1.1 Models of the Structure of Semi-Crystalline Polymers

The first model that attempted to describe the semi-crystalline character of polymer materials was the "fringed micelle" model. According to this model, semi-crystalline polymers consist of crystalline and amorphous regions. Each polymer molecule, with its long chain character, contributes to several crystalline and amorphous regions. In the crystalline regions, the chain segment is aligned with segments from other polymer chains. In the amorphous region, the chain segments have disordered conformations. Because of the physical (covalent) connections (the fringes) between the amorphous and crystalline regions, this model could explain the mechanical properties in semi-crystalline polymers. However, it is difficult to apply this model to explain the morphological features in polymers such as spherulites that are commonly found in melt-crystallized polymer samples.

The fringed-micelle model was eventually replaced by the chain-folding model. First proposed by Keller[15], the chain-folding model was the result of studies on poly(ethylene) single crystals grown from dilute solutions[15-17]. With the observations by electron microscopy and electron diffraction in particular, it was found that the chains pack preferentially parallel to the crystal thickness direction. While the length of a polymer chain is of the order of several thousand angstroms, the typical thickness of a polymer single crystal is only approximately 100 Å. For this to happen, the polymer chains must be folded in the lamellar structure. This observation is one direct proof that chain-folding is indeed occurring during polymer crystallization. The adjacent re-entry chain folding model of Keller was subsequently challenged by Flory who proposed the

random re-entry chain folding model or switch board model. After extensive studies, especially with the help of atomic force microscopy (AFM)[18] and transmission electron microscopy (TEM)[19] in the past ten years or so, there seems to be little doubt that under crystallization from dilute solution, the chain folding is very regular conforming nearly to Keller's model. It is now generally accepted that for a single crystal grown from dilute solution, the polymer chains fold back into the crystal in an adjacent re-entry manner.

In melt crystallization, even though the chain folding character remains the same, there has been a never-ending controversy about the regularity of the adjacent re-entry folding process. Today, it is believed that the chain folding in lamellae crystallized from the melt is somewhere between the adjacent re-entry and the switched board models. The true nature depends on many factors, such as polymer chain stiffness, crystallization temperature, molecular weight, etc.

2.1.2 Morphology of Semi-Crystalline Polymers

Semi-crystalline polymers form single crystals when crystallized from dilute solutions (with polymer concentration less than 0.1% w/v). The common feature among all these single crystals is chain-folding. However, the geometry of these single crystals depends on the individual polymer crystal unit cell type, solvent, polymer concentration and crystallization temperature[7]. At higher polymer concentration (larger than 0.1% w/v), multi-lamellar structures are formed. They appear as lamellar stacks, sheaves of lamellae

(axialites, hedrites) or spherically symmetrical entities--spherulites. A review on this subject can be found in ref. 7.

When crystallized from the melt, semi-crystalline polymers generally form a super structure called spherulites. The building block of a spherulite is the lamella. A lamella is a single crystal with thickness of the order of 100 Å. The original lamellae that grow outward from the nucleus branch at dislocation points and splay. As further branching and splaying occur, eventually a spherical structure called spherulite is formed. The spherulite continues to grow until neighboring spherulites impinge on each other. Typical dimensions of spherulites is of the order of microns to tens or hundreds of microns. Fig. 2.1 shows the typical structure of a spherulite. Lamellar branching as well as entangled polymer chains are shown in the enlarged portion in Fig. 2.1. As can be seen, the morphology of semi-crystalline polymers does not lack complexity. An in-depth study of this morphology requires the use of many different experimental techniques. A concise introduction to this subject can be found in the book by Woodward[20].

Beside the morphological structures mentioned above, which result from quiescent crystallization, other types of morphology can be observed. A "Shish Kebab" morphology, for example, is the result of crystallization under flow. While the morphology resulting from specific processing conditions is not a subject of discussion in this dissertation, it is an important issue in applications.

In polymer crystallization from the melt state, it is often found that the density (crystallinity) of the sample still increases over a long period of time after the impingement of the spherulites. This phenomenon is called secondary crystallization. During the pri-

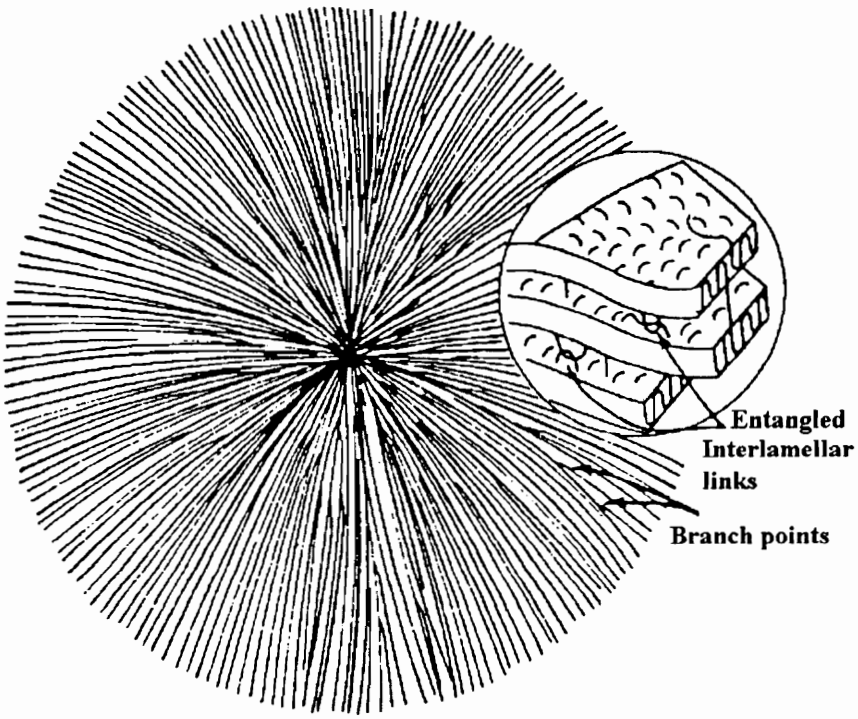

Fig. 2.1 Polymer spherulite showing the chain folding lamellae and branching (adapted from ref. 8).

mary crystallization, where the three dimensional spherulitic structure is formed, impurities and defective polymer chains are trapped in the inter-lamellar and inter-fibrillar regions. Crystallizable chains are also trapped in the those regions. These polymer chains will eventually organize themselves and crystallize. Though the nature and implication of the secondary crystallization is not the subject of discussion here, its importance in polymer crystallization research has been realized[21].

The linear growth rate observed under isothermal crystallization conditions indicates that the diffusion process cannot be the rate determining step in polymer crystallization. For this to be the case, the time dependence of the radius of the spherulite should follow a $t^{1/2}$ dependence.

According to Keith and Padden[22], there is an impurity rich layer of thickness $\delta = (D/G)$ at the growth front, where D is the impurity diffusion constant and G the lamellar crystal growth rate. The impurity material diffuses laterally away from the growth front. This provides a mechanism for the lamellar fibril to form. That is, δ controls the morphology resulting from polymer crystallization.

The Keith and Padden theory is general in nature and does not specifically consider the chain-like characteristics which are fundamental in polymer molecules. Moreover, it does not explain the low angle lamellar branching which is a necessary step for the spherulite to develop into a three dimensional structure, neither does it explain the banding of spherulites, which is related to the twisting of lamellar fibrils due to internal or external stress on the lamellae.

2.1.3 Polymer Crystallization Theory

The theory developed by Lauritzen and Hoffman[23] for polymer crystal growth is the most used and best developed theory on the subject. This theory is based on the fact that the polymer morphology resulting from crystallization is kinetically controlled. Therefore, this theory is sometimes called the kinetic theory of polymer crystallization.

In the Lauritzen and Hoffman secondary nucleation theory, it is suggested that the rate of crystal growth is controlled by two elementary processes: the secondary nucleation process of rate i and the lateral spreading of rate g. The theory then predicts that the polymer crystal growth can fall into three regimes. In regime I, g is much larger than i. Single nucleus (stem) is formed on the surface and a new layer is formed by the spreading of a single crystalline patch along the surface. In regime II, the magnitude of i and g are comparable. Multiple nuclei form and spread laterally at the growth front to give rise to a new crystalline layer. This leads to a crenulated growth front. In regime III, the secondary nucleation rate i is much larger than the rate of spreading g and becomes the rate determining step because there is no longer time for lateral spreading of the secondary nuclei. In this regime, crystal growth is so fast that the fold surface it the closest to what one expects for the switch board model.

Over the years, this theory has been modified numerous times[24-27]. It has been extended to include polymer blend systems[28] as well.

In the following, the melting behavior of semi-crystalline polymers and the Gibbs-Thomson equation will be discussed. This relationship is at the basis of the popular

Hoffman-Weeks plot. It will be used in Chapter 3 where the equilibrium melting temperature of the copolymer is discussed.

The free energy of fusion of a polymer crystal can be written as

$$\Delta G_f = xyl\,\Delta G_f^{\infty} - 2xy\sigma_e - 2l(x + y)\sigma \tag{2.1}$$

where ΔG_f^{∞} is the free energy of fusion per unit volume for an infinitely large and perfect crystal, σ_e the free energy per unit area of the crystal fold surface and σ the free energy per unit area of the crystal lateral planes. x, y and l are the dimensions of the lamellar crystal as shown in Fig. 2.2.

For an infinitely large crystal, in which surface effects can be neglected,

$$\Delta G_f = xyl\,\Delta G_f^{\infty} = xyl[\,\Delta H_f^{\infty}(T) - T\,\Delta S_f^{\infty}(T)\,] \tag{2.2}$$

The equilibrium melting temperature, T_m, is defined by $\Delta G_f = 0$. This gives

$$T_m = \Delta H_f^{\infty}(T_m) / \Delta S_f^{\infty}(T_m) \tag{2.3}$$

For small crystals, substitution of (2.3) into equation (2.1), together with the approximations $\sigma << \sigma_e$ and $x, y >> l$, gives for the observed melting temperature, T_m', of the small crystal

$$T_m' = T_m(1 - 2\sigma_e / l\,\Delta H_f^{\infty}) \tag{2.4}$$

Equation (2.4) is called the Gibbs-Thomson-Tammann equation.

The Lauritzen-Hoffman theory predicts the initial thickness of polymer lamellar crystal, l_g^* as

$$l_g^* = 2\sigma_e T_m / \Delta H_f^{\infty}\,\Delta T + \delta l \tag{2.5}$$

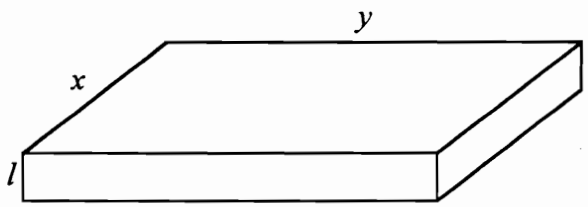

Fig. 2.2 Schematic of a lamellar crystal

where δl is an increment in stem length which allows the growing crystal to enter the range of stability.

During crystallization or subsequent heating the thickness of the crystal may change which leads to the definition of the thickening constant γ by the relation: $l = \gamma l_g^*$. From (2.4), under conditions where $\delta l \Delta H_f^\infty \Delta T / 2\sigma_e T_m$ is small compared to 1, then equation (2.6) results, which provides a relationship between the crystallization temperature, the observed and equilibrium melting temperatures.

$$T_m' = T_m [1 - (1/\gamma)] + (T_x/\gamma) \qquad (2.6)$$

Equation (2.6) is the basis of the Hoffman-Weeks plot. To construct a Hoffman-Weeks plot, the observed melting temperature, T_m', is plotted against the corresponding crystallization temperature T_x. The equilibrium melting temperature T_m is determined as the intercept between the extrapolation of this line and the $T_m' = T_x$ line.

Before leaving this section, one should discuss further the lamellar thickening process. The lamellar thickening process occurs for thermodynamic reasons. During lamellar thickening, the surface energy per unit volume of the crystal is reduced. One of the many ways to investigate the thickening effect is through the use of Hoffman-Weeks plot. From equation (2.5), the slope of the T_m' vs. T_x plot is $1/\gamma$, where γ is the thickening coefficient. Hence a steeper slope in the Hoffman-Weeks plot indicates the sample under investigation does not thicken as much as one which has a smaller slope. Note that a linear plot of T_m' vs. T_x would imply that the thickening rate is temperature independent, which is generally not to be expected. Although a lamella would always become more

stable if it thickened, there are many factors which can limit or prohibit this thickening process. Under the context of the Lauritzen-Hoffman theory, Mezghani *et al.*[29] suggest a connection between lamellar thickening and the regimes of polymer crystallization. Basically, the idea behind this connection is that the interfacial region is involved in the lamellar thickening process. Their argument is, that interfacial region (or the surface roughness) is different for different growth regimes. For regime III, in which the rate of secondary nucleation is larger than the spreading rate, the fold surface of the lamella may resemble the one described by the switch board model. The roughness or irregularity at the fold surface makes the thickening process much more difficult. On the other hand, in regime I, like most of the poly(ethylene) crystallization studies in the past, polymer chains arrange in an adjacent re-entry manner. Thickening is much easier in this case.

Lamellar thickening is also related to the α_c relaxation process in semi-crystalline polymers. Temperature T_{α_c}, where the α_c relaxation process is activated, indicates the on-set of chain mobility within the lamellar crystal. Since lamellar thickening requires chain mobility within the lamellar crystals, it can only be observed at temperatures above T_{α_c} and below the melting temperatures. For polymer systems that do not have α_c relaxation, such as isotactic poly(styrene) (it-PS), poly(ethylene terephthalate) (PET), poly(butylene terephthalate) (PBT), poly(ether-ether-ketone) (PEEK), etc., lamellar thickening is not observed. These polymers usually have a bulky side group or a stiff backbone that lowers chain mobility.

2.2 Copolymer Crystallization Theory

Crystallization models built for statistical copolymers with a non-crystallizable component display two extreme cases which are shown schematically in Fig. 2.3. In the first case, the non-crystallizable component is rejected from the crystal lattice during crystallization. This is called the complete exclusion model. In the second case, the non-crystallizable component is included uniformly in the crystal lattice and the co-unit concentration in the crystal lattice is the same as that in the initial melt. This is called the uniform inclusion model.* In his copolymer crystallization theory, Flory[30] considered the minor co-units as defects on the crystallizable polymer chains. By assuming that these "defects" are completely excluded from the crystal lattice, he derived the conditions for the melting of the copolymer crystals based on a phase equilibrium theory. From that derivation, the minimum stable crystallite length and the degree of crystallinity as a function of temperature and sequence distribution length was obtained. However, the application of this theory to several copolymer systems has shown only poor agreement. One of the most cited discrepancies was the consistently lower value of heat of fusion calculated for a homopolymer on the basis of the exclusion model analysis on copolymers of that homopolymer, as compared, for example, with the analysis using other experimental methods, such as the diluent method.

* Note that the two schematic drawings in Fig. 2.3 by no means suggest the two models have the same lamellar thickness.

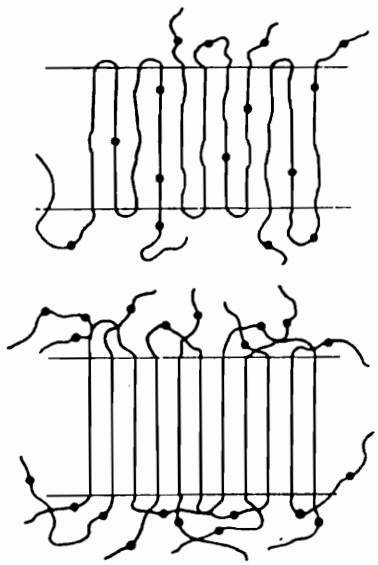

Fig. 2.3 Schematic drawings showing the extreme states of crystalline random copolymers. Uniform inclusion model, top; complete exclusion model, bottom (adapted from ref. 32).

Later, Sanchez and Eby[31] used another scheme to derive the conditions for the inclusion model. The theory was modified later by the same group to include kinetic effects[32]. Under the modified theory, the copolymer composition in the crystal lattice is kinetically-controlled. Depending on the crystallization temperature, the departure from the equilibrium co-unit concentration X_{eq} varies. Here X_{eq} can be expressed as

$$X_{eq} = \frac{Xe^{-\varepsilon/RT}}{1 - X + Xe^{-\varepsilon/RT}} \tag{2.7}$$

where T is the temperature at which the crystallization process takes place and ε is the excess free energy of the defect in the crystal lattice. The uniform inclusion model and the complete exclusion model correspond to the two limiting cases where ε equals to zero and infinity, respectively.

The free energy of crystallization for the copolymer crystal is given by:

$$\Delta G = \Delta G^{\circ} - RT\left\{\frac{\varepsilon X_c}{RT} + (1 - X_c)\ln\left[\frac{1 - X_c}{1 - X}\right] + X_c \ln\left[\frac{X_c}{X}\right]\right\} \tag{2.8}$$

with the symbols define as follows:

ΔG°: free energy of crystallization for the homopolymer;

X_c: actual concentration (mole fraction) of the co-unit in the crystal;

X: overall mole fraction of the co-unit in the copolymer.

As can be seen from equation (2.8), the modified free energy consists of three terms. The first term is an enthalpic term. The second and the last term are entropic in nature. Several important predictions can be made with this theory. First, it predicts an

equilibrium melting temperature depression in the copolymer system. This can be obtained by letting $\Delta G = 0$ in equation (2.8) which gives:

$$\frac{1}{T_m^o} - \frac{1}{T_m} = -\frac{R}{\Delta H_f^o}\left\{\frac{\varepsilon X_c}{RT_m} + (1-X_c)\ln\left[\frac{1-X_c}{1-X}\right] + X_c \ln\left[\frac{X_c}{X}\right]\right\} \qquad (2.9)$$

where T_m^o the equilibrium melting temperature of the homopolymer. For the uniform inclusion model, i.e. $X_c = X$, equation (2.9) reduces to

$$T_m = T_m^o\left(1 - \frac{\varepsilon}{\Delta H_f^o} X\right) \qquad (2.10)$$

Equilibrium melting temperature depression for the copolymer with respect to the homopolymer was also predicted by Flory in his exclusion model. However, there is a fundamental difference between these two predictions. In Sanchez and Eby's words[31], in the inclusion model, the equilibrium melting temperature depression is caused by the defective heat of fusion, an enthalpic effect whereas in the exclusion model, it is caused by the requirement of a preferential ordering of the copolymer chains during crystallization, an entropic effect.

By assuming that the fold surface energy σ_e and the lamellar thickening at the crystallization temperature are independent of the co-unit content, Sanchez and Eby showed that the observed lamellar thickness at a given crystallization temperature increases linearly with the co-unit content of the copolymers. It should be noted that Flory's equilibrium theory (exclusion model) also predicts that the lamellar thickness increases with the co-unit content. Therefore, these two theories are qualitatively equivalent in this consideration.

Sanchez and Eby's theory also predicts that under isothermal crystallization conditions, the rate of crystal growth should decrease with co-unit content. They also suggest that, from the kinetic point of view, the co-unit inclusion should increase with crystal growth rate.

As can be seen from above, similar predictions can be made from both models. In principle, however, results from thermal analysis and X-ray crystallinity studies should result in the determination of which model is more appropriate for different copolymer systems. For the exclusion model, the ratio between the observed heat of fusion ΔH_f^* and crystallinity x_c is independent of the co-unit concentration:

$$\Delta H_f^*/x_c = \Delta H_f^\infty - 2\Delta H_e/l \tag{2.11}$$

However, $\Delta H_f^*/x_c$ is linearly dependent on X for the inclusion model:

$$\Delta H_f^*/x_c = \Delta H_f^\infty - X\Delta H_d - 2\Delta H_e/l \tag{2.12}$$

where ΔH_d is the defect heat of fusion, l the lamellar thickness and ΔH_e the excess enthalpy associated with forming the basal surfaces of the lamellar crystal.

Before leaving this section, one should also mention a similar theory on copolymer crystallization by Helfand and Lauritzen[33]. Their theory is based on the kinetic theory by Lauritzen, DiMarzio and Passaglia[34]. In addition to the kinetic theory employed in homopolymers, free energy costs of incorporating the co-units in the crystal stems are also accounted for by this theory. Without going into details, the major predictions from Helfand and Lauritzen's theory are:

1. The faster the crystal growth, the greater is the inclusion of excess co-unit.

2. Conditions that speed up the growth process will increase the inclusion of co-unit.
3. Lamellar thickness of the copolymer is larger than that of the homopolymer crystallization at the same temperature.

These conclusions are very similar to those made by Sanchez and Eby.

2.3 Poly(propylene)

2.3.1 Stereo-Isomerism of Poly(propylene)

The chemical structure of poly(propylene) is very similar to that of poly(ethylene) except that one of the hydrogen atoms is replaced by a methyl group on every other carbon atom. The chemical structure of a poly(propylene) repeat unit is shown in Fig. 2.4. When the repeat units are assembled to form a linear polymer chain, it can occur with two different isomerisms. Isomerism has significant consequences on the polymer properties. This will be explored in more details in the following sections.

There are two different types of isomerisms: positional and stereo isomerisms. Positional isomerism, also known as regio-isomerism or orienticity, involves the orientation of the repeat unit when it is added to the growing polymer chain. Usually, this is also referred as head-to-head or tail-to-tail on head-to-tail arrangements. A polymer chain is regio-regular when its repeat units are in the head-to-tail arrangement. Head-to-head or tail-to-tail defects cause interruptions in the regular monomer sequence in the polymer chain and have the resulting effect of decreasing crystallinity. Regio-regularity depends strongly on the catalyst systems used in polymerization. For example, isotactic poly(propylene) and isotactic propylene-ethylene copolymers are highly regio-regular[35,36] and practically no inversion is present in commercial isotactic poly(propylene) samples[37]. On the other hand, syndiotactic poly(propylene) and syndiotactic propylene-ethylene copolymers obtained from the vanadium-based catalyst systems have a non negligible amount of head-to-head or tail-to-tail defects[38,39].

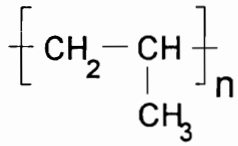

Fig. 2.4 Chemical structure of the poly(propylene) repeat unit

Stereo isomerism can be seen in Fig. 2.5, where three different "configurations" of successive repeat units exist. For poly(propylene), the side group "R" is the methyl group. In polymer physics terminology, these different configurations are called tacticities. When the side groups are on the same side of the fully extended carbon back bone, as in Fig. 2.5a, the configuration is called "isotactic". When the position of the side group alternates in consecutive repeat units, as in Fig. 2.5b, the configuration is called "syndiotactic". Atactic configuration (Fig. 2.5c) is one in which the position of the side group follows a random sequence. Degree of tacticity, or randomness of the sample, can be measured by solution ^{13}C NMR experiments.

Tacticity has a significant effect on polymer crystallization and other polymer properties. As an example, isotactic (a) and syndiotactic (b) poly(propylene) are semi-crystalline materials while atactic (c) poly(propylene) is amorphous. Moreover, crystal structure, melting behavior and physical properties of the isotactic and syndiotactic poly(propylene) are very different.

Until recently, isotactic poly(propylene) was mainly synthesized using Ziegler-Natta catalysts system. Ziegler and Natta received the Nobel Prize for this important discovery in 1963. Nowadays, it-PP is also made using the new metallocene catalysts[41-48]. These catalysts are also called single site catalysts. Metallocene catalysts have already made it possible to produce isotactic[45], isotactic-stereoblock[46], syndiotactic[47], and isotactic-atactic propylene block copolymers[48]. Compared to materials synthesized from Ziegler-Natta catalyst systems, polymers synthesized by these new catalysts have higher tacticities. Defects of the polymers are also better controlled. Moreover, poly(propylene)

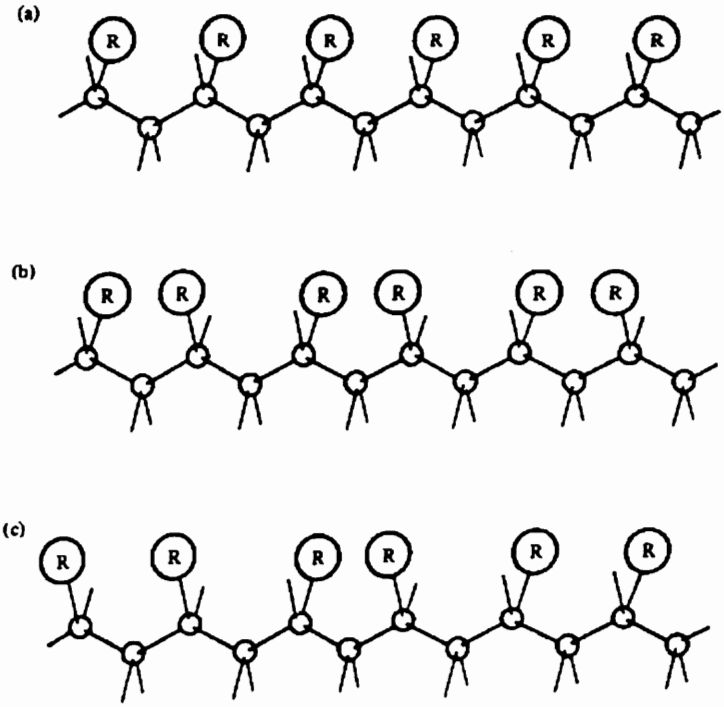

Fig. 2.5 Sections of polymer chains with different tacticities: (a) isotactic (b) syndiotactic (c) atactic (adapted from ref. 40).

with a narrower molecular weight distribution (with M_w/M_n approximately equals to 2) can also be produced with these catalysts[44].

In comparison with isotactic poly(propylene), syndiotactic poly(propylene) (s-PP) has a relatively shorter history. Even though it was first synthesized almost at the same time as it-PP with the Ziegler-Natta catalyst systems, s-PP materials used in the early studies usually contained a non-negligible amount of isotactic sequences, along with head-to-head or tail-to-tail defects. The complexity of the molecular structure of s-PP synthesized in the earlier days has made the characterization of its properties more difficult than in the case of the isotactic material. Namely, results and conclusions derived from studies with different s-PP samples were difficult to compare and correlate. However, the situation has changed recently. The interest in this polymer has become larger since the 80s and a number of studies have been carried out. Using the metallocene catalyst based synthesis[47], s-PP samples with higher syndiotactic content, higher yields and higher purity can now be synthesized, which has led to a better characterization of their properties.

Like it-PP, syndiotactic poly(propylene) also exhibits polymorphism. Among the several crystal forms reported in the literature[49-57], one is the high temperature orthorhombic form[53,54]. It is the most stable crystal structure for s-PP. Polymer chains in this crystal form assume a $(T_2G_2)_2$ helical conformation and have an S(2/1)2 symmetry. Three different unit cells (cell I, II and III) have been proposed for this crystal structure. Another orthorhombic form exists at low temperature or under quenched conditions[51,52]. This crystal form is less stable than the first one and transforms into the more stable crystal structure upon heating. The polymer chains in this crystal form assume the planar zigzag

conformation. Finally, there is another crystal form with a triclinic unit cell[55]. More recent studies of s-PP have been concentrated on the analysis of crystal structures in oriented and unoriented samples[54]. Effects of chain disorder were also investigated[53,56]. Due to the difficulties in s-PP synthesis, the literature reporting the physical properties of syndiotactic poly(propylene) has been limited. Equilibrium melting temperature and crystallization kinetics were studied by Miller *et al.*[58]. A more recent study on equilibrium melting temperature, enthalpy of fusion and glass transition temperature were reported by Haftka and Könnecke[59]. The crystallization behavior and morphology have been recently reviewed by Rodriguez-Arnold *et al.*[60]

The most widely used poly(propylene) today is the isotactic poly(propylene) (it-PP). It-PP has one of the lowest density (0.90-0.91 g/cm^3) among the large-volume, low-cost thermoplastics[3]. Its high melting temperature (~170 °C) enables a usable temperature up to 120 °C[3]. One of the most important benefits of it-PP is its ease of processing and low cost[61]. It can undergo almost any processing method: injection molding, extrusion, thermoforming, blow molding, melt spinning, etc. Since it can be processed into fibers, films, sheets, it-PP finds applications in diapers, carpet backings, packaging, food containers, data transmission cable sheathing, etc. Because of its light weight (low density) and high impact properties, it-PP is becoming an important component used in the auto industry and for other applications. Its good moisture barrier properties, low odor/taste transfer properties, relatively high melting temperature among other polyolefins and low cost make it one of the best choice to be used in the food industry for packaging

and storage. As mentioned in Chapter 1, it-PP has the fastest rate of growth in the world wide thermoplastics market.

The polymorphism of it-PP will be discussed in the next section.

2.3.2 Polymorphism of Isotactic Poly(propylene)

Isotactic Poly(propylene) has at least five different crystal phases: α_1, α_2, β, γ and the smectic form. In all its crystal forms, including the less ordered smectic form, it-PP crystallizes with the trans-gauche [$(TG_+)_3$ and $(G_-T)_3$] conformation that forms a 3/1 helix with a repeat period of 6.5 Å. Extensive studies of these crystal forms have been conducted and discussed in several review articles[62,63].

As mentioned above, it-PP assumes a 3/1 helical conformation in all of its crystal forms. This conformation can be further divided into left- and right-handed helices according to the internal rotation angles of the backbone. Moreover, one can also define the orientation of the chain within the crystals. For a given reference axis, the 3/1 helical conformation can be identified with, in addition to the left- and right-handed conformations, the up and down orientations. This can be best illustrated in Fig. 2.6, where sections of the 3/1 helix with the left- and right-handed conformations as well as the up and down orientations are shown. While all these conformations have the same conformational energy, their arrangement within the crystals can affect the packing energy. In fact, polymorphism in it-PP, which has identical chain conformations but with different modes of packing (hence different packing energies), is called "packing polymorphism".

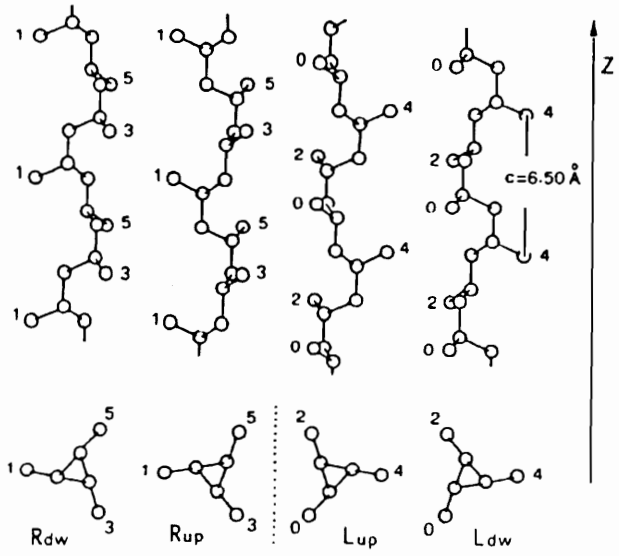

Fig. 2.6 The right- (R) and left-handed (L) conformations of it-PP with the up and down orientation w.r.t. to the reference Z axis (adapted from ref. 63).

The monoclinic α-form is the most common crystal form found in it-PP. Fig. 2.7 shows the WAXD pattern of α-form it-PP. The unit cell parameters for the α-form, determined by Turner-Jones *et al.*[62] are: a = 6.66 Å, b = 20.78 Å, c = 6.495 Å, β = 99.6° and α = γ = 90°. The α-form is further divided into two limiting structures: α_1 and α_2[64]. The difference between these two polymorphs is the different degrees of disorder in the up and down positioning of chains in the unit cell. The α_1 structure is the limiting disordered structure with random distribution of the up and down chains whereas α_2 denotes a limiting ordered structure with well-defined up and down positioning of chains within the unit cell. In many cases, it-PP samples are found to have different amounts of α_1 and α_2 forms. Transition from the disordered α_1 form crystals to ordered α_2 form crystals in it-PP homopolymer and propylene-ethylene copolymer with 2.7% ethylene content was studied by De Rosa *et al.*[65] who suggested that the transition involves partial melting and subsequent recrystallization. Quantitative studies of these two structures by WAXD analysis is difficult. Because of the similarity of these two structures, they can only be distinguished using the two high order Bragg peaks in the 34° to 38° 2θ range[66].

Morphologically, α-form lamellae exhibit an unique lamellar branching characteristic which is very different from any other semi-crystalline polymers. Namely, the branching lamellae in α-phase crystals always form an 80.67° angle with respect to the parent lamella. This branching behavior, resulting in the "cross-hatched" morphology, is found in it-PP spherulites grown from the melt or from solution[67-71]. It is responsible for the low birefringence in the α-form spherulites when observed by microscopy under polar-

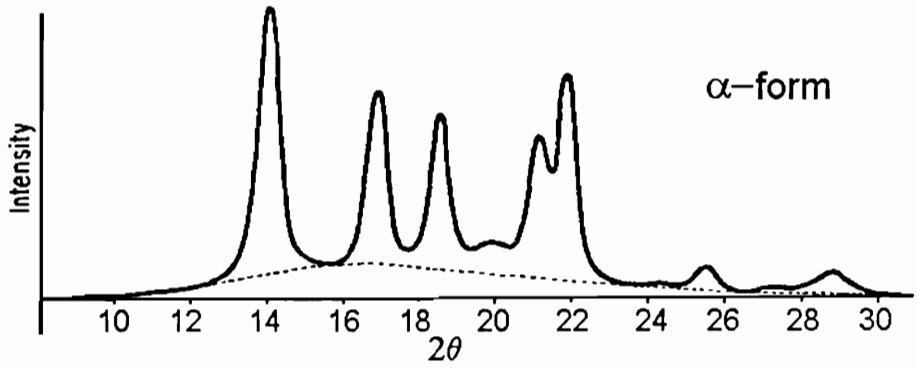

Fig. 2.7 Powder X-ray diffractogram for an α-form it-PP bulk sample (adapted from ref. 62).

ized light. Olley and Bassett[70] studied the morphology development in melt grown it-PP crystals. They showed that at high crystallization temperatures (160 °C), the development is more or less similar to other polymer systems with dominant lamellae growing outward. In the temperature range of 150 to 155 °C, however, lamellar branching (cross-hatching) at the center of the spherulites is observed, with higher frequency of occurrence as the crystallization temperature is lowered. These results were consistent with an earlier finding by Norton and Keller[71], who used optical and electron microscopy to study the correspondence between the lamellar branching habit and the birefringence change in α-form poly(propylene) spherulites. Using transmission electron microscopy, Khoury[67] discussed the morphology in the it-PP dendrites crystallized from solutions. He found that the dendrites consist of "twinned" crystals that form an acute angle of 80.67°, which is the same angle observed in cross-hatching . This unique branching behavior is closely related to the α and γ-form crystal structures and is consistent with the α-γ branching.

Chain orientation within the lamellae was also determined from electron diffraction patterns[69]. Moreover, the contact plane at the branching point has been identified as the (010) plane by Padden and Keith[72] and the branching is an epitaxial growth with a fit of molecular subgroups[68]. It should be noted that this observation is not a coincidence. This and other observations found in the α-form structure as well as those found in the γ-form structure are inter-related. Only after a thorough understanding of each of these behaviors then a complete picture of the crystal growth behavior can be fully understood. More recent studies[73-75] suggested that the α-form structure consists of bi-layers of left-handed and right-handed helices. In α-form crystals, two adjacent bi-layers contact each other

through helices of opposite chirality, resulting in a parallel chain structure within the crystals. Occasionally, the contact between the two bi-layers occurs through helices with the same chirality. This causes lamellar branching and results in the cross-hatched morphology. This bi-layer structure is also found to be the building block of γ-form structure[76]. In γ-form crystals, the two adjacent bi-layers contact each other through helices with the same chirality and give a 80.67° tilting angle between the two bi-layers. This packing occurs in a periodic way and gives rise to the non-parallel chain structure of the γ-phase crystals.

β-form it-PP has a hexagonal unit cell. Fig. 2.8 shows the WAXD pattern for the β-form crystals. It can coexist in small amount with the much more common α-form when the melt is quenched in water-glycerol mixtures at 100 to 130 °C[62]. Other conditions that promote the β-phase formation such as crystallization from an oriented melt, shear-induced crystallization and temperature gradient method have also been reported in the literature[77-79]. Over the temperature range 100 to 130 °C, β-form has a higher crystal growth rate than the α-form. This makes it kinetically favored in this window of crystallization temperature. β-form crystals can transform to the α-form upon heating above 130 °C[80-82]. The β-α transformation depends on the thermal treatment prior to heating. Moreover, this β-α transition can also be promoted by deformation[80]. It has also been reported that a small amount of certain nucleating agents can promote the formation of the β-form[83-85]. In fact, this is the most common approach in studies of the β-form.

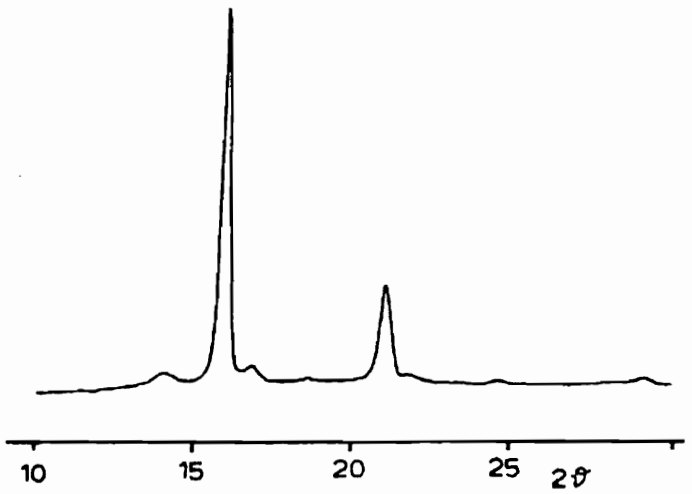

Fig. 2.8 Powder X-ray diffractogram for a β-form it-PP bulk sample (adapted from ref. 63).

Pure β-form samples have been obtained by this approach[83]. Unlike α-spherulites, which have the special cross-hatched morphology, β-spherulites consist only of lamellae radiating from the center of the spherulites.

The γ-form crystal is probably the most interesting crystal form among all crystal forms of poly(propylene). It is known that several factors can promote the γ-form crystal formation: low molecular weight[86,87], slow cooling from the melt[62], crystallization under high pressure[88] and defects on the poly(propylene) backbone such as ethylene or 1-butene repeat units in some propylene copolymers[89]. Since the first discovery of the γ-form[86,90], its crystal structure had been considered as triclinic[62]. Morphology of the γ-form crystals based on this triclinic unit cell and its relation to the α-form crystals were studied by Lotz *et al.*[91] The similar X-ray diffraction patterns of the α and γ forms have suggested the γ-form unit cell can be obtained by a slight deformation of the α-form unit cell. However, this suggestion has been ruled out on the basis of energy calculations[73]. Moreover, it has been reported that some of the diffraction peaks in the γ-form X-ray pattern (Fig. 2.9) cannot be explained by the triclinic unit cell. In 1989, Brücker and Meille[76] proposed a new crystal structure for the γ-form. The new crystal structure is a face-centered orthorhombic cell with unit parameters: a = 8.54 Å, b = 9.93 Å, c = 42.41 Å. It should be noted that the c-axis in this new unit cell is unusually large. More importantly, the new unit cell consists of non-parallel chains. Furthermore, unlike many other semi-crystalline polymers, which have the chain axis normal to the lamellar surface, the chain axis in the γ–

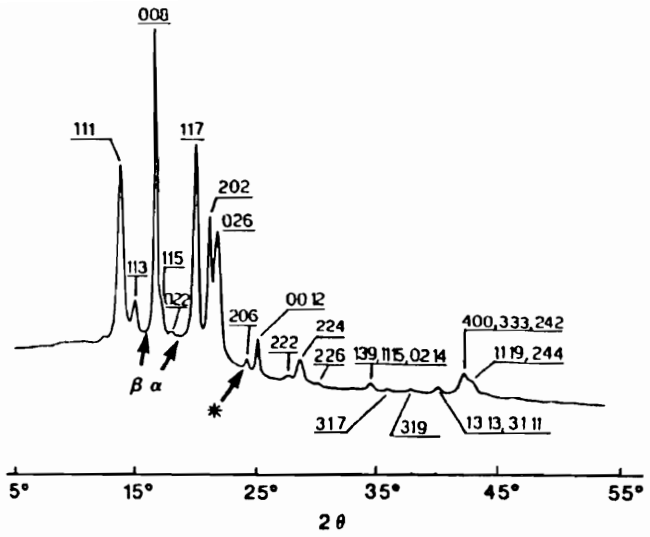

Fig. 2.9 The X-ray diffraction pattern of γ-form it-PP (adapted from ref. 76).

form crystals makes a 40° tilting angle with respect to the lamellae surface normal. This particular chain arrangement is a systematization of the chain overlapping pattern at the crystallographic branching point of α-form lamellae, which gives rise to the cross-hatched morphology. Some other similarities between this crystal form and the α-form have been mentioned above. With this unit cell, the previous inconsistencies among the crystal growth behavior and the formation of coexistent α- and γ-form crystals can now be better explained. Continuing studies based on this new unit cell include refining the crystallographic parameters[92] and investigation of the contact faces of the α- and γ-phase it-PP[93].

γ-form single crystals were successfully obtained by Lotz *et al.*[94] In that paper, they clearly showed the consistency between the non-parallel chains in the γ-form unit cell structure and the specific 80.67° angle at the lamellar branching in the α-form spherulite. Another important consequence with this finding, as mentioned in the same publication, is the morphological possibility of γ–α branching. Such an event is rare but nonetheless has been observed[94]. This again further supports the validity of this new unit cell.

The smectic form, sometimes referred to as the mesomorphic or liquid crystal-like form, is obtained by fast quenching the it-PP samples from the melt to below room temperature. It is characterized by a low degree of lateral chain order and broad and less defined diffraction peaks in the WAXD pattern[95-97]. Furthermore, the smectic form is unstable. Upon heating or long-time residence above T_g, it transforms into the more common α-form. Using IR, WAXD, SAXS and DSC experiments, Yan *et al.*[98] have

shown that the smectic form does not consist of it-PP α-form crystals of small size but is formed by chains in the 3/1 helical conformation with less lateral packing order than in the α-form.

2.4 Propylene Based Copolymers

Propylene can form copolymers with several other olefins: ethylene, 1-butene, etc.[99] Depending on the comonomer composition and the catalyst systems used, copolymers of propylene and ethylene can be either semi-crystalline or amorphous rubbery materials. The crystal structures of copolymers of propylene and ethylene are similar to that of poly(ethylene) for low propylene content copolymers and to that of poly(propylene) for low ethylene content copolymers. Polymorphism similar to that of the propylene homopolymer also exists in the latter copolymer in the low ethylene content range. Amorphous rubbery materials (EPR--ethylene-propylene rubbers and EPDM--ethylene-propylene-diene elastomers) synthesized by catalyst systems different from those used to prepare statistical PP copolymers are obtained for ethylene content ranging from 40 to 90 mol%.

When the copolymers of propylene and ethylene are under study, the content of each monomer unit should first be emphasized. Random copolymers of propylene and ethylene with ethylene content as high as 29.2 mol% have been shown to form only poly(propylene) type crystals[100]. For samples with higher ethylene content, mixed crystals of poly(propylene) and poly(ethylene) were detected. Like many other copolymer

systems, the crystallization behavior and many other physical properties of copolymers of propylene and ethylene cannot be solely determined by the copolymer composition. The microstructure of the copolymer (i.e. random or blocky nature of the ethylene and propylene sequences) is just as important.

Statistical copolymers of propylene and ethylene, often referred to as random copolymers, have different properties from the poly(propylene) homopolymer. Generally speaking, as compared with the homopolymer, random PP copolymers exhibit a reduced stiffness, higher impact resistance, lower melting temperatures and better optical clarity[3]. In terms of their chemical resistance and water vapor barrier properties, PP copolymers are comparable to the it-PP homopolymer. Commercial PP copolymers usually contain 1 to 7 wt% ethylene unit. Because of the insertion of ethylene repeat unit, the copolymer has lower stiffness. The interruption of the propylene sequence leads to a lower crystallinity, lower melting temperature, and higher impact resistance. A wide range of properties can be obtained from different grades of materials with different compositions, different molecular weights and different molecular weight or composition distributions[3,61].

In addition to all the physical property modifications provided by copolymerization, PP copolymers have another important property. As reported by Turner Jones[89] in the early 70s, a small amount of comonomer units in the poly(propylene) backbone can promote the formation of the γ-form structure. Details of this behavior will be discussed later in Chapter 3.

Bearing in mind the significance of microstructure, it is of essence to have the microstructure characterized when the polymer properties are studied. One of the most

powerful tools for this task is ^{13}C NMR. ^{13}C NMR has been widely used to characterize the microstructure of numerous polymer systems. Due to the low natural abundance of ^{13}C (only 1.11%), a ^{13}C NMR experiment usually takes hours as compared with a ^{1}H NMR experiment. Nonetheless, ^{13}C NMR has proved to be an invaluable tool for poly-(olefin) characterization. One of its benefits is the resolution. ^{13}C NMR covers a chemical shift range of over 200 ppm, which is 20 times that usually covered by ^{1}H NMR. Several issues associated with this characterization technique will be briefly addressed below.

First of all, the microstructure of a propylene-ethylene copolymer involves several structural variables. Besides the content of the two monomer units, the microstructure also involves the distribution of these units in the polymer chains. This is normally characterized by the dyad, triad or sometimes tetrad distributions of the monomer units. Whereas the analysis of the tetrad distribution of the monomer units gives more information than that of the dyad or the triad distributions, the requirement of higher resolution and higher signal to noise ratio in the recorded spectrum limits its use. In this study, the propylene-ethylene co-unit distribution will be characterized by the triad concentration. Moreover, as in the homopolymer poly(propylene), there can be inversion in the propylene addition sequence which causes head-to-head or tail-to-tail inversion. It should be mentioned that the inversion level for some vanadium-based catalysts systems used for producing EPR and amorphous materials can be very high[101]. On the other hand, it is nearly undetectable in the titanium-based catalysts system[102]. Similar observations for propylene copolymers were confirmed with ^{13}C NMR experiments by Simonazzi and Abis[103]. Beside inversion in the propylene addition sequence, there are also tacticity of the

propylene sequence in the polymer chains. Kanezaki *et al.*[104] showed that isotacticity of the propylene block in propylene-ethylene block copolymers can be determined by ^{13}C NMR experiments. Even though characterization of the propylene inversion and tacticity is possible from tedious ^{13}C NMR studies, it is felt that the ethylene content and comonomer distribution can be considered to be the most important factors in controlling the properties of propylene-ethylene copolymer samples under study.

Peak assignments in the ^{13}C NMR spectrum of propylene-ethylene copolymers have been reported by several authors[105-108]. More on this issue can be found in the review on ^{13}C NMR characterization of ethylene-based copolymers published by Randall[109].

2.5 Poly(1-butene)

Poly(1-butene) is another member of the polyolefin family. Isotactic poly(1-butene) (it-P1B) was first synthesized in the 50's by Natta and coworkers[110]. The chemical structure of an it-P1B repeat unit is shown in Fig. 2.10. Over the years, the share of it-P1B in the thermoplastics market has been relatively small. The homopolymer still has limited applications in industry[61]. Poly(1-butene) films have found applications in food and meat packaging. It-P1B is also used in making blends with other polyolefins, such as poly(propylene), to improve the toughness of the latter.

Like it-PP, isotactic poly(1-butene) also exhibits polymorphism. There are three major crystal forms: form I, form II and form III. Two other forms, the untwinned hexagonal form I' and form II', however, are less often documented in the literature. The

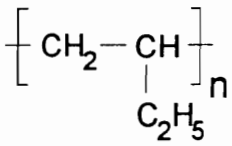

Fig. 2.10 Chemical structure of the poly(1-butene) repeat unit

orthorhombic form III and the less common form I' are formed by crystallization from suitable solvents. Form II' is formed by crystallization under pressure. Form I crystal has a twinned hexagonal unit cell. It has the highest equilibrium melting temperature 135 °C and is the most stable it-P1B crystal form.

Form II crystal has a tetragonal unit cell. The kinetically favored form II structure is metastable. When it-P1B is crystallized from the melt, it will first crystallize into the form II structure. Immediately, it starts to transform into the more stable form I crystal and the transformation is irreversible. Depending on the crystallization conditions, the process of transformation will be complete in the order of 4 to 40 hours at room temperature. This form II $\rightarrow$ form I transformation has been studied by many research groups[111-116]. Since form I crystal has a higher density than form II crystal (0.951g/cm^3 vs. 0.902g/cm^3), a significant shrinkage accompanies this transformation. This shrinkage is undesirable from any application point of view. In practice, poly(1-butene) products have to be stored until this shrinkage is completed. This adds to the cost and is the main reason for it-P1B's slow growing market in spite of its promising properties. Studies have been conducted to accelerate this transformation. Many factors, such as molecular weight, copolymerization, additives, pressure, temperature, sample thickness, ultrasonic wave, heat treatment and γ-ray irradiation, have been found to affect the rate of this transformation[111-116].

2.6 Polymer Blend Miscibility

The essence of research in polymer blends is to develop new materials with optimal materials properties that are derived from the properties of the individual components. When two or more polymer materials are mixed together, the very first question often addressed is whether they are miscible. In some areas, the term "compatibility" is used instead of "miscibility" when the properties of a polymer blend are under study. Though in some cases the two terms are used interchangeably, there is a difference between them. When a polymer blend is said to be "compatible", it usually implies the blend has good mechanical and optical properties, etc. Usage of the term "compatible" in this case is more or less a practical one. It implies no knowledge on whether or not mixing in the polymer blend occurs at the molecular level. It should be noted that some two-phase, immiscible polymer blends are "compatible" under this usage. On the other hand, "miscibility" is a thermodynamic term. A miscible blend is a thermodynamically stable one phase system. The behavior of a miscible blend can be described by phase diagrams. Therefore, while a miscible system is always "compatible", the reverse is not necessarily true.

Miscible blends are desirable in many applications since they provide stability and uniformity within the material. Good mechanical properties are often the result of miscibility. Though immiscible polymer blends are very common in industry, some of these blends show poor adhesion at interfacial regions, resulting in much lower ultimate properties than what would have been expected from averaged properties. More

importantly, properties of miscible systems are more predictable than for their immiscible two phase counterparts whose properties depends on many factors such as phase morphology, phase size, interfacial properties, etc. Finally, the usable range of an immiscible system is often limited to compositions where one phase is the major continuous phase in contrast to the fact that the entire composition range can provide usable properties for miscible systems. It should be pointed out, however, that miscibility is not necessary desirable for all polymer blend applications. In many areas, a two phase system has advantages over a miscible, one phase system. For example, in rubber toughened thermosets, the rubber phase prevents crack development and delays failure.

A brief review of polymer miscibility is given below.

2.6.1 Flory-Huggins Theory

Theoretical works on polymer miscibility usually fall into two approaches: the Flory-Huggins lattice model and the equation of state. Although there are shortcomings in the classical Flory-Huggins lattice model, it continues to be used in polymer miscibility studies. Various modifications of the model have been proposed and have had success in specific applications to various systems, including those with specific interactions. In this work, where miscibility of poly(propylene) and poly(1-butene) is under investigation, it is found that the Flory-Huggins model is more convenient. In the following, the assumptions and the key equations of this theory will be discussed. It is then followed by the derivation of the binodal and spinodal curves, which will define the phase diagram.

Although a complete derivation of the Flory-Huggins theory is not given in this review, it is necessary to mention the assumptions made in this classical theory. These assumptions include: 1) the mixing does not involve any volume change, and 2) even though some favorable or unfavorable interactions may be involved, the interactions are not strong enough to produce clustering. (In statistical mechanical terms, assumption 2) is the same as saying entropy is still governed by the Boltzmann distribution). It also assumes that the system can be described on a regular lattice. Moreover, the system has narrow molecular weight distributions and interactions are limited to neighboring segments which are characterized by z, the coordination number.

The derivation of the theory involves writing down the expression of the free energy of mixing. A complete derivation usually starts with mixing in ideal solutions, after which the departure from ideality is introduced for real solutions. This is followed by the formulation of the enthalpy and entropy of mixing. Separately proved by Flory[117] and Huggins[118], the equations for polymer solutions were in fact similar to the classical ones applied to real solutions except that the mole fractions were replaced by volume fractions. Later, Scott[119] applied the Flory-Huggins theory to polymer mixtures. For polymer solution and polymer blend systems, Raoult's law does not apply. Therefore, in addition to the athermal mixing term, another term that contributes to the polymer-solvent interaction or polymer-polymer interaction is introduced.

For polymer blend systems, the free energy of the system ΔG_{mix} can be written in the general form:

$$\Delta G_{mix} = \Delta H_{mix} - T\Delta S_{mix} \qquad (2.13)$$

Where ΔH_{mix} and ΔS_{mix} are the enthalpy and entropy of mixing, respectively. (In order to limit the number of notations used and for the convenience of the discussion in later chapters, the symbols in the following will refer to the poly(propylene)/poly(1-butene) blend system.)

The enthalpy of mixing is given by

$$\Delta H_{mix} = Vzw\phi_P(1 - \phi_P)/V_s \tag{2.14}$$

where $w = \frac{1}{2}\varepsilon_{PP} + \frac{1}{2}\varepsilon_{BB} - \varepsilon_{PB}$ is the energy of interaction or exchange, V and V_s the total volume and the interacting segment volume, respectively. ε_{PP}, ε_{BB} and ε_{PB} are the energies of contacts between the propene-propene, butene-butene and propene-butene segments. The combinatorial entropy of mixing, ΔS_{mix}, is given by

$$\Delta S_{mix} = -k[N_P \ln\phi_P + N_B \ln(1 - \phi_P)] \tag{2.15}$$

Where N_P and N_B are the number of polymer-occupied lattice sites for propylene and butene segments, respectively. If the Flory-Huggins interaction parameter χ is defined as

$$\chi = zw/RT \tag{2.16}$$

then the free energy of mixing can be rearranged into the form:

$$\Delta G_{mix} = RT\left[\frac{\phi_P \ln(\phi_P)}{m_P v_P} + \frac{(1-\phi_P)\ln(1-\phi_P)}{m_B v_B} + \frac{\chi}{v_0}\phi_P(1-\phi_P)\right] \tag{2.17}$$

with the individual symbols defined as follows:

v_P, v_B: molar volume per repeat unit

m_P, m_B: weight average number of repeat units

ϕ_P: volume fraction of poly(propylene)

v_0: lattice cell volume, generally taken as $v_0 = \sqrt{v_P v_B}$

where subscripts P and B stand for the propylene and butene repeat units (segments), respectively.

Equation (2.17) is the basic equation in the Flory-Huggins theory. The phase behavior of the system can be predicted from (2.17), based on the criteria for equilibrium, the limits of stability and criticality evaluated at constant temperature and pressure.

Before proceeding any further, (2.17) will be rewritten by using the Hildebrand solubility parameter approach.

2.6.2 Solubility Parameter Approach

While there are several approaches in theoretical works on polymer miscibility, only the Hildebrand solubility parameter approach[120] will be mentioned here. The solubility parameter approach has been successful in characterizing the strength of dispersive interactions in simple liquids. The concept was extended to polymer solutions and polymer mixtures. Various refinements of the solubility parameter concept have been made to accommodate systems with polar and hydrogen bonding interactions[121].

The solubility parameter, δ, is defined as:

$$\delta \equiv \left(\frac{\Delta U_{vap}}{V} \right)^{1/2} (cal / cm^3)^{1/2}$$

Where ΔU_{vap} is the heat of vaporization at constant volume and V the volume of the sample.

For simple liquids, δ can be calculated directly from measurements of the heat of vaporization at constant pressure. For polymers, however, solubility parameters can only be determined indirectly, either by experiments or by calculation using the group contribution method[122]. One of the experimental methods for determining δ is the swelling experiment. In this method, polymer samples, either lightly cross-linked or semi-crystalline, are swollen by different solvents. The interaction and thus the swelling is at its maximum when the polymer and the solvent have the same solubility parameter. Therefore, from the maximum in a plot of swelling vs. solvent solubility parameter, the solubility parameter of the polymer can be determined. Other experimental methods of solubility parameter determination rely on heat of solution measurements and extrapolation methods from homologous series.

Once the solubility parameters are determined for the system of interest, they can be applied to (2.17). To do so, the following two steps are involved:

1) ε_{PB} is assumed to be the geometric mean of ε_{PP} and ε_{BB}., i.e. $\varepsilon_{PB} = \sqrt{\varepsilon_{PP}\varepsilon_{BB}}$. This assumption is only good for non polar or slightly polar systems.

2) From Hildebrand[120], $(\delta_P - \delta_B)^2 \equiv z\left(\sqrt{\varepsilon_{PP}} - \sqrt{\varepsilon_{BB}}\right)^2 / 2V_s$

Then, the interaction parameter χ can be expressed as

$$\chi = \frac{v_0(\delta_P - \delta_B)^2}{RT} = \frac{v_0(\Delta\delta)^2}{RT} \qquad (2.18)$$

Where $\Delta\delta = \delta_P - \delta_B$ is the solubility parameter difference between poly(propylene) and poly(1-butene).

From (2.18), (2.17) can be rewritten in the form

$$\Delta G_{mix} = RT\left[\frac{\phi_P \ln(\phi_P)}{m_P v_P} + \frac{(1-\phi_P)\ln(1-\phi_P)}{m_B v_B} + \frac{\Delta\delta^2}{RT}\phi_P(1-\phi_P)\right] \tag{2.19}$$

2.6.3 Binodal Curve, Spinodal Curve and Phase Diagram

The binodal curve in a phase diagram describes the location on a temperature vs. composition plot where the chemical potential ($\Delta\mu_P = \partial(\Delta G_{mix})/\partial\phi_P$) of a component is the same in both phases. Conditions for the binodal curve are:

$$\Delta(\mu_P)' = \Delta(\mu_P)'' \text{ and } \Delta(\mu_B)' = \Delta(\mu_B)'' \tag{2.20}$$

From (2.19), this gives

$$\begin{aligned} &\ln\phi'_P + \left(1-\frac{1}{r}\right)(1-\phi'_P) + \frac{m_P v_P(\delta_P-\delta_B)^2}{RT}(1-\phi'_P)^2 = \\ &\ln\phi''_P + \left(1-\frac{1}{r}\right)(1-\phi''_P) + \frac{m_P v_P(\delta_P-\delta_B)^2}{RT}(1-\phi''_P)^2 \end{aligned} \tag{2.21}$$

and

$$\begin{aligned} &\ln(1-\phi'_P) + \left(1-\frac{1}{r}\right)\phi'_P + \frac{m_B v_B(\delta_P-\delta_B)^2}{RT}\phi'^2_P = \\ &\ln\phi''_P + \left(1-\frac{1}{r}\right)(1-\phi''_P) + \frac{m_B v_B(\delta_P-\delta_B)^2}{RT}\phi''^2_P \end{aligned} \tag{2.22}$$

Where $r = \frac{m_B v_B}{m_P v_P}$. The superscripts ' and " refer to the separate phases.

The condition for the spinodal curve is:

$$\left(\frac{\partial \Delta\mu_P}{\partial \phi_B}\right)_{T,P} = 0 \tag{2.23}$$

From (2.19), this gives the expression for the spinodal curve:

$$T = \frac{2(\delta_P - \delta_B)^2}{R}\left[\frac{1}{\phi_P m_P v_P} + \frac{1}{(1-\phi_P) m_B v_B}\right]^{-1} \tag{2.24}$$

The critical conditions are:

$$\left(\partial^2 \Delta G_{mix} / \partial \phi_P^{\,2}\right)_{T,P} = \left(\partial^3 \Delta G_{mix} / \partial \phi_P^{\,3}\right)_{T,P} = 0 \tag{2.25}$$

From (2.19), the critical χ parameter of the system can be calculated as

$$\chi_c = \frac{v_0}{2}\left(\frac{1}{\sqrt{m_P v_P}} + \frac{1}{\sqrt{m_B v_B}}\right)^2$$

$$= \frac{\sqrt{v_P v_B}}{2}\left(\frac{1}{\sqrt{m_P v_P}} + \frac{1}{\sqrt{m_B v_B}}\right)^2 \tag{2.26}$$

with

$$\phi_{Pc} = \frac{(m_B v_B)^{1/2}}{(m_B v_B)^{1/2} + (m_P v_P)^{1/2}} \tag{2.27}$$

and $$\phi_{Bc} = \frac{(m_P v_P)^{1/2}}{(m_B v_B)^{1/2} + (m_P v_P)^{1/2}} \tag{2.28}$$

The subscript 'c' used in the ϕ's above stands for the critical compositions for each polymer. For a given blend system, ϕ_{Pc} and ϕ_{Bc} are only dependent on the weight average number of repeat units. The critical χ parameter, χ_c and the critical temperature, T_c can be related to each other through equation (2.18). According to this approach, as it can be

seen from the equations above, molecular weights of the two components are the only variables that can affect the phase behavior. In other words, if the molecular weights are given, the critical temperature, critical χ parameter as well as the whole phase diagram can be determined.

A phase diagram for systems with an UCST (upper critical solution temperature) is shown in Fig. 2.11. This phase behavior is usually seen in mixtures with positive enthalpies of mixing (systems with dispersive interactions only and without any specific interactions). On the other hand, mixtures that have negative enthalpies of mixing (systems with specific interactions) usually show an LCST (lower critical solution temperature) behavior in their phase diagrams.

Besides the one phase region, two more regions in the phase diagram can be defined from Fig. 2.11. The region between the spinodal and the binodal curves is called the metastable region. The region within the spinodal curves is called the unstable region. These two regions can be defined in a LCST phase diagram in the same manner.

Phase separation develops through two different processes. In the metastable region, phase separation involves nucleation and growth. A new and more stable phase is developed within the metastable one phase system. This nucleation process is an activated process and a finite undercooling below the binodal curve (for a UCST diagram) is needed for the phase separation to proceed.

On the other hand, phase separation in the unstable region involves a process called spinodal decomposition. The spinodal decomposition process originates with small amplitude composition fluctuations within the unstable region. These fluctuations con-

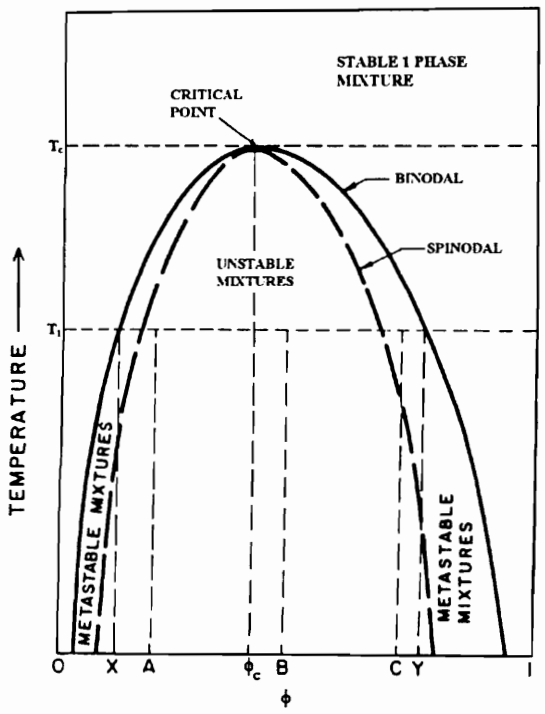

Fig. 2.11 Phase diagram of a polymer blend system exhibiting a UCST behavior.

tinue and eventually a two phase system develops. Spinodal decomposition is often characterized by a high interconnectivity in both phases. Moreover, spinodal decomposition does not require activation energy. It is only limited by diffusion process and occurs spontaneously.

The expression in (2.19) indicates that the solubility parameter approach will work for systems with positive enthalpies of mixing only. Hence, it can only predict UCST behavior in the phase diagram. This is apparently a significant limitation for polymer blend studies. However, the solubility parameter approach should still be useful for the poly(propylene)-poly(1-butene) blend. Since a positive enthalpy of mixing works against miscibility, the polymers will be miscible only when they have very similar solubility parameters and when the molecular weights of the components are not too high.

2.6.4 Group Contribution Method

The solubility parameter difference $\Delta\delta$ for the propylene and 1-butene repeat units can be calculated empirically by group contribution methods[122], where the solubility parameters are estimated by:

$$\delta = \frac{\sum F_i}{\sum v_i} \tag{2.29}$$

F_i and v_i are the molar attraction constant and molar volume of the chemical group in the polymer repeat unit, respectively.

This method is based on the additivity of the quantity $F_i = (E_i v_i)^{1/2}$. Where E_i is the cohesive energy of the chemical group. The summation is taken over the polymer repeat unit. F_i can be calculated by regression analysis for various common structural groups in low molecular weight compounds. Several tables of F_i values have been reported in the literature[123-125]. Group contribution methods have also been refined to accommodate the polar and hydrogen bonding interactions[126-128].

The drawback of this approach is the choice of the group contribution data set. The choice of molar attraction constants has a vital effect on the final result. Different authors use different experimental methods to obtain their data set. In practice, when δ is determined from this method, the F_i for different functional groups within the polymer repeat unit must be taken from the same table. Otherwise, erroneous value of δ may result. Even for polymer blend systems with weak or without any favorable intermolecular interactions, such as the poly(propylene)/poly(1-butene) blend in this study, the task of obtaining a reliable interaction parameter from the group contribution approach is difficult. Using this approach by no means verifies the validity of this method, but shows the agreement of this relatively simple approach and the experimental result from this study. The agreement between predicted and measured $\Delta\delta$ should be considered as incidental.

Moreover, it should be noted that the effect of tacticity is not included in this general approach. In many polymer blend systems, especially for those with specific interactions between the components, it has been shown that tacticity can play a significant role in the miscibility. The phase diagrams can shift by tens of degrees between polymer blends with various tacticities, given that the other parameters such as blend composition

and molecular weights remain unchanged. For example, for blends such as poly(vinyl methyl ether) (PVME)/polystyrene (PS)[129-132], poly(methyl methacrylate) (PMMA)/poly (vinyl chloride) (PVC)[133], and poly(methyl methacrylate) (PMMA)/poly(vinylidene fluoride) (PVF_2)[134], tacticity has been shown to have a significant effect on miscibility. In these systems, the specific interactions are very directional and their magnitude does depend on the respective tacticity of the interactive groups along the polymer chain. For polymer systems without strong interactions, tacticity effect on miscibility is less significant but can still change the miscibility behavior of the polymer blend system. Recently, Trask and Roland[135] reported in their study on blends of cis-1,4-poly(isoprene) (PIP) and atactic poly(vinyl ethylene) (PVE) an order of magnitude change in the interaction parameter when the PVE is syndiotactic. It suggests that the general prediction of critical temperatures for blends of isotactic materials from data on atactic polymers may be inaccurate. Similarly, miscibility in blends involving copolymers is expected to be dependent on the copolymer microstructure.

2.6.5 Measurement of the Flory-Huggins Interaction Parameter

The interaction parameter between two polymers can be obtained by various methods such as heat of mixing measurement, inverse gas chromatography, solvent vapor sorption, light, X-ray and neutron scattering experiments[136]. For semi-crystalline polymer systems, observation of a melting temperature depression for the highest melting component in the blend is also viewed as a good indication of miscibility. However, such

studies should be inspected with caution, as a depression in the observed melting temperature can also result from mere kinetic or morphological effects[137,138]. Establishing the miscible character of a semicrystalline polymer blend using the concept of melting point depression is only valid if the composition dependence of the equilibrium melting temperature is investigated through extrapolative techniques such as the Hoffman-Weeks or the Gibbs-Thomson methods[8]. The Flory-Huggins χ_{FH} interaction parameter can be obtained from melting point depression experiments by using the expression derived by Nishi and Wang[139]. Although this method is useful for systems with a moderate to large and negative χ_{FH}, Rim and Runt[138] correctly pointed out that it is fairly inaccurate for systems exhibiting a small χ_{FH}.

For miscible polymer blends, the expression of equilibrium melting temperature depression can be written as

$$\frac{1}{T_{mb}} - \frac{1}{T_m} = \frac{-Rv_c}{\Delta H_f^\circ v_a}\left[\frac{\ln(1-\phi_a)}{m_c} + \left(\frac{1}{m_c} - \frac{1}{m_a}\right)\phi_a\right] + \frac{-Rv_c}{\Delta H_f^\circ v_a}(\chi_{FH}\phi_a{}^2) \qquad (2.30)$$

with the individual symbols defined as follows:

T_m, T_{mb}: equilibrium melting temperatures for the pure homopolymer and for the homopolymer in the blend, respectively.

R: Universal gas constant

ΔH_f°: heat of fusion per mole of segment

v_a, v_c: molar volume of the repeat units

ϕ_a : volume fraction of amorphous component

m_a, m_c: degree of polymerization

Where the subscripts 'c' and 'a' represents the crystalline and amorphous components, respectively.

For high molecular weight polymers, equation (2.30) is often rewritten in a more common expression with the limit: m_a and $m_c \rightarrow \infty$.

$$\frac{1}{T_{mb}} - \frac{1}{T_m} = \frac{-Rv_c}{\Delta H_f^\circ v_a}(\chi_{FH}\phi_a^{\,2}) \qquad (2.31)$$

2.6.6 Methods for Evaluating Polymer Blend Miscibility

As mentioned at the beginning of this section, "miscibility" is a thermodynamic term. While various experimental methods are used to determine the miscibility of polymer blend systems, it should be noted that the length scales that can be resolved by the probes are different for different techniques. For example, small angle neutron scattering provides an atomic level resolution, while optical microscopy can barely resolve sub-micron details. While there are many experimental methods developed over the years to study the miscibility behavior of polymer blends, the following is only a brief summary for the common approaches. For details and references of these experimental techniques, the book written by Olabisi *et al.*[136] should be consulted.

- Glass transition temperature: It is one of the most common approaches for miscibility studies. It is a useful method when the components in the polymer blend system have different glass transition temperatures. If the components are totally immiscible, the polymer chains of each polymer are segregated with their own kind, thus retaining their own characteristic glass transition temperatures. Depending on the degree of

mixing, sometimes a broad glass transition temperature is observed for systems with marginal miscibility. For systems with partial miscibility, two separate glass transition temperatures may be observed between those of the two constituents. This is an indication of the existence of a component-1 rich phase and a component-2 rich phase in the system. For miscible blends, a single, composition dependent glass transition temperature is observed. Experimental techniques for this approach include thermal analysis (DSC), dynamic mechanical analysis (DMA), dielectric spectroscopy, etc. These techniques find limited usage in polymer systems with high crystallinity. In those systems, it is extremely difficult to keep the sample in the amorphous state without significant crystallization during quenching from the melt. As a result, the signal, which originates from the amorphous phase, can be very weak. Moreover, for polymer systems with close glass transition temperatures, it is often difficult to determine the miscibility of the system from glass transition temperature measurements. These limitations can be partially resolved by the method suggested by Jorda and Wilkes[140]. Their approach takes advantage of the physical aging process common to glassy polymers. Glassy polymers, when stored below their glass transition temperatures, in time will approach the equilibrium state. During the process, an enthalpic peak near the glass transition region can be registered by subsequent DSC heating scan. Using this "physical aging" approach, Jorda and Wilkes demonstrated that two separate enthalpic peaks correspond to the two phases in an immiscible polymer blend with similar glass transition temperatures can be clearly resolved.

- Optical microscopy: This method takes advantage on the fact that most polymers have different refractive indices. For an immiscible system, the phases can be distinguished from each other by optical microscopy. Usually, the effect can be enhanced by using phase contrast optics. The disadvantage of this technique is the phases must be large enough to be observed in the optical microscope and the difference in refractive indices of the two polymers must be sufficient.
- Scattering method: Different scattering techniques have been successfully applied to determine the miscibility of polymer blend systems. That includes: conventional light scattering (cloud point method), small angle light scattering (SALS), small angle X-ray scattering (SAXS) and neutron scattering. All these scattering methods rely on the existence of fluctuations in some fundamental properties within the systems. Light scattering relies on density and concentration fluctuations; X-ray scattering depends on electron density fluctuation; and neutron scattering depends on the fluctuation in the neutron scattering cross-section.
- Melting temperature depression method: As mentioned in section 2.6.5, melting temperature depression is often found in miscible, semi-crystalline polymer blends. This method is useful for systems with specific interactions, where significant melting temperature depression is expected. For systems with weak interactions, such as the poly(propylene)/poly(1-butene) blend in this study, the melting temperature depression may be so small that this method is not promising.

- Other experimental techniques, including nuclear magnetic resonance, viscosity measurements and others, will not be discussed in this text. Useful references on these approaches can be found in ref. 136.

2.7 Competition between Phase Separation and Crystallization

For polymer blend systems with one or more components being crystallizable, the phase behavior and, more specifically, the final morphology of the systems, are strongly influenced by the crystallization behavior of the crystallizable components. Moreover, phase separation in these systems also affects the crystallization process and other properties of the polymer blend systems.

The competition between the phase separation and crystallization processes in polymer blend systems will now be discussed. The situation can be comprehended more easily with the aid of a phase diagram. Depending on the relative position between the binodal curve, the spinodal curve and the melting curve in the phase diagram, the respective influences of the phase separation process on the crystallization behavior and vice-versa will be different. Schematic phase diagrams in Fig. 2.12 describe the different possible situations. As will become clear in chapter 4, the it-PP/it-P1B polymer blend system in this study has a situation that resembles that depicted in Fig. 2.12a and therefore it would be convenient to concentrate on this particular phase diagram in the following discussion.

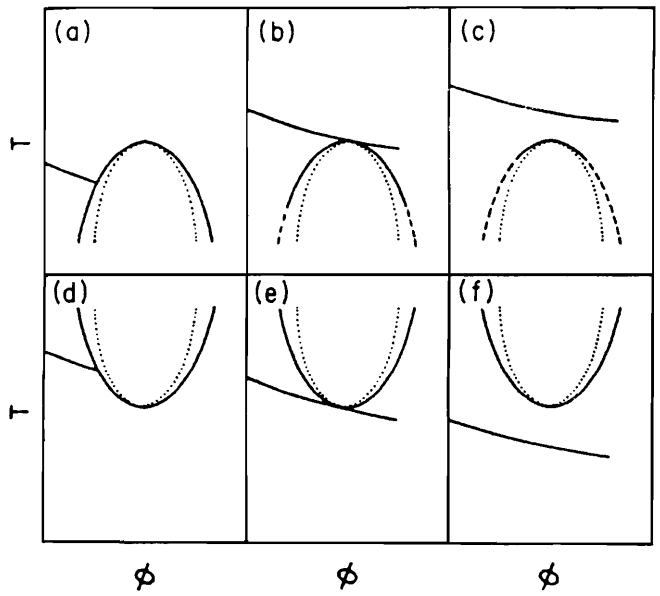

Fig. 2.12 Schematic phase diagrams for various kinds of polymer blend systems (adapted from ref. 141).

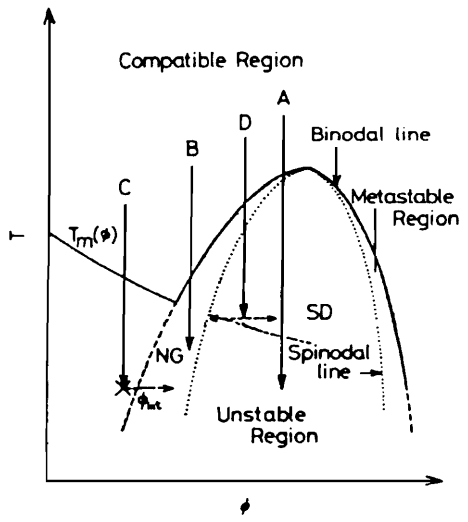

Fig. 2.13 Schematic phase diagram with the melting point curve $T_m(\phi)$ (adapted from ref. 142).

The situation of Fig. 2.12a is redrawn in Fig. 2.13, where a schematic phase diagram for a polymer blend system with a UCST behavior is shown. $T_m(\phi)$ is the melting point curve of the crystallizable component. Depending on the final temperature, the resulting morphology of the system is determined by the competition between the phase separation and the crystallization kinetics. Various quenching situations indicated by arrows A to D in Fig. 2.13 were described by Tanaka and Nishi[142]. For example, arrow A and B indicate two situations in which the quenching temperatures are within the unstable and metastable regions, respectively. The phase separation and crystallization processes take place simultaneously. The final morphology is determined by the relative rate of the two processes. Arrow C indicates a quenching into the miscible region. Crystallization starts within the one phase system. As crystallization continues, the composition of the system changes as one of the components is crystallized and removed from the melt. Eventually, crystallization induces phase separation. Arrow D indicates a situation in which the phase separation process induces crystallization. Since the final temperature is higher than the melting temperature $T_m(\phi)$ at that initial composition, no crystallization will occur at the beginning. The phase separation continues until a crystallizable-polymer-rich phase (with a melting temperature higher than the final temperature) is formed. At that point, crystallization can proceed.

Although phase diagrams can provide the information as how the two processes compete with each other, the final morphology of the system cannot be determined by thermodynamics alone. Supercooling, composition of the system and molecular weights determine the crystallization rate of the crystallizable component, whereas the phase

separation rate is governed by system viscosity (kinetic factor, limited by the reptation of the polymer chains) and the relative location within the metastable or unstable region of the phase diagram (thermodynamic factor).

2.8 Previous Studies of PP/P1B Blend

Miscibility Studies of it-PP/it-P1B mixtures have been reported in the literature for quite some time but have not provided a definite answer as to the conditions under which these mixtures are miscible at the molecular level in the liquid state[4,5,143-151]. Examination of the pertinent literature clearly demonstrates the controversial nature of this subject. For example, Boor and Mitchell[143], on the basis of dilatometric data, reported that when small amounts of isotactic poly(propylene) are added to isotactic poly(1-butene), the rate of crystallization for the latter is significantly increased but that this behavior is not highly reproducible, thereby suggesting the difficulty in obtaining a truly homogeneous mixture of the two polymers. Piloz and Decroix[144] using dynamic mechanical analysis and dilatometry inferred from the observed variation in the glass transition temperature with blend composition that the mixture is "compatible". Berticat *et al.*[145] using differential scanning calorimetry (DSC), thermal mechanical analysis (TMA), and dilatometry suggested these blends to be incompatible. However, it should be noted that their conclusion was not based on an unambiguous observation of two distinct glass transition temperatures but on a statistical analysis of their data which favored a two-phase model. Siegmann[4,5] observed a depression in the observed melting temperature and in the

crystallization rate of the it-PP component with added P1B, a crystallinity in each component that is lower than that expected on the basis of the linear rule of mixtures and morphological variations of the it-PP spherulites with small amounts of the it-P1B component. From these observations, he concluded that the poly(1-butene) acts as a miscible diluent which is rejected from the it-PP spherulites during crystallization and that the two components are highly compatible in their amorphous phase, Gohil and Petermann[146] using transmission electron microscopy and differential scanning calorimetry suggest the blends to be miscible for it-PP content larger than 80% or less than 20% and immiscible in the intermediate composition range. They also confirmed Siegmann's observation of a melting temperature depression for the it-PP component in blends containing less than 30% P1B and observed a complex melting behavior for it-PP in blends containing larger than 30% P1B. Finally, Hsu and Geil[147] studied the glass transition, crystallization and melting behavior, and the morphology of it-PP /it-P1B blends prepared by a combination of compression molding at 235 °C and quenching either in air or with isopentane. While some of their specific conclusions, such as the invariance of the it-PP melting point with changes in blend composition and the observation of two separate glass transition temperatures in ultra-quenched blend samples, differ from those of Siegmann's work, they concluded that "there is a considerable degree of compatibility, possibly even miscibility, of it-PP and it-P1B in the melt but that miscibility is difficult to obtain by ordinary melt mixing processes".

Physical properties of polymer blends depend markedly on the crystalline morphology and the level of phase segregation that results from crystallization and

potential phase separation processes. The variation of mechanical properties with blend composition has been used in the past to characterize the level of compatibility in polymer blends[148]. However, mechanical compatibility and molecular-level miscibility must be clearly differentiated. As pointed out by Hsu and Geil[147], low-strain properties such as the modulus are unable to differentiate compatible blends from miscible ones. The composition dependence of large-strain properties such as the elongation at break or the toughness may be more significantly related to the molecular-level homogeneity of a given material. Siegmann[4,5] and Hsu *et al.*[147] showed that it-PP/it-P1B blends exhibit a linear variation of the modulus and yield strength with blend composition but a nonlinear variation of tensile strength and ultimate and yield strength with blend composition. It was suggested that the efficient stress transfer between the two components of a compatible blend arises from a good adhesion between their amorphous phases. As will be apparent in chapter 4, a different point of view will be suggested to account for the mechanical properties of these polyolefin blends that will be based on consideration of phase mixing and in the observation of competing phase separation and crystallization processes. Noting that many of the previous investigations of the state of miscibility in these blends relied either on room temperature measurements or on analyses carried out on samples that had been crystallized under non-isothermal conditions and were subsequently heated during the analysis, the state of miscibility of this blend in the liquid state prior to crystallization will be investigated, followed by the study of the influence of crystallization of the poly(propylene) component on the extent of liquid-liquid demixing.

3. PROPYLENE-ETHYLENE COPOLYMERS

3.1 Materials

Two sets of propylene-ethylene copolymers were used in this study. The first copolymer (labeled ER) has a 4.5 mol% ethylene content. The second set of copolymers consists of six different grades labeled by the manufacturers as DX6E62, DS6D20, DS6D81, PP9122, PD9012E1 and PD9282E2. They will be relabeled as the P-series samples according to their ethylene content determined from ^{13}C NMR experiments. Melt flow rates (MFR) of the P-series samples provided by the manufacturer are shown in Table 3.1.

Melt flow rate is a measure of relative polymer melt viscosity (ASTM D1238-85). It is defined as the weight of polymer that flows in 10 min through a die of specified length and diameter under constant temperature and load. In general, samples with higher molecular weight exhibit lower MFR values. However, the MFR values are affected by the physical dimension of the die, the measurement temperature, etc.

Table 3.1 Melt flow rate (MFR) of the P-series propylene-ethylene copolymers

Grade	New designation	MFR*
DX6E62	P1	3.0
PP9122	P2	2.0
PD9012E1	P3	6.0
DS6D20	P4	1.9
DS6D81	P5	4.0
PD9282E2	P6	5.0

* Data provided by manufacturers. Conditions for the measurement not available.

3.2 Experimental Procedures

3.2.1 Fractionation (Solution Crystallization)

To study the effect of ethylene content on the crystallization and polymorphic behavior of propylene-ethylene copolymers, fractions of the copolymer with different ethylene contents were obtained by fractionating the bulk materials by solution crystallization. The procedure employed here is similar to the one reported by Alamo *et al.*[152], though a lower solution concentration was used in their case. It has been reported that this procedure preferentially fractionates according to microstructure of the polymer chains rather than molecular weight. For example, Nandi and Mandelkern used this procedure to obtain PVF_2 fractions with different head-to-head concentrations[153].

Since the fractionation process can take days, it is important to remove any trace amount of oxygen from the solution in order to prevent oxidative degradation of the polymer samples. A pre-weighed copolymer sample and *p*-xylene for a 2% (w/v) solution were placed on the same side of a fractionation tube for degassing under vacuum. The design of the glass fractionation tube is shown in Fig. 3.1. The fritted-glass filter in the middle had a pore size of 10 μm. The tube was sealed under vacuum to prevent degradation during the fractionation process. The polymer sample was then dissolved at 120 °C to form a homogeneous solution. The tube was then quickly transferred into a silicon oil bath set at the crystallization temperature. The bath temperature is controlled to within ±0.05 °C. After remaining at the crystallization temperature for 4 to 7 days, the

tube was inverted to separate the crystals from the solution through the filter. Depending on the crystallization temperature, the exact time for crystallization varied from 7 days for the highest crystallization temperatures to no less than 4 days for the lowest crystallization temperatures. Then, the crystals and the solution were collected by breaking the tube. The fraction remaining soluble at the crystallization temperature was further precipitated by adding an excess amount of acetone at room temperature. This resulting fraction was then recovered by filtering and dried under vacuum. The insoluble fraction formed under isothermal treatment is also dried under vacuum. Further fractionation was repeated for the soluble fraction at a lower temperature.

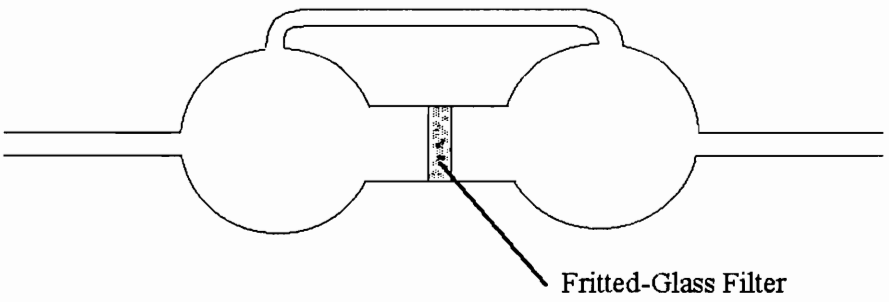

Fig. 3.1 Design of the fractionation tube

3.2.2 ^{13}C NMR

Ethylene content and triad distribution for the bulk sample and for each fraction obtained from the fractionation were determined by ^{13}C NMR experiments. The samples were dissolved in *o*-dichlorobenzene to make a 10% (w/v) solution. A coaxial glass tube, 2 mm in outer diameter and sealed with dimethyl sulfoxide (DMSO), was placed at the center of the 10 mm NMR tube. DMSO in the smaller glass tube provides the lock signal for the NMR experiment. The experiment was conducted on a 400 MHz Varian FT-NMR instrument at 110 °C with a frequency of 100.577 MHz under proton-decoupling condition. It should be noted that the pulse spacing should be five times the spin-lattice relaxation time (T_1) to ensure 99% relaxation. Considering the fact that the T_1 values for the methyl, methine and methylene carbons are 2.1, 1.5 and 0.7 sec, respectively (in both 1,2,4-trichlorobenzene and *o*-dichlorobenzene at 120 °C)[154,155], the data acquisition time and relaxation time in all the ^{13}C NMR experiments were chosen at 1.2 and 8.8 sec, respectively. About 1000 repetitions for each sample were used to improve the overall signal to noise ratio.

The ethylene content in each sample is calculated from the following:

$$\text{ethylene content} = [E]/([E] + [P]) \tag{3.1}$$

where [P] and [E] are the concentrations of the propylene and ethylene units, respectively and are given by the Bovey relationships[156]:

$$[P] = [PP] + \tfrac{1}{2}[EP] \text{ and} \tag{3.2}$$

$$[E] = [EE] + \tfrac{1}{2}[EP] \tag{3.3}$$

where the above dyad concentrations are given by the equations:

$$[PP] = I_{\alpha\alpha} \tag{3.4}$$

$$[PE] = I_{\alpha\gamma} + I_{\alpha\delta} \tag{3.5}$$

$$[EE] = \tfrac{1}{2}(I_{\beta\delta} + I_{\delta\delta}) + \tfrac{1}{4}I_{\gamma\delta} \tag{3.6}$$

The peak assignments and notations in equations (3.4) to (3.6) were given in Randall's review paper[109].

Triad distributions were determined by using the triad sequence assignments given by Randall and Hsieh[106]. First, peak areas of each of the eight regions [region A, 45-48 ppm; region B, 30-20 ppm; region C, 33.3 ppm; region D, 29.5-31.5 ppm; region E, 28-29.5 ppm; region F, 27-28 ppm; region G, 24-25 ppm; region H, 19-22 ppm] were calculated. Then, the triad concentrations in the copolymer were obtained from the following equations:

$$[PPP] = T_E \tag{3.7}$$

$$[PPE] = 2(T_A - T_E) \tag{3.8}$$

$$[PEP] = T_G \tag{3.9}$$

$$[EPE] = T_C \tag{3.10}$$

$$[PEE] = T_F \tag{3.11}$$

$$[EEE] = \tfrac{1}{2}(T_C + T_D + T_E - \tfrac{1}{2}T_F - T_H) \tag{3.12}$$

The T_i's in equations (3.7) to (3.12) are the total areas under the peaks in the corresponding regions. The concentration of each triad can then be obtained after normalization of the total concentration to one.

3.2.3 Intrinsic Viscosity Measurements

3.2.3.1 Background

Molecular weight of a polymer sample is related to its intrinsic viscosity [η] with the Mark-Houwink equation:

$$[\eta] = KM_v^a \tag{3.13}$$

K and a are the Mark-Houwink coefficients and the values of both constants are dependent on the solvent and temperature used in the measurement.

Intrinsic viscosity of the polymer solution can be determined as follows.

- The elution time of the polymer solution (t) at various concentrations as well as that of the pure solvent (t_o) is determined.
- From the elution time, the corresponding reduced viscosity η_{red} and inherent viscosity η_{inh}, defined in equation (3.14) and (3.15), are calculated.

$$\eta_{red} = (1/c)(\eta/\eta_o - 1) \approx (1/c)(t/t_o - 1) \tag{3.14}$$

$$\eta_{inh} = 1/c\ ln(\eta/\eta_o) \approx 1/c\ ln(t/t_o) \tag{3.15}$$

- [η] is determined from the y intercepts by extrapolating the η_{red} vs. c plot and the η_{inh} vs. c plot to zero concentration.

(To minimize the need to apply correction for kinetic effects, usually the elution time is kept longer than 100 sec. This can be achieved by a choosing viscometer with a suitable capillary diameter.)

3.2.3.2 Experimental Procedure

Intrinsic viscosity of the copolymer samples was measured using an Ubbelohde-type viscometer. The measurements were carried out in *p*-xylene at 85 °C. The Mark-Houwink coefficients K and a are 0.096 ml/g and 0.63, respectively[157]. The whole setup was placed in a silicon oil bath with the temperature controlled to within ±0.05 °C. A pre-weighed sample of about 55 mg was dissolved in 6 ml *p*-xylene and transferred into the viscometer. After the temperature of the system was equilibrated, the elution time of the solution was measured and averaged. After the elution time of the solution at the first concentration was measured, additional solvent was injected into the viscometer with a syringe. The weight difference of the syringe before and after injecting the solvent into the viscometer was measured with an electronic balance to obtained the total weight of solvent added. To improve the accuracy of the final results, elution times were measured at five different concentrations. The volumes of solution used in the measurements are about 6 ml and 25 ml for the most concentrated and the most diluted solution, respectively. The elution time of the solution ranges from 100 sec to 200 sec. t/t_o varies from 1.2 for the most diluted to 1.7 for the most concentrated solution.

3.2.4 Wide Angle X-Ray Diffraction (WAXD)

Samples for the wide angle X-ray diffraction studies were crystallized between two cover slips in a Linkam THM 600 hot stage operated under dry nitrogen purge. They were kept in the melt at 200 °C for 5 min followed by isothermal crystallization at various crystallization temperatures for 1 to 48 hours. Different crystallization times were used to maximize the crystallinity for each sample. The samples so prepared were about 300 μm in thickness. The wide angle X-ray diffraction (WAXD) patterns were collected at room temperature with a Scintag powder diffractrometer model XDS 2000 with a nickel filtered Cu Kα radiation of an X-ray source operated at 45 kV and 25 mA. The patterns were acquired from $2\theta = 10°$ to 30° with a step size of 0.01 degree and a scan rate of 0.5 degree per minute. They were then analyzed with the Scintag DMS 2000 analysis software.

γ-form content (w.r.t. total crystallinity) of each sample was determined from the heights of the (117) Bragg peak of the γ form and the (130) Bragg peak of the α-form according to the method of Turner-Jones[89].

It should be pointed out here that changes in the profile of the amorphous halo were observed for samples having different ethylene contents. As a result, the absolute crystallinity estimation was not conducted from the WAXD data.

3.2.5 Thermal Analysis

For thermal analysis, a Perkin-Elmer differential scanning calorimeter model DSC2 was used. The calorimeter was interfaced to a PC compatible computer through a PE

Nelson 950 Intelligent Analog to Digital Interface. The data were acquired and analyzed using the MC^2 Thermal System software. Two types of thermal analysis experiments were conducted. In the first set of experiments, the samples were crystallized isothermally after melting for 3 min at 200 °C. The heating curves were then recorded by scanning from the crystallization temperature. In the second set of experiments, the samples were dynamically cooled from the melt to room temperature and then reheated to 200 °C. All heating and cooling scans were conducted at a rate of 10 °C/ min. From the recorded dynamic cooling curves, the temperature at maximum crystallization rate T_{cmax} for each fraction was obtained.

The overall crystallinity in each fraction was determined from the area under the endotherms in the DSC scans during heating. The samples were crystallized isothermally for 6 to 8 hours at temperatures 20 degrees above the temperature of maximum crystallization rate T_{cmax} which was determined in the dynamic cooling crystallization study. In the crystallinity calculations, it was assumed that the heat of fusion of the γ-form crystals is the same as that of the α-form. To the best of my knowledge, the heat of fusion of the it-PP γ-form has not been documented in the literature. The latter approximation can be justified by considering the packing energy calculations carried out for the α- and γ-forms by Ferro *et al.*[158] Their calculations showed that the packing energy difference between these two crystal phases is not significantly different (0.05 kcal/mol for space groups without statistical up-down disorder and 0.11 kcal/mol for space groups with statistical up-down disorder). It is also interesting to note that in the above calculation the total packing energy for γ-form crystals is slightly lower.

Hoffman-Weeks analysis

Equilibrium melting temperatures of the α-form in each of these fractions were determined by the Hoffman-Weeks analysis. Samples were crystallized isothermally until a 10% total crystallinity is obtained. (When calculating the total crystallinity, both the α- and γ-form endothermic melting peaks were included and the heat of fusion for each phase were assumed to be the same.) Heat of fusion for 100% crystallinity was taken as 35.2 cal/g), the value for it-PP homopolymer[159]. The choice of this value is incidental since the reported values of ΔH_f for it-PP cover a wide range (15-62 cal/g)[160] and the best value of ΔH_f has been argued. The "observed" melting temperature of α-form crystals was determined from the endothermic maximum. To construct the Hoffman-Weeks plot, the melting temperature T_m' is plotted against the corresponding crystallization temperature T_x. The equilibrium melting temperature T_m is determined as the intercept between the extrapolation of this line and the $T_m' = T_x$ line.

3.2.6 Small Angle X-Ray Scattering (SAXS)

3.2.6.1 Background

Small angle X-ray scattering as a morphological probe has been used for investigating structures with size ranging from 50 to 1000 Å. The Bragg relationship

$$n\lambda = 2d \sin\theta \qquad (3.16)$$

also applies to SAXS for periodic morphologies. In equation (3.16), n represents the order of the scattering, λ the wavelength of the X-ray being used, d the periodic distance

of interest and θ the Bragg scattering angle. If Cu Kα radiation (λ = 1.54178 Å) is used and only the first-order scattering is considered, it can be seen from equation (3.16) that the scattering angle would be very small for structures with dimensions ranging from 50 to 1000 Å. Applications of SAXS include proteins, inorganic substances, polymer solutions and solid state polymers.

While the theory of small angle X-ray scattering is not to be discussed in the following, there are a few things that should be mentioned. Firstly, the "contrast" of the scattering in semi-crystalline polymers comes from the electron density difference between the amorphous phase and the crystal phase[161]. Secondly, for optimum scattering signal, the sample thickness should be equal to $1/\mu$, where μ is the linear absorption coefficient of the sample[162]. For poly(propylene) samples, the optimum thickness is about 3 mm.

The analysis to be used in the following is based on the ideal two phase model. It assumes that the structure can adequately be described by assuming the electron density variations to occur in one coordinate direction only. At the end, the long period L of the sample, defined as the sum of the lamellar thickness l_c and the amorphous phase thickness l_a, can be determined. In this model, the structure consists of alternate crystalline phase (the lamellae) and amorphous phase, which are organized in stacks. The dimension of the stacks can be assumed to be large enough so that it does not affect the small angle scattering. It should be noted, however, there are several assumptions in this model. This model assumes that there are only the crystal phase and the amorphous phase in the sample. Moreover, this model assumes uniform density distribution within each phase. In this simplest case, the possibility of crystallinity distribution within the sample, which

includes the variation in the thickness of amorphous inter-lamellar regions, and existence of large inter-spherulitic and inter-fibrillar regions, is neglected. Finally, this simplified model works best on systems with moderate to high crystallinities and the propylene-ethylene copolymer in this study falls into this category.

3.2.6.2 Experimental Procedure

The variation in the long spacing as a function of crystallization temperature for copolymer samples with different ethylene contents was studied by small angle X-ray scattering. Polymer samples were crystallized in a crystallization chamber. The design of the main component of the crystallization chamber--the heating block is shown in Fig. 3.2. The chamber was purged with dry nitrogen gas and the temperature of the heating block was controlled to within ±0.1 °C. Each sample was contained in a stainless steel mold (25 mm × 8 mm × 3 mm) and melted on a hot plate at 200 °C for 5 minutes. (The surface temperature of the hot plate was monitored using a surface thermometer). The mold was then transferred to the crystallization chamber. Three different crystallization temperatures were used: 95, 110 and 120 °C. In order to obtain maximum crystallinity, these samples were kept at their crystallization temperatures for 12 hrs, 24 hrs and 7 days, respectively. Another set of samples were prepared by air-quenching in the stainless steel mold upon removal from the hot plate after 5 minutes at 200 °C. WAXD experiments were also conducted in all these samples with the same experimental procedures described in section 3.2.4.

Since the amount of samples obtained from the fractionation were not sufficient for the SAXS experiment, another set of propylene-ethylene copolymer samples with ethylene content from 0.2 to 6.1 % (wt%), were used in this set of experiment. These samples were called the P-series. As to be reported in the result and discussion session, the microstructure and the other properties such as polymorphism, crystallization and melting behaviors of these samples are similar to those of the fractionated samples with similar ethylene content.

SAXS measurements were conducted at room temperature in a Kratky camera (Anton Paar KG, model A-8054) with a nickel filtered Cu Kα X-ray source operating at 50 kV and 30 mA. The camera was aligned with a 3° take-off angle. Slit width and slit length used in the experiments were 80 μm and 15 mm, respectively. Data were collected with a M. Braun position sensitive proportional counter (model OED-50m) and the Canberra system 100 MCA hardware and software package. Data acquisition time in these experiments were 15 min. Background scattering profile for each sample was collected by putting the sample in between the X-ray tube tower and the entrance of the camera. In the desmearing process, the intensity profile of the X-ray beam along the slit length direction is required. This beam profile is recorded by rotating the detector by 90 degree from its horizontal position.

The computer program--HMSAXS used in data analysis was developed by Dr. Hervé Marand. It includes background scattering subtraction, smoothing, desmearing (along the slit length direction), and Lorentz correction. The program uses an iterative method developed by Glatter[163] for the desmearing. The long spacing of each sample is

calculated from the position of the scattering maximum using lead stearate as a calibration standard.

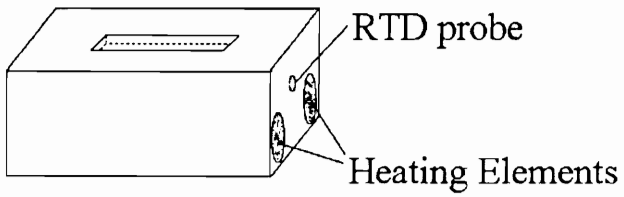

Fig. 3.2 Design of the heating block for the crystallization chamber

3.3 Results and Discussion

3.3.1 Fractionation

From ER (the first copolymer sample), nine fractions were obtained through two separate series of fractionation experiments. The difference between the two series came from the choice of different initial solution concentrations (2.5 % in fractionation series I vs. 2.0 % in fractionation series II) and different fractionation temperatures. The fractionation temperatures used in series I are: 79.5 °C, 75 °C and 61 °C. The fractionation temperatures used in series II are: 75.5 °C, 70 °C, 56 °C and 53 °C. Since no attempt will be made to present separate analysis of the fractions obtained from these two series, they were labeled in the order of increasing ethylene contents according to the results of the ^{13}C NMR analysis as E1 to E9. For reference, Table 3.2 lists the corresponding fractionation series for each fraction.

Fractionation was also carried out on the P-series propylene-ethylene copolymers. According to their ethylene contents obtained from ^{13}C NMR analysis (see section 3.3.2), these bulk samples were labeled in the order of increasing ethylene content as P1 to P6, respectively. Fractions of each of these samples were labeled as P1-A, P1-B, etc. The weight percents of each fraction for the P-series samples and the temperatures used for the fractionation procedures were given in Table 3.3.

Table 3.2 Fractionation series for the sample ER

Fractions	Series	wt %*
E1	II	33.2
E2	I	32.8
E3	II	13.6
E4	I	11.9
E5	II	20.1
E6	I	29.8
E7	II	12.5
E8	I	17.2
E9	II	11.3

(mass loss in fractionation series I: 8.3%; mass loss in fractionation series II: 9.3%)

* Numbers in the third column are wt% of the fractions w.r.t. their own series.

Table 3.3 Results of fractionation for the P-series copolymers

Samples	Fraction	% in Weight	T_X's (°C)
P1	A	65.5	77
	B	5.8	74
	C	20.0	68
	D	3.5	
	loss	5.2	
P2	A	19.0	74
	B	79.7	
	loss	1.3	
P3	A	28.0	71
	B	47.0	69
	C	20.5	
	loss	4.5	
P4	A	41.8	76
	B	30.0	74
	C	9.3	68
	D	13.5	
	loss	5.4	
P5	A	2.3	74
	B	31.4	71
	C	11.6	68
	D	50.4	
	loss	4.3	
P6	A	14.0	68
	B	21.1	65
	C	59.0	
	loss	5.8	

3.3.2 Sample Characterization

A typical ^{13}C NMR spectrum of the propylene-ethylene copolymer used in this study is shown in Fig. 3.3. Ethylene contents for the bulk material (ER) and its fractions (E1 to E9) are shown in Table 3.4. Ethylene contents for the P-series samples are shown in Table 3.5.

Triad concentrations for the bulk material (ER) and its fractions (E1 to E9) are shown in Table 3.6. Triad concentrations for the P-series samples are shown in Table 3.7. Tables of triad concentrations for fractions of the P-series samples are shown in Appendix. A three dimensional plot of the triad concentration for the fractions of sample P4 is also presented in Fig. 3.4.

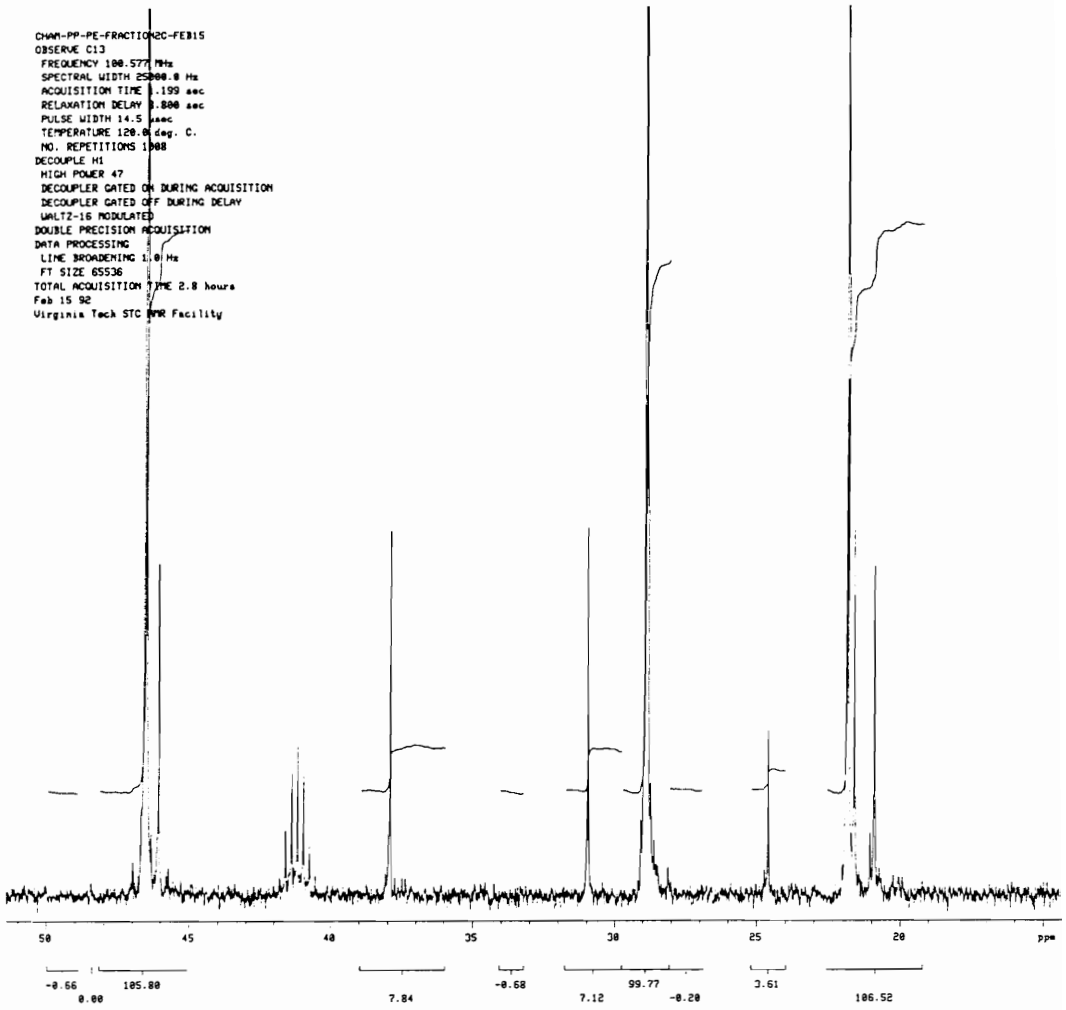

Fig. 3.3 A typical NMR spectrum of propylene-ethylene copolymer

Table 3.4 Ethylene content of the propylene-ethylene copolymer fractions

	ethylene content (mole %)	ethylene content (wt %)
ER	4.5	3.0
E1	1.6	1.1
E2	1.6	1.1
E3	3.0	2.0
E4	3.4	2.3
E5	4.0	2.7
E6	4.2	2.8
E7	7.0	4.8
E8	8.8	6.1
E9	11.0	7.6

Table 3.5 Ethylene content of the P-series propylene-ethylene copolymers

	% ethylene (wt%)	% ethylene (mol%)
P1	0.2	0.3
P2	1.9	2.8
P3	2.7	4.0
P4	2.7	4.0
P5	4.9	7.1
P6	6.1	8.9

Table 3.6 Triad concentration for the propylene-ethylene copolymer fractions

	Triad concentration (%)					
	[PPP]	[PPE]	[PEP]	[PEE]	[EPE]	[EEE]
ER (bulk)	83.5	11.7	4.0	0.5	0.0	0.4
E1	93.8	4.5	1.6	0.0	0.0	0.0
E2	87.4	10.4	1.2	0.0	0.0	1.0
E3	88.9	8.7	1.5	0.8	0.0	0.0
E4	86.3	10.4	3.1	0.0	0.0	0.2
E5	83.9	12.5	3.1	0.5	0.0	0.0
E6	83.4	12.8	3.4	0.4	0.0	0.0
E7	77.7	15.2	4.8	1.2	0.6	0.4
E8	71.7	18.8	6.2	1.2	1.0	1.1
E9	68.7	19.4	7.6	1.5	1.6	1.2

Table 3.7 Triad concentration of the P-series propylene-ethylene copolymers

	Triad concentration (%)					
	[PPP]	[PPE]	[PEP]	[PEE]	[EPE]	[EEE]
P1	94.2	3.9	1.0	0.0	0.0	0.9
P2	88.4	7.4	2.5	0.2	0.0	1.4
P3	86.2	8.3	3.0	0.3	0.0	2.2
P4	88.7	5.7	2.4	0.8	1.0	1.5
P5	80.2	12.6	4.4	1.2	0.8	0.8
P6	75.7	15.5	4.9	1.9	1.2	0.8

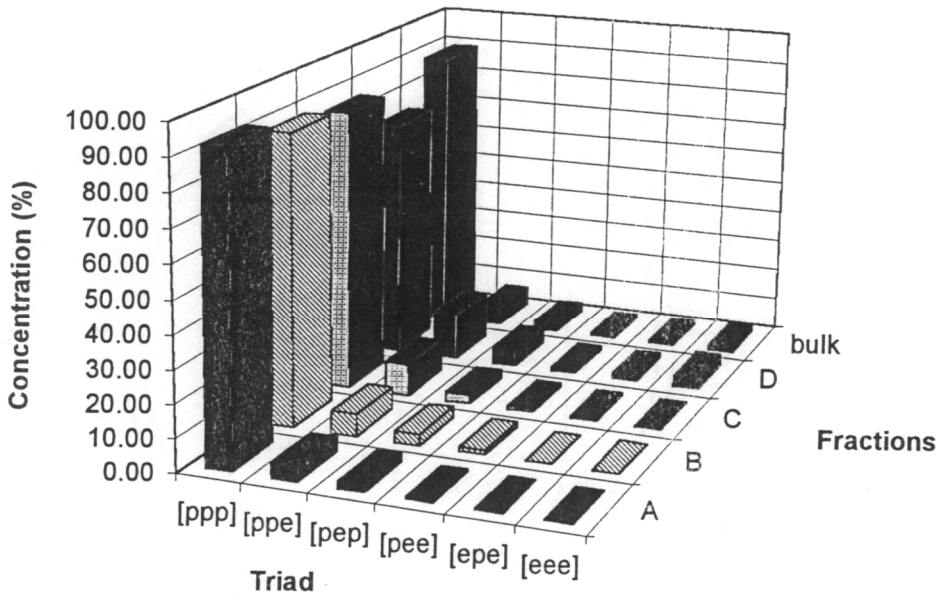

Fig. 3.4 Triad concentrations for fractions of sample P4

As can be seen in Table 3.4, starting with the bulk material with 4.5 mol% ethylene content, fractions with ethylene content ranging from 1.6% to 11.3% were obtained. As mentioned at the beginning of this section, these 9 fractions were obtained separately in two fractionation series. It should be noted that there was a slight difference in the solution concentration as well as the crystallization temperatures used in these two series. However, as long as the fractions were characterized by their ethylene content and microstructure (triad distribution) from the C^{13} NMR data, no attempt was made to distinguish the fractions between the two fractionation series. Moreover, it will become more evident that the ethylene content is the most important factor affecting the crystallization behavior and the polymorphism in the propylene-ethylene copolymer system under this study.

From Table 3.6, the highest [EEE] triad concentration in all the fractions is 1.2%, i.e. in fraction E9. Thus, there is no significant amount of ethylene block in the copolymer fractions. Moreover, the lack of ethylene block can be visualized by calculating the number-average sequence length of the ethylene co-units. According to Randall[164], for copolymer systems capable of containing inverted monomer units, which is the case for the propylene-ethylene copolymer system, the number-average sequence length of un-interrupted methylene carbons would be a better representation of the real situation. In terms of ethylene and propylene contents, the number-average sequence length of un-interrupted methylene carbons is given by[164]:

$$n_o = 1 + 2[E]/[P] \qquad (3.17)$$

Even for E9, the fraction with the highest ethylene content (11.0%), n_o is only 1.25 as calculated from equation (3.17). Therefore, when the crystallization behavior is discussed in the following sections, the possible crystallization of the "ethylene blocks" can therefore be neglected.

Although it has been shown from the triad distribution and the value of n_o that the existence of ethylene block is negligible even for the fraction with the highest ethylene content, it would be of interest to use a single parameter to describe the randomness of the copolymer microstructure. The randomness parameter χ_R, as defined in equation (3.18), is used as a measure for randomness in the sequence distribution of the copolymer repeat units[165].

$$\chi_R = \frac{P_2(PE)}{P_1(P)P_1(E)}$$

$$= \frac{[PE]}{2[P][E]} \qquad (3.18)$$

Since for a completely random process

$$P_2(PE) = P_1(P)P_1(E) \qquad (3.19)$$

values of χ_R correspond to different situations can be deduced and are listed in Table 3.8:

Table 3.8 Values for the randomness parameter χ_R for various types of copolymerization reactions (adapted from ref. 165)

Randomness parameter	
$\chi_R = 1$	random statistics
$\chi_R > 1$	more alternating tendency process
$\chi_R < 1$	more block character
$\chi_R = 2$	completely alternating
$\chi_R = 0$	completely block

Table 3.9 shows the values of χ_R for the copolymer fractions. The uncertainties shown in Table 3.9 for each fraction were calculated by error estimation under the assumption: $\Delta[PE] = \Delta[P] = \Delta[E] = 0.001$. It can be seen that there is no significant change in χ_R among these fractions. The unusually low χ_R value for fraction E3 is caused by a lower signal to noise ratio for that particular sample run. A larger uncertainty is assigned to it. As the average value of χ_R equals 0.943, the microstructure distribution of the copolymer fractions is not strictly "random" as compared with the "ideal" case. Such departure from the Bernoullian distribution (more block character) is typical for $TiCl_3$ based Ziegler-Natta catalysts[166]. However, since the [EEE] triad concentration remains extremely low in all the fractions and the departure from the true "random" distribution is slight, the term "random copolymer" will still be used throughout the text.

Similarly, the values of χ_R for the P-series copolymers are shown in Table 3.10. There seems to be an increased block character as the ethylene content increases. The extremely large uncertainty for the χ_R of P1 is due to the low ethylene content of this sample (0.3 mol%). Again, in view of the overall low ethylene content in these copolymers, the block character for this case will not be an issue. Though not shown here, comparable χ_R values were also obtained for fractions prepared from these samples.

Table 3.9 χ_R for various copolymer fractions

Fractions	χ_R
ER	0.94±0.02
E1	1.02±0.07
E2	1.02±0.07
E3	0.75±0.10
E4	1.04±0.03
E5	0.92±0.03
E6	0.94±0.02
E7	0.88±0.01
E8	0.95±0.01
E9	0.97±0.01

Table 3.10 χ_R for the P-series copolymers

Samples	χ_R
P1	1.00±0.38
P2	0.95±0.04
P3	0.95±0.03
P4	0.83±0.02
P5	0.89±0.01
P6	0.86±0.01

The results of intrinsic viscosity measurements and the resulting calculated molecular weights for the bulk sample ER and its fractions are shown for each fraction in Table 3.11. The viscosity average molecular weight M_v varied between 40,000 to 98,700 g/mol. In fact, except for fraction E9, there was only a slight variation in molecular weight among the fractions. Compared with the 7-fold change in ethylene content, the molecular weight effect should be less significant for the crystallization behavior and polymorphism of the system. Therefore, in the following discussion about the crystallization and polymorphism of the copolymer, it is safe to concentrate on the ethylene content effect. As a side note, the extremely low molecular weight of fraction E9 was expected since E9 is the last fraction of the fractionation process.

Table 3.11 Intrinsic Viscosity and Molecular Weight of the fractions of propylene-ethylene copolymer

Fractions	[η] (dL/g)	M_v (g/mol)
ER	1.203	82,700
E1	1.136	75,600
E2	1.147	76,600
E3	1.114	73,200
E4	1.345	98,700
E5	0.914	53,400
E6	1.194	81,800
E7	1.298	93,300
E8	–	–
E9	0.761	40,000

(–: data not available)

3.3.3 γ-Phase Content

A typical WAXD pattern of the propylene-ethylene copolymer is shown in Fig. 3.5. Compared with the diffraction patterns in Fig. 2.7 and Fig. 2.9, it is clear that the WAXD pattern of the copolymer is a combination of those of the α- and γ-form. A mixture of α and γ it-PP crystal phase structure was found in the fractions as well as in the bulk samples. Similar observations were also found in the P-series samples prepared for the SAXS study (see section 3.2.6). There was no detectable it-PP β-form crystal in any of these crystallized samples. As mentioned in section 2.3.2, α_1 and α_2 structures were reported to co-exist in propylene-ethylene copolymers. Due to the difficulties for quantitative studies of these two structures, there was no attempt here to investigate the α_1 and α_2 forms in these samples.

The presence of γ-form crystals can be confirmed with the (117) Bragg peak of the γ-phase in the diffractograms. Analysis of the diffractograms recorded from samples crystallized isothermally at different temperatures shown in Fig. 3.6 and Fig. 3.7 indicates that the γ-phase content not only increases with ethylene content as reported by Turner-Jones[89], but also with crystallization temperature. Note that there is a Bragg reflection developing at $2\theta \approx 15°$ in both Fig. 3.6 and Fig. 3.7 along with the development of the (117) Bragg peak of the γ-phase. A comparison with Fig. 2.9 shows that this is the (113) Bragg peak of the γ-phase. The result of the WAXD study for the P-series is summarized quantitatively in Table 3.12 and Fig. 3.8, which show the γ-form content for the P-series samples at various crystallization temperatures. Similarly, the result of the WAXD study

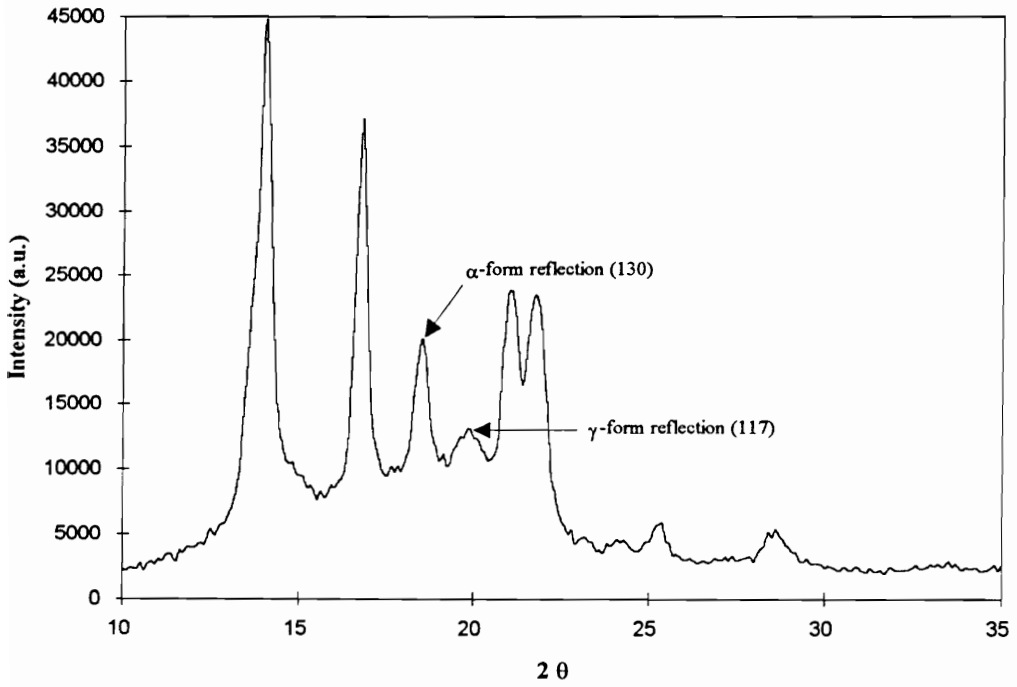

Fig. 3.5 A typical WAXD pattern of propylene-ethylene copolymer

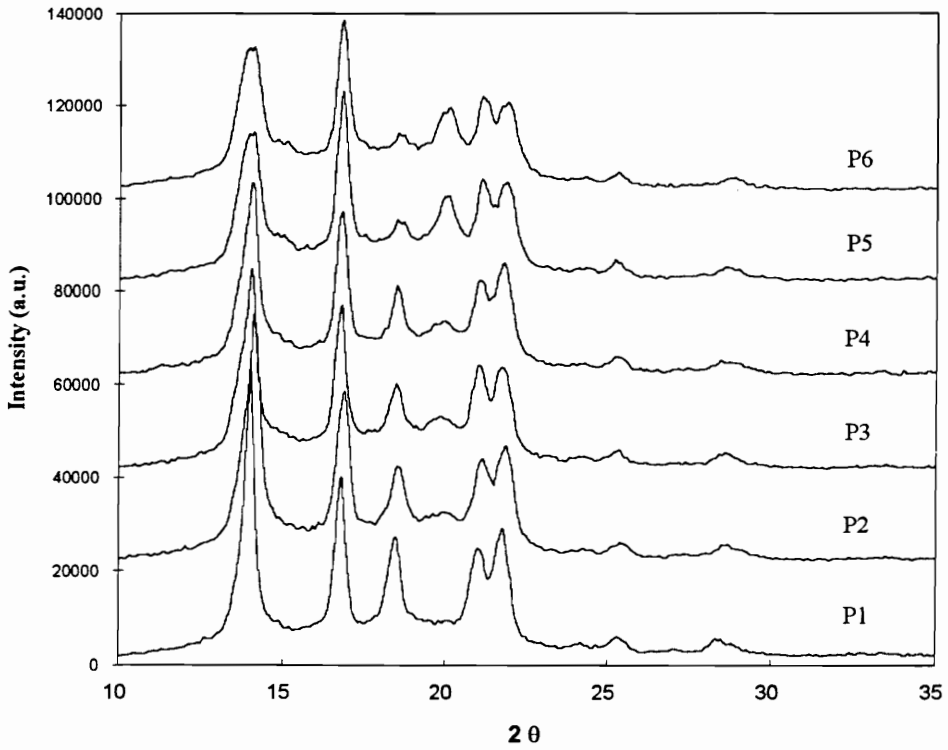

Fig. 3.6 WAXD patterns of P-series copolymers crystallized isothermally at 110 °C

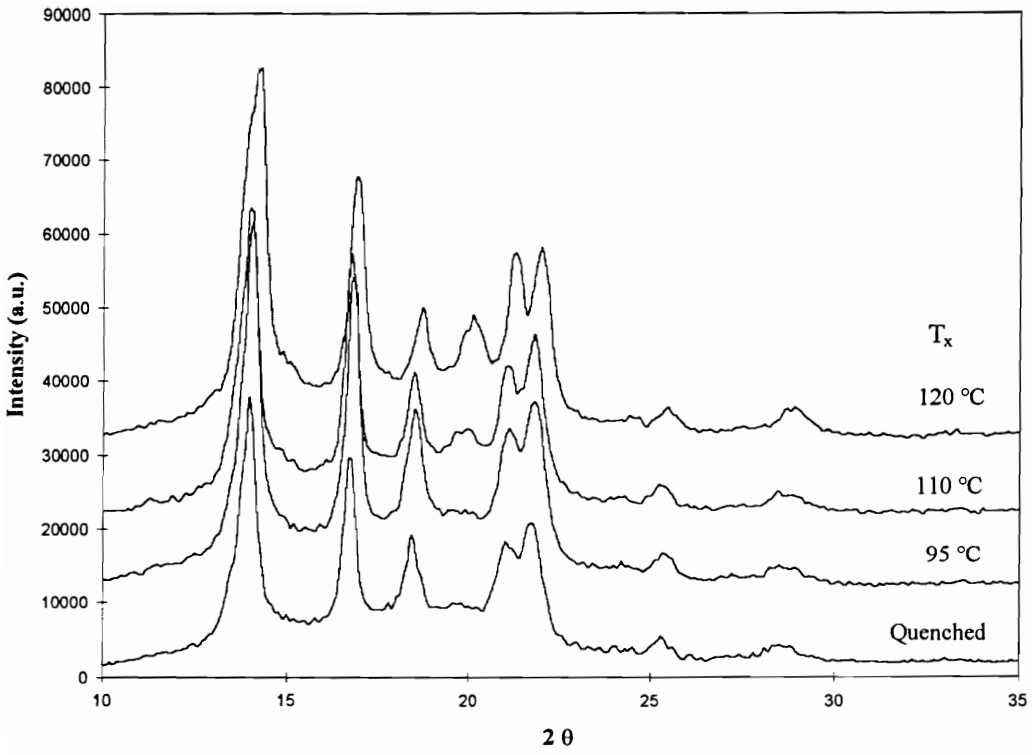

Fig. 3.7 WAXD patterns of P4 crystallized at different temperatures

Table 3.12 γ-phase content (%) for the P-series propylene-ethylene copolymer crystallized at various temperatures

Samples	Air quenched	T_x = 95 °C	T_x = 110 °C	T_x = 120 °C
P1	–	–	–	7
P2	–	10	18	36
P3	–	12	23	42
P4	6	12	20	46
P5	27	31	69	82
P6	28	31	71	83

(Uncertainty in the γ-phase content is estimated to be 5%)

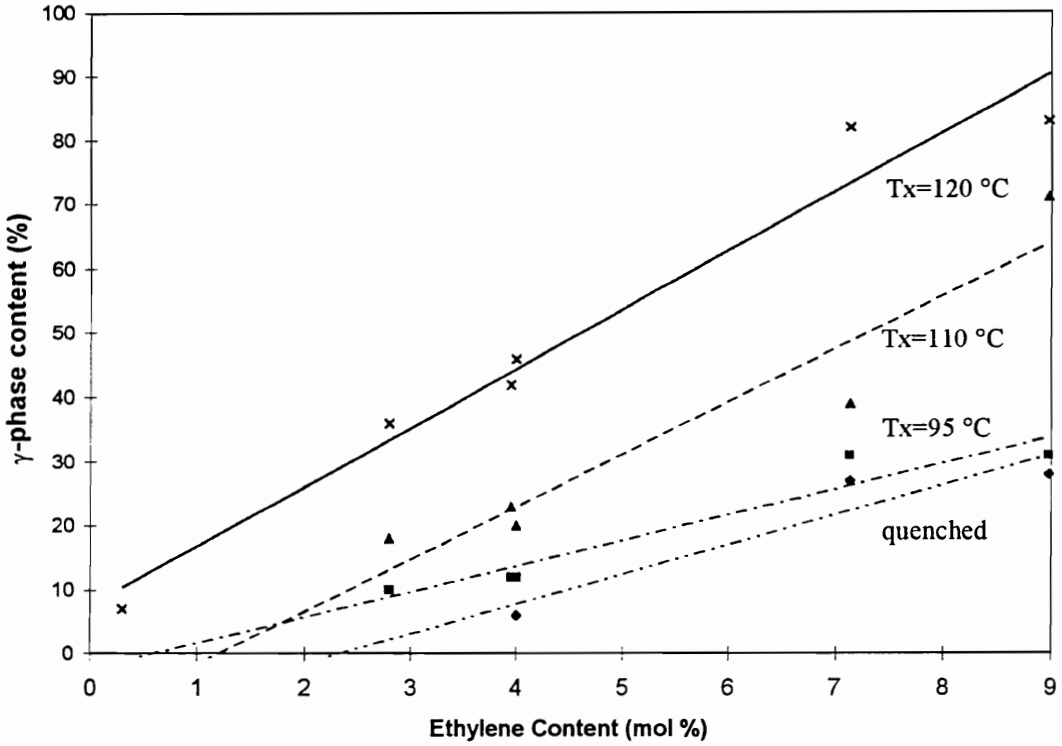

Fig. 3.8 γ-phase content (%) for the P-series propylene-ethylene copolymer crystallized at different temperatures

for the copolymer fractions is summarized in Table 3.13. As will be discussed in the following section, this information, together with the melting behavior of the fractions, lead to the conclusion that the lower melting endotherm should be partially responsible for the γ-form crystal melting. This observation also implies that for copolymers with sufficiently high ethylene content, crystallization at high crystallization temperature results exclusively in γ-phase crystals. On the contrary, it can be seen from Table 3.12 that, for the sample with the lowest ethylene content--P1, the γ-Phase Bragg peak can be observed only at the highest crystallization temperature. Moreover, the effect of quenching on γ-phase content is also demonstrated.

The effect of cooling rate (between 1 and 80 °C/min) on the γ-form content was also studied in the bulk sample (ER). As shown in Fig. 3.9, the γ-form content decreases as the cooling rate increases. At a cooling rate of 80 °C/min, no γ-form Bragg peak can be seen in the WAXD pattern. These latter results are consistent with the previous observation that crystallization at high temperature promotes formation of γ-phase crystals.

Finally, within experimental error, positions of the diffraction peaks in all WAXD patterns are independent of ethylene content, indicates that the unit cell dimensions for both the α- and γ-form crystals do not change with ethylene content.

Table 3.13 γ-phase content (%) for the propylene-ethylene copolymer fractions crystallized at various temperatures

Tx (°C)	ER	E2	E5	E6	E7	E8	E9
80					10	44	90
90					36		
95	12					85	
100					56	100	
115	38	29	71	81	88		100
120					95		
125	55	42	76	84			

(Uncertainty in the γ-phase content is estimated to be 5%)

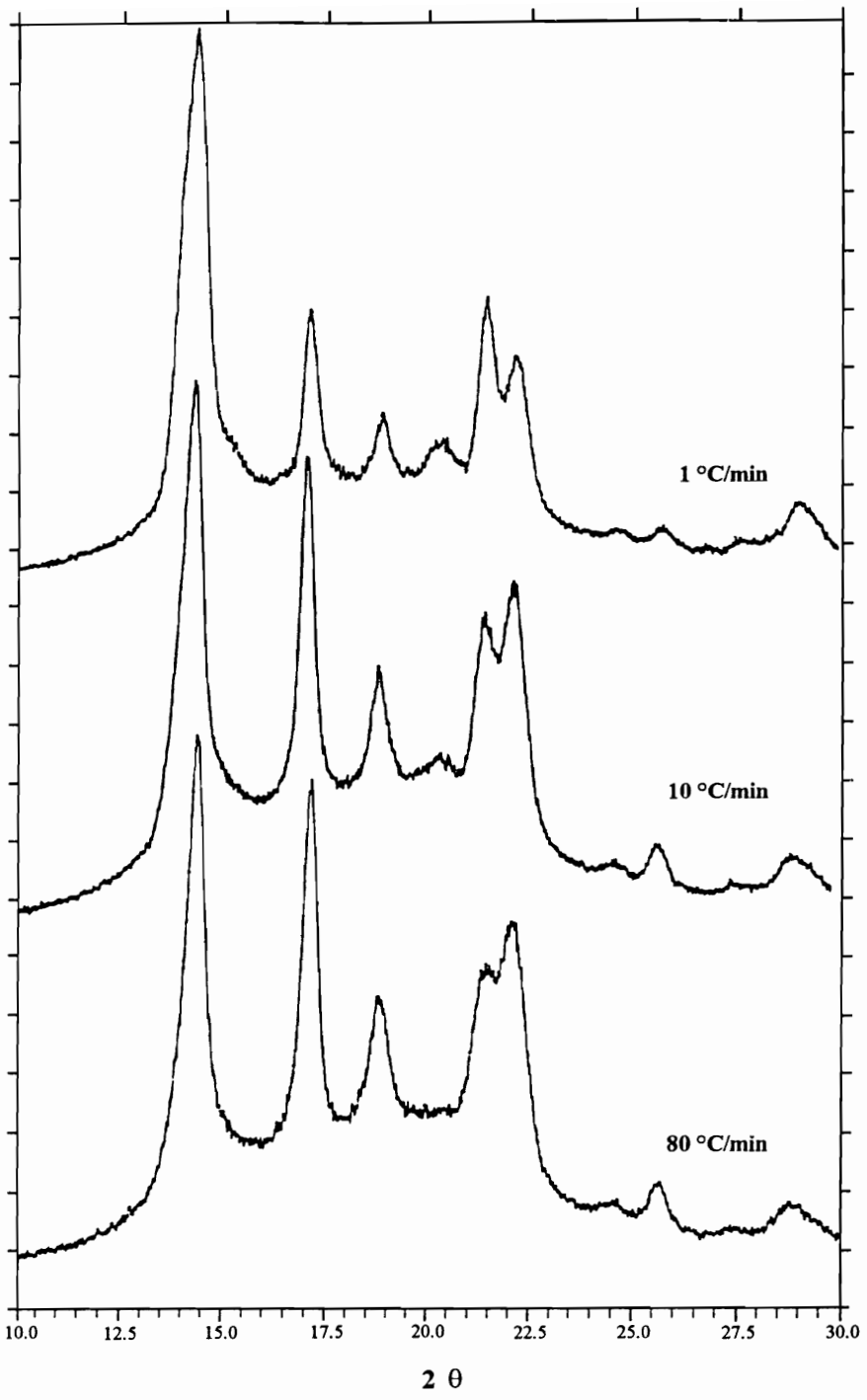

Fig. 3.9 WAXD patterns of the bulk sample (ER) after cooling from the melt at different cooling rates.

3.3.4 Melting Behavior

The melting endotherms of fractions E2, E4 and E6 crystallized at 110.5 °C are shown in Fig. 3.10. It can be seen that a broadening on the low temperature tail of the endotherm starts to develop as the ethylene content increases. This same behavior is also observed for the same fraction at increasing crystallization temperatures. Crystallization studies for various crystallization times at the same crystallization temperature show a simultaneous development of the lower and upper endothermic peaks with crystallization time. This indicates that the lower endotherm is not associated with lamellar in-filling at the later time of the crystallization. This point of view is supported by the results in a paper by Marigo *et al.*[167] In their study, WAXD patterns of propylene-ethylene copolymer samples with 4 wt% ethylene were recorded by synchrotron radiation during slow cooling at 1 °C/min from the melt. The results indicate a simultaneous development of the α- and γ-phases.

The ratio of the area under the lower endotherm to the area under the upper endotherm increases with ethylene content and crystallization temperature. This observation agrees with the observed increase in the γ-phase with ethylene content and crystallization temperature from the WAXD experiments (see section 3.2.2). For the highest ethylene content fraction (E9) and at high crystallization temperatures, this lower endotherm even dominates the upper endotherm peak. The resulting breadth of melting range agrees with the suggestion by Turner-Jones[89], that γ-form crystals can be promoted by irregularities along the poly(propylene) backbone. In this case, the ethylene co-units

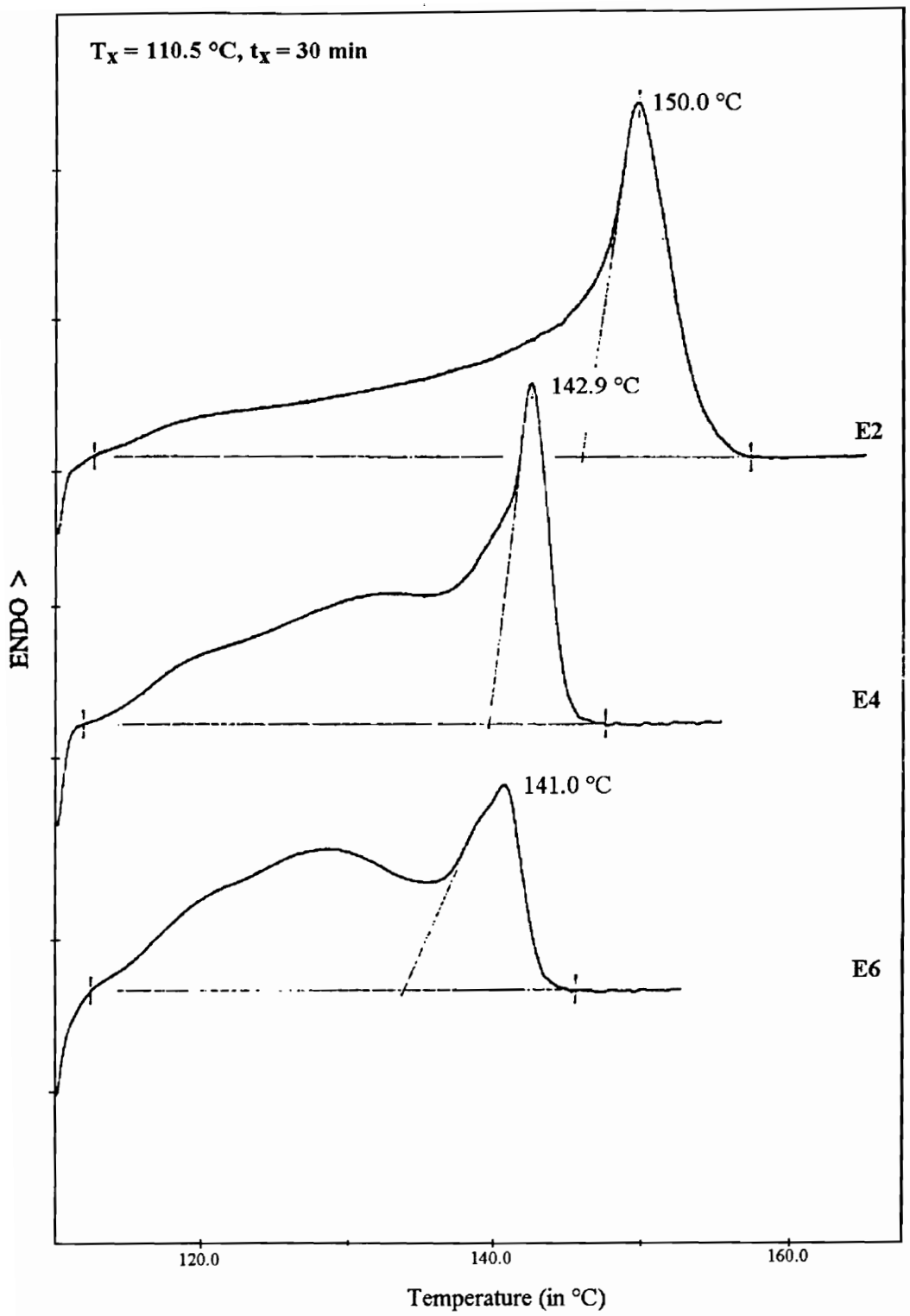

Fig. 3.10 DSC scans of copolymer fractions crystallized at 110.5 °C

correspond to the irregularities. It is therefore reasonable to believe that this lower endotherm is associated with the melting of γ-form crystals. This point of view is shared by other researchers[89,166,168]. However, it is not clear whether a very broad lamellar thickness distribution of the γ-form crystals is responsible for this broad endotherm at lower temperature. Once again, the breadth of the lower endotherm does not change with crystallization time, suggesting that this broadening cannot be completely due to lamellar thickening or reorganization processes.

From the above discussion, the higher peak is associated with the melting of α-form crystals. Taking the temperature at the peak maximum as the α-form melting temperature, a Hoffman-Weeks plot can be constructed in the way described in section 3.1.5. Fig. 3.11 shows the Hoffman-Weeks plots for the α-form crystals for some of the fractions together with the starting bulk material. Attempts to obtain the equilibrium melting temperature for γ-form crystals were unsuccessful because of the breadth of the γ-form melting endotherm. In fact, the equilibrium melting temperature for the γ-form it-PP is still unknown in the literature.

From Fig. 3.11 it can be seen that the experimental data exhibit some upward curvature at the highest crystallization temperatures. This observation suggests that the lamellar thickening of α-form crystals in these fractions is temperature dependent. In other words, the thickening coefficient γ in the Hoffman-Weeks equation--equation (2.6), as opposed to the conventional opinion, is temperature dependent. It should be noted that for each data point in the Hoffman-Weeks plot, the sample was kept at the corresponding

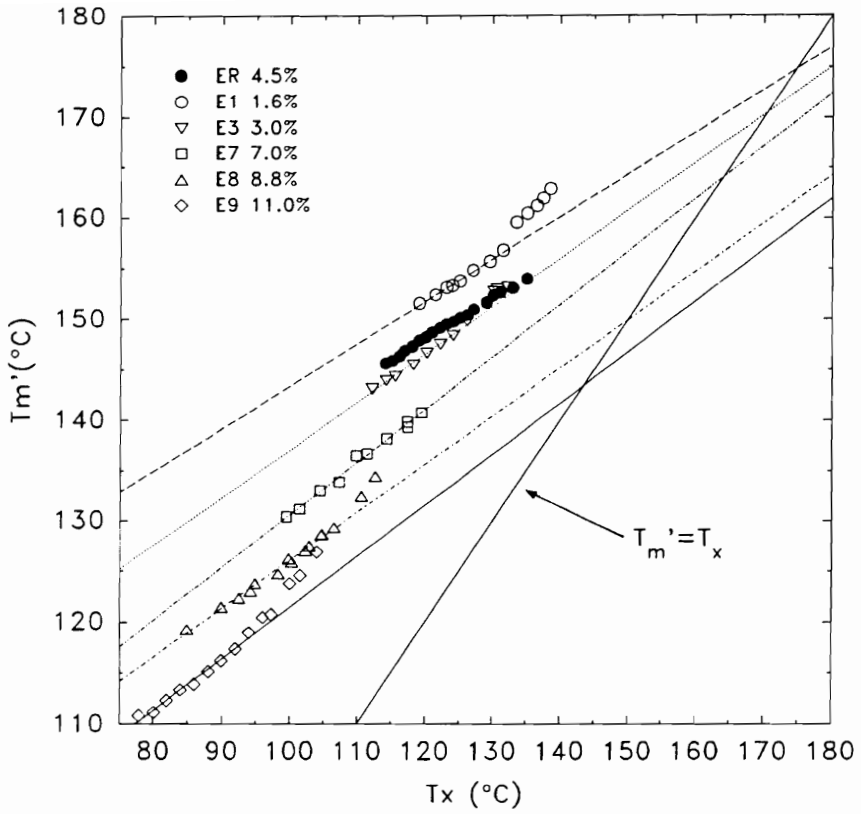

Fig. 3.11 Hoffman-Weeks analysis of the α-form crystals in the propylene-ethylene copolymer fractions

crystallization temperature until a 10% crystallinity is achieved. While this only takes about a minute at the lowest crystaillization temperature, such process would take many hours at the highest ones. In other words, there is more time for the lamellae to thicken under those high crystallization temperature situations. Another factor that would affect the thickening process is the ethylene content. With increasing ethylene content, there are more and more interruptions along the polymer backbone and therefore lamellar thickening becomes more and more difficult. This argument should hold regardless of whether the ethylene units are excluded or included in the crystal. As suggested by Mezghani *et al.*[29], the mechanism of thickening must involve a "snaking" through the crystals. Such snaking process will be hindered by the increasing irregularities along the polymer chains, regardless of whether such irregularities are within the lamellar crystals or not. Keeping this in mind, it is unexpected to see that curvatures are also observed in fractions with high ethylene contents. This discrepancy can be justified qualitatively by the following.

An explanation for the thickening of α-form crystals from fractions with higher ethylene content is the fractionation effect during crystallization. From the wide angle X-ray diffraction experiments, it has been shown that the majority of polymer chains in the fractions with higher ethylene content will crystallize into γ-form crystals as the crystallization temperature increases. Since the connection has been established between γ-phase formation and ethylene content of the copolymer, one can expect that the polymer chains within the α-form crystals under this circumstance have a lower ethylene content.

Therefore, these α-form crystals will thicken more or less the same way as the it-PP homopolymer crystals.

The equilibrium melting temperature of the α-form crystal for each fraction under study was obtained from extrapolation of observed melting temperatures vs. crystallization temperature plot. The result is shown in Fig. 3.12. It indicates a strong dependence of equilibrium melting temperature on ethylene content. This is quite different from the results of propylene-ethylene block copolymers reported by Greco *et al.*[169] They reported that the equilibrium melting temperatures of block-type propylene-ethylene copolymers with ethylene content ranging from 8 to 19 wt% are independent of co-unit concentration and have the same value as that of it-PP homopolymer.

To estimate the excess free energy ε of the ethylene co-unit in the crystal lattice, equation (2.10) for the uniform inclusion model is used. From the equilibrium melting temperature data, ε is estimated to be 30.3±2.5 cal/g (~0.06 eV/defect), which is 86% of the heat of fusion for the pure it-PP homopolymer. The large magnitude derived for the excess free energy may be the reason for the observed decrease in crystallinity for the propylene-ethylene copolymer as the ethylene content increases. The value of ε calculated here is comparable with the values for other copolymer systems (0.04 eV/defect for co-polymers of tetrafluoroethylene and hexafluoropropylene[31], 0.03 eV/defect for copolymers of L- and DL- lactides[32] and 0.06–0.12 eV/defect for copolymers of β-hydroxybutyrate and β-hydroyxyvalerate[170]). Note also that this relatively large value of ε (in comparison

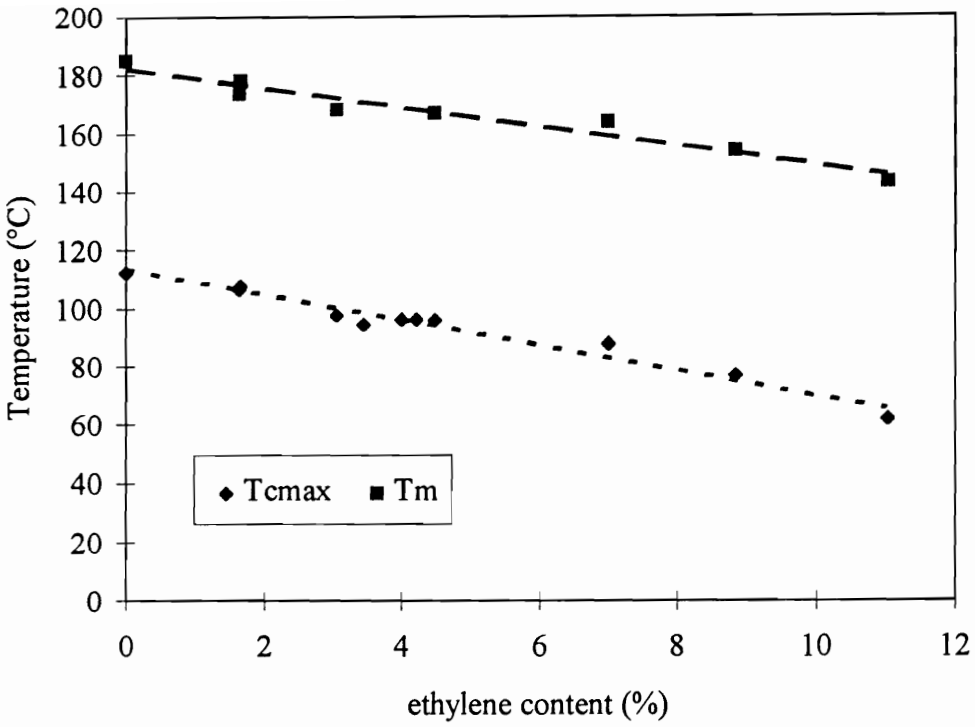

Fig. 3.12 Equilibrium melting temperature of the α-form crystal and temperature at maximum crystallization rate under cooling at 10 °C/min as a function of ethylene content

with ΔH_f^*) probably comes from the use of the uniform inclusion model equation (2.10) which would give an overestimation of ε.

The ethylene content dependence of the temperature of maximum crystallization rate (T_{cmax}) under dynamic cooling at 10 °C/min from the melt are also presented in Fig. 3.12. It can be seen that the temperature of maximum crystallization rate decreases with increasing ethylene content as expected.

The crystallinities of the fractions were measured from the area of the endothermic peaks obtained by heating at 10 °C/min in the DSC after crystallization for 6 to 8 hours at 20 °C above T_{cmax}. Fig. 3.13 shows that the apparent crystallinity of the copolymer decreases drastically as the ethylene content increases. It should also be noted that in Fig. 3.13 the extrapolation to zero percent ethylene content gives a crystallinity of about 70%, which matches what is known for pure it-PP homopolymer[3].

Table 3.14 summarizes the result of the DSC study of the P-series copolymers. In this series of study, the samples were slowly cooled from the melt at 10 °C/min. After they have been cooled to room temperature, the samples were heated immediately and the heating curves were recorded. It can be seen that crystallization starts at a lower temperature for samples with higher ethylene content. This is accompanied with a lower melting temperature and a lower heat of fusion. In general, the melting behavior of the P-series samples is very similar and consistent with that observed for the E-series fractions. The apparent crystallinity of the P-series copolymers from Table 3.14 is plotted against ethylene content in Fig. 3.14. It is clear that the general trend of crystallinity decrease with increasing ethylene content is also observed in the P-series samples.

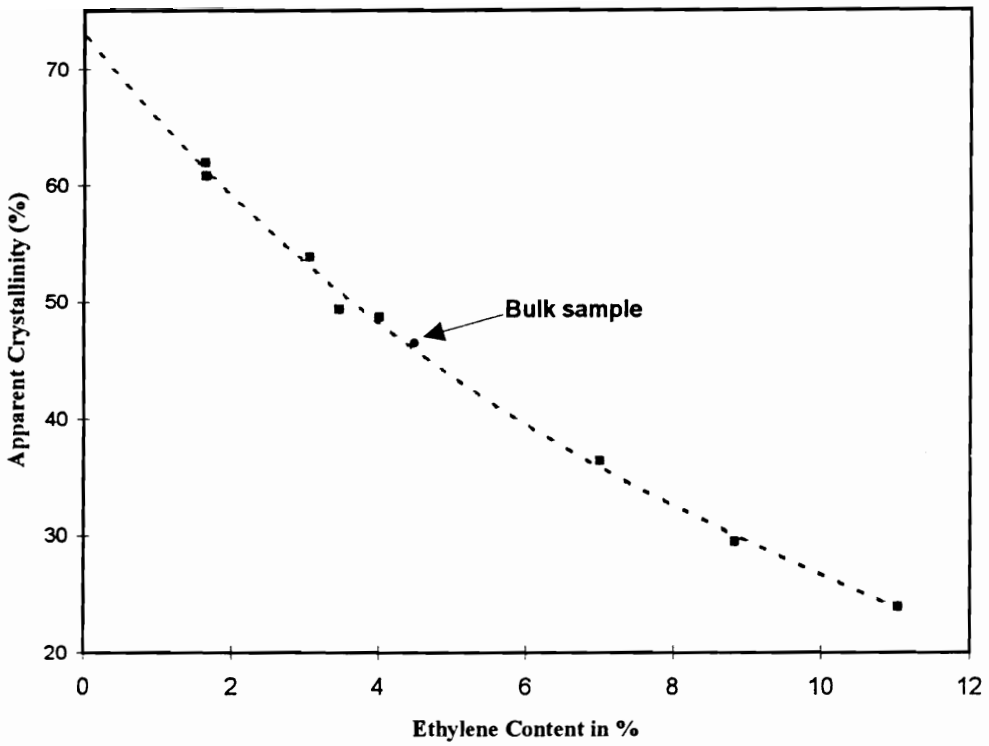

Fig. 3.13 Apparent crystallinity of propylene-ethylene copolymer fractions (E-series) vs. ethylene content

Table 3.14 Results of the DSC study of the P-series copolymers

Samples	Fractions	T_{cmax} (°C)	T'_m (°C)	ΔH_f(cal/g)	x_c
P1	bulk	108.7	156.1	21.6	61
	A	112.4	156.5	23.1	66
	B	113.8	156.3	20.8	59
	C	110.6	152.3	22.3	63
	D	84.3	113.8	7.3	21
P2	bulk	99.1	145.2	20.1	57
	A	106.0	148.2	21.9	62
	B	83.9	127.3	12.0	34
P3	bulk	99.9	143.4	21.7	62
	A	105.5	149.1	21.5	61
	B	103.1	144.4	18.0	51
	C	83.9	124.7	13.3	38
P4	bulk	99.5	143.0	19.8	56
	A	106.0	148.2	22.0	62
	B	102.5	144.4	19.6	56
	C	101.5	141.2	19.9	57
	D	85.6	124.0	14.2	40
P5	bulk	91.5	133.4	16.8	48
	A	102.0	140.7	18.6	53
	B	98.0	135.0	19.3	55
	C	97.7	139.6	18.9	54
	D	88.9	125.6	15.1	43
P6	bulk	86.5	131.2	15.8	45
	A	102.6	140.3	21.3	60
	B	97.1	134.8	17.9	51
	C	88.1	126.6	15.5	44

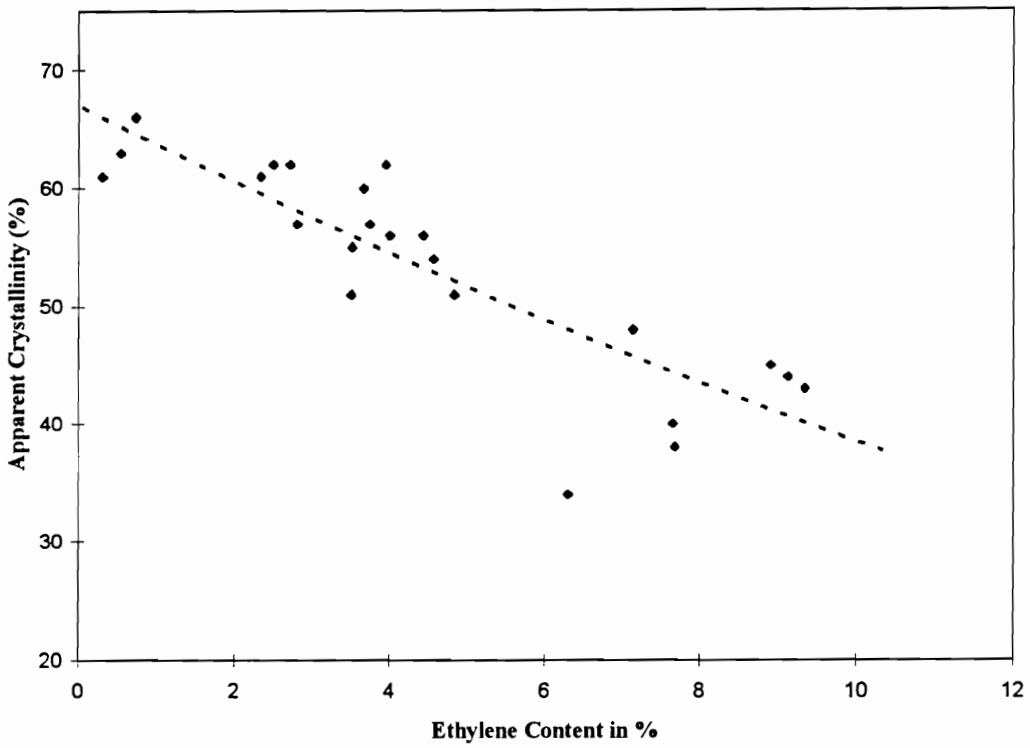

Fig. 3.14 Apparent crystallinity of propylene-ethylene copolymer (P-series) vs. ethylene content

Using unfractionated high conversion propylene-ethylene copolymers, Avella *et al.*[171] showed that there is a strong dependence of ethylene content on the overall apparent enthalpy of fusion and the equilibrium melting temperature of the copolymer. The apparent enthalpy of fusion drops drastically as the ethylene content increases. This finding agrees with the observations reported there. They also reported an increase in γ-phase content with ethylene co-unit concentration in samples prepared by compression molding. As was shown earlier, the cooling rate and thermal history have a significant effect on the γ-phase content. Unfortunately, the processing conditions of these samples were not provided and the comparison of the two results is not possible.

The drastic change in crystallinity measured by DSC, according to Sanchez and Eby's inclusion model, can be the result of a decrease in crystallinity as well as a decrease in heat of fusion of the copolymer as the ethylene content increases. From equation (2.12) it can be seen that the ratio between the observed heat of fusion ΔH_f^* and crystallinity x_c is linearly dependent on the ethylene content for the inclusion model. There is evidence from the WAXD experiments that the total crystallinity did decrease. However, the change was smaller as compared with the DSC results. A decrease of total crystallinity with increasing ethylene content was also observed by Zimmerman[172]. Keeping this in mind, it can be seen that the decrease of observed heat of fusion cannot be explained by the reduction of total crystallinity alone. The incorporation of ethylene unit into the crystal reduces the total crystallinity as well as the heat of fusion of the copolymer. This observation, however, cannot provide any quantitative prediction on the level of ethylene unit inclusion and the reduction of heat of fusion in the α- and γ-phase individually.

The slight difference on the crystallinity (especially at higher ethylene content samples) between the E-series and the P-series samples in Fig. 3.13 and Fig. 3.14 can be rationalized as follows. The samples from the E-series fractions were crystallized isothermally at temperatures 20 °C above their T_{cmax} for 6 to 8 hours while the P-series samples were crystallized by dynamic cooling from the melt to room temperature at 10 °C/min. Given the fact that the crystallization time for the E-series polymers may not have been sufficient, and that these materials were not cooled down to room temperature, it is not surprising that they exhibit lower crystallinity than the P-series samples which crystallize over a larger temperature range. In the latter case, chains that remain uncrystallized at the highest temperatures can eventually crystallize at lower temperatures.

3.3.5 Small Angle X-Ray Scattering

Small angle X-ray scattering experiments were conducted at room temperature on bulk samples of the P-series copolymers crystallized at different temperatures. Fig. 3.15 shows the desmeared SAXS patterns for sample P6 crystallized at different temperatures. The result of long spacing calculation is summarized in Table 3.15. Since sample thickness correction and incident beam intensity normalization were not conducted on these samples, the difference in intensity between the SAXS patterns, as can be seen in Fig. 3.15, does not have any significance in the analysis. Moreover, other data analysis approaches such as correlation function were not used in this discussion. Recalling that

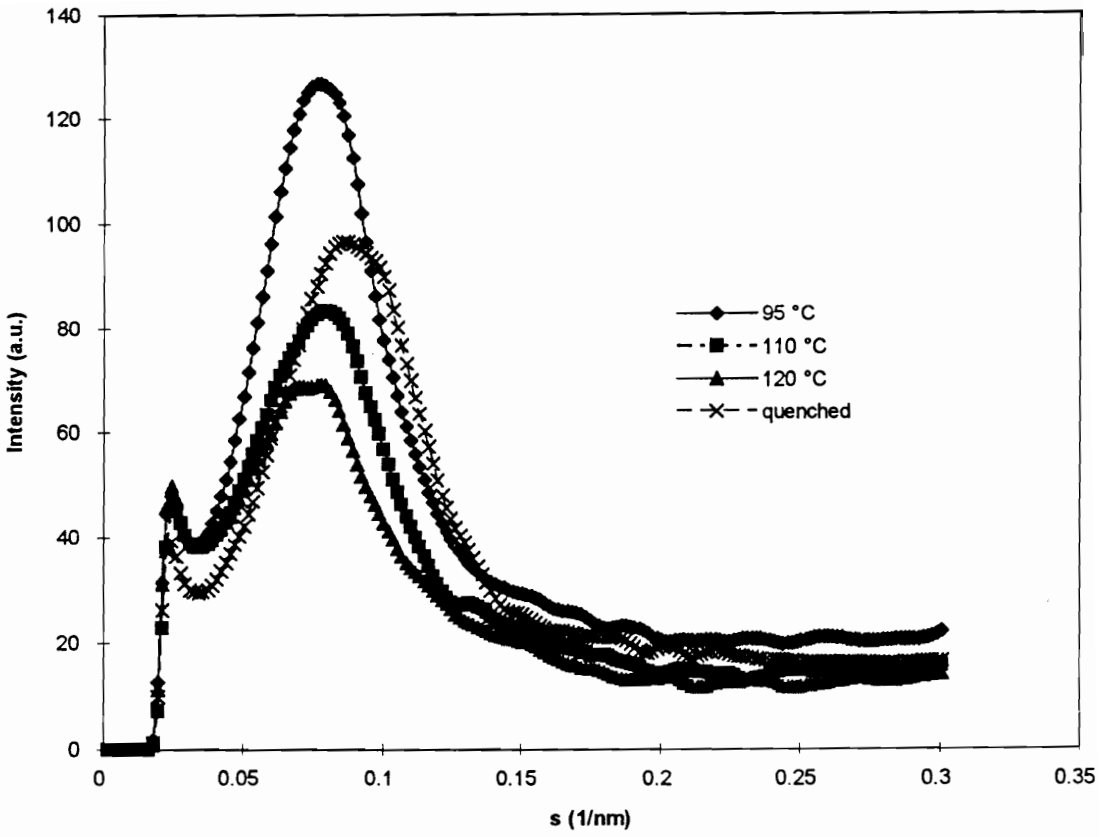

Fig. 3.15 Desmeared SAXS patterns of propylene-ethylene copolymer P6 at different crystallization temperatures

Table 3.15 Long spacing of the P-series propylene-ethylene copolymers obtained from SAXS

	L (nm)			
Samples	quenched	T_x = 95 °C	T_x = 110 °C	T_x = 120 °C
P1	13.2	14.4	15.1	17.2
P2	12.1	13.4	14.7	16.3
P3	12.1	12.9	14.4	16.3
P4	12.4	13.2	14.4	16.3
P5	11.7	12.9	12.9	15.1
P6	11.7	12.8	12.6	14.4

the P-series samples were labeled in the order of increasing ethylene content, it can be seen that the long spacing of these copolymers increases with crystallization temperature and decreases with ethylene content. This second observation agrees with the recent findings by Zimmermann[172].

According to Sanchez and Eby's theory[31,32], at a fixed crystallization temperature the crystal thickness increases as the co-unit content in the copolymer increases. This prediction was also mentioned by Flory[30] in his exclusion model, in which the minimum stable thickness of the crystal increases with the co-unit content.

With the two phase model (see section 3.2.6), the long spacing L is written as:

$$L = l_c + l_a \tag{3.20}$$

where l_c and l_a are the thicknesses of the lamella and of the interlamellar amorphous region, respectively. According to Sanchez and Eby, equation (3.20) implies that at constant crystallization temperature, the thickness of the amorphous region, l_a must decrease as the ethylene content increases. It has been mentioned earlier (section 3.3.4) that the total crystallinity X_c decreases with increasing ethylene content. If the linear crystallinity follows the trend of X_c, l_c must decrease faster than l_a. Since this is in contradiction with the prediction by Sanchez and Eby's theory, it must be examined more closely.

From Table 3.12, it can be seen that the γ-phase content in some of the SAXS samples is not negligible. At high crystallization temperatures and high ethylene content samples, γ-phase crystal becomes the dominant crystal component. One of the main consequences comes from the non-parallel chain structure of the γ-phase crystals. As

noted by Lotz *et al.*[91], The tilting of chain axis w.r.t. the lamellar normal in γ-form crystals makes the surface to volume ratio much larger than that of the α-form crystals. Moreover, because of this tilting, for a fixed stem length the ratio of the thickness of α- and γ-form crystals is 1:0.77. As the γ-form content increases, one should expect a bi-modal distribution of the lamellar thickness contributed by the two crystal forms. Keeping in mind that these two types of crystals have their own lamellar thickness distribution, the end result is a broad lamellar thickness distribution registered by the SAXS experiments. This situation was overlooked by Zimmermann[172] in his SAXS analysis of a series of similar propylene-ethylene copolymers. Unfortunately, information of the individual lamellar thickness distribution cannot be extracted from the SAXS results. On the other hand, since the γ-form lamella is thinner for a fixed stem length, having more and more crystals in the γ-phase as the ethylene content increases essentially decreases the overall crystal thickness. Owing to the two crystal forms involve, Sanchez and Eby's prediction on the variation in l_a at constant temperature cannot be verified from the result of the SAXS experiment.

3.3.6 Further Discussion

In section 3.3.3 it has been shown that the ethylene co-unit has a significant effect on the formation of γ-phase crystals in propylene-ethylene copolymers. The influence of copolymer content on polymorphism is also found in other copolymer systems. For example, in the study by Baltá Calleja *et al.*[173], it was found that the content in ferro-

electric phase in copolymers of vinylidene fluoride (VF_2) and trifluoroethylene (F_3E) is dependent on the copolymer composition. For copolymers containing 50 to 80% mole fraction of VF_2, the polymer chain can only crystallize in an extended all-trans planar conformation and the crystal structure is similar to β-PVF_2. For copolymers with VF_2 content in the range of 12 to 82%, there exist a well-ordered ferroelectric phase and a less-ordered phase with non-polar character. The content in ferroelectric phase increases with VF_2 content. Moreover, the unit cell dimension of the copolymer crystals is also affected by the co-unit. The a and b axis in the unit cell of β-PVF_2 in the copolymer are longer than that of the homopolymer. This is the result of the additional fluorine atoms in the trifluoroethylene co-unit.

The effect of co-unit on polymorphism should be considered as a fundamental factor in copolymer crystallization. For PVF_2 copolymer, inclusion of the co-unit reduces the number of conformations accessible to the polymer chains. For propylene-ethylene copolymers, however, ethylene co-unit does not cause reduction of the accessible chain conformations. Nonetheless, the ethylene co-unit clearly plays a significant role on the formation of γ-phase in poly(propylene) and at the same time has a similar effect as a defect during crystallization.

The presence of ethylene co-unit, as well as some other types of defects in poly-(propylene) homopolymer in general, promotes the formation of γ-phase. However, it should be pointed out that there is a significant difference between the copolymers under this discussion and another type of random copolymers studied by Cheng *et al.*[174] They investigate the crystalline structures and thermodynamic property changes of a series of

poly(propylene) homopolymer fractions with similar molecular weights but different isotacticities. Cheng *et al.*[174] report that crystal unit-cell parameters, crystallinity, lamellar thickness and crystal size are dependent on the isotacticity of what they called "random" stereo-copolymers. However, they did not report any presence of γ-phase crystal in all their samples. Considering the hindrance caused by the interruption of the isotactic sequence in their fractions, it can be seen that the "defect" in their copolymers not only significantly reduces crystallinity, but also prohibits the formation of γ-phase. This second observation is supported by the fact that the non-parallel chain structure in the γ-phase places a special restriction on chain packing at the contact surface between two adjacent layers. The size of the ethylene co-unit may just be small enough so that it does not cause any conflict at the contact surface of two adjacent layers.

Another puzzling observation in this study is the crystallization temperature dependence of the γ-phase content. Why is the formation of γ-form crystals more favorable at high crystallization temperatures? By reasoning from crystallization kinetics, this would indicate that the γ-phase crystals crystallize faster than the α-form crystals at high crystallization temperatures. Unfortunately, this has not been confirmed by experiments since no growth rate data of the γ-form crystals is available. There is other experimental evidence, however, that suggests the crystallization rate of the γ-phase crystals is higher than that of the α-phase crystals at higher crystallization temperatures. In section 3.3.4 it was mentioned that during the melting behavior study under isothermal crystallization conditions the lower and the upper endotherms develop simultaneously. However, it was

also observed that the ratio between the heights of the lower and the upper endotherms increases with crystallization time. This suggests two possibilities.

The first possibility is, the γ-phase crystal growth outruns the α-phase crystal growth at higher crystallization temperatures. While this can explain the crystallization temperature dependence of the γ-phase content, it also implies that the γ-form has a higher equilibrium melting temperature. This is possible according to Ferro *et al.*[158]'s calculation, which gives a slightly lower packing energy (hence a more stable state) for the γ-phase structure than that for the α-phase structure. However, the fact that γ-form crystals have lower observed melting temperatures makes it necessary to take a closer look at the situation.

If $T_{m\gamma}$ is higher than $T_{m\alpha}$, from the Gibbs-Thomson-Tammann equation (eq. 2.4), it would require

$$\sigma_{e\gamma}/l_\gamma \Delta H_{f\gamma}^{\infty} > \sigma_{e\alpha}/l_\alpha \Delta H_{f\alpha}^{\infty}$$

Using lattice theory, Yoon and Flory[175] showed that the interfacial free energy (same as σ_e) can be reduced by the tilting of the polymer chain w.r.t. the lamellar normal. Since the chain axis in γ-phase crystals is tilted by an angle of 40° w.r.t. the lamellar normal, their result suggests that $\sigma_{e\gamma}$ should be smaller than $\sigma_{e\alpha}$. While this conclusion would work against the above argument, one should be reminded that both l_γ and $\Delta H_{f\gamma}^{\infty}$ are smaller than their corresponding counterparts for the α-phase crystals. The former is due to the tilting chain axis w.r.t. the lamellar normal and the latter is due to inclusion of defects and ethylene co-units into the γ-phase crystals. As a result, the argument that γ-phase has a

higher equilibrium melting temperature can still hold as long as the resulting contribution from these three components ($\sigma_{e\gamma}$, l_γ and $\Delta H_{f\gamma}^{\infty}$) gives a larger $\sigma_{e\gamma}/l_\gamma \Delta H_{f\gamma}^{\infty}$ term.

The second possibility that would provide the observed increase in the ratio between the lower and upper endotherms at long crystallization time is, that the polymer chains with higher ethylene content and/or defects, which have not crystallized, preferably crystallize into the γ-form crystals at a later time. This agrees with the observed ethylene content dependence of the γ-phase content.

The next question is, does the ethylene co-unit enter the crystal lattice during the crystallization? If it does, will the inclusion be different in the γ-form crystals and in the α-form crystals?

In propylene-ethylene random copolymers, the polymorphic behavior makes the interpretation of inclusion and exclusion of the co-units more complicated. As mentioned earlier, the γ-form content increases with the ethylene content. One cannot ignore the possibility that the co-unit can be excluded in one crystal structure but be included in the other one. Moreover, even if the co-unit is included in both crystal structures, the inclusion level may not be the same.

As mentioned by Sanchez and Eby[32], both inclusion and exclusion models predict that the lamellar thickness changes with co-unit concentration. The justification of these models in any random copolymer system will rely on the study of crystallinity and heat of fusion of the system. This approach was successfully applied on the L- and DL-lactides copolymer system[176].

For ethylene-propylene copolymers, it was reported that the propylene co-units can be accommodated into the poly(ethylene) crystal lattice[177]. On the other hand, reports on whether the ethylene co-unit is included in the crystal lattice of propylene-ethylene copolymers have been controversial. It was mentioned in section 3.3.3 that the unit cell dimensions for the α- and γ-form crystals are independent of ethylene content. In a more recent study of propylene-ethylene copolymers with ethylene content up to 11 mol%, Zimmermann[172] reported that the unit cell dimension of α-form crystals is independent of ethylene content. In another study, Busico *et al.*[166] investigated propylene-ethylene copolymer system with ethylene content ranging from 4 to 20 mol%. By comparing the Bragg distances corresponding to the most intense diffraction peaks of both the α- and γ-form structures, they found that the crystallographic unit cells of both crystal forms are independent of the copolymer concentration and coincident with those for it-PP homo-polymers. These observations would imply that ethylene co-units are excluded from the two crystal structures. However, in the same publication, Busico *et al.* also presented several indirect experimental evidence to support the inclusion model. For example, the X-ray crystallinities of their samples were relatively high which suggests that inclusion should occur at some extent (exclusion model would predict a much lower crystallinity, especially for samples with higher co-unit content).

In contrast to those findings by Zimmermann and Busico *et al.*, Avello *et al.*[171] reported a systematic contraction of the unit cell dimension for the α-form crystal as the ethylene content increases. They also reported that the Bragg interplanar distance of the most intense reflection of the γ-form decreases systematically with ethylene content. As

suggested by these authors, this systematic decrease suggests the inclusion of a small amount of ethylene units into the it-PP crystal lattice. However, the claim by these authors was ambiguous and the original data were not presented in that paper. It can be seen that the arguments supporting either the inclusion model or exclusion model based on WAXD data are not conclusive. On one hand, the changes in unit cell parameters caused by ethylene unit inclusion can be too small to be registered in these experiments. Unfortunately, there is no theoretical calculation or simulation on unit cell dimension changes based on ethylene inclusion available in the literature. On the other hand, changes in unit cell parameters are not necessary due to inclusion of the co-unit in the crystals. It can also be caused by lamellar thickness changes, such as the case in poly(ethylene) lamellae[178].

The inclusion hypothesis for propylene-ethylene copolymer is supported by some computer calculations, however. By molecular mechanics calculation in their model studies of propylene-ethylene copolymers, Starkweather *et al.*[100] suggest that copolymer with low [E]/[P] ratio is equivalent to a homopolymer it-PP from which a few methyl side groups have been removed. Therefore, isolated ethylene units may be incorporated into the PP 3/1 helix without much difficulties. Microstructure should play a significant role in determining whether the ethylene units be included in the 3/1 helix. Starkweather *et al.* also suggest that, as the ethylene content increases, propagation of the 3/1 helix will depend on randomness of the copolymer. Inclusion is less likely to happen in propylene-ethylene copolymers with increasing block characters since blocks of ethylene will hinder the propagation of the 3/1 helix. This is nothing unexpected since the preferred planar

zigzag conformation of the ethylene block is not compatible with the helical structure of the poly(propylene) crystals. This argument once again demonstrates the importance of microstructural analysis in studies of copolymer crystallization behavior.

From these results it is not surprising to see that both the inclusion model and the exclusion model of copolymer crystallization be applicable to the propylene-ethylene copolymer system. In the thermal analysis study (section 3.3.4), the inclusion model was used to explained the observation of a upward curvature in the Hoffman-Weeks plots for fractions with high ethylene contents. Though it is not a proof for the inclusion model, the inclusion model should be a reasonable one to apply to this copolymer system in view of the consistency between this and the model study by Starkweather *et al.*[100]

So far the discussion on the ethylene co-unit inclusion was limited to the α-form crystal. Discussion of this issue on the γ-form crystal is absent in the literature. This is due to the complication of this crystal structure and the limited knowledge about it. Important parameters such as equilibrium melting temperatures, heat of fusion of the γ-phase crystal are yet to be determined. In view of the similarities between the α- and γ-phases, one can speculate that should ethylene co-unit be included in the α-form structure, it could be included in the γ-form structure as well. On the other hand, the fact that ethylene co-unit plays a significant role in the formation of γ-phase implies that it might be excluded to the fold surface.

The details of the crystallization will depend on the crystallization conditions and, more importantly, the microstructure of the particular copolymer samples. This further illustrates why fractionation of the copolymer samples according to their ethylene content

is so important in the study of copolymer crystallization. The consistency between the P-series samples and the fractions obtained from solution crystallization fractionation proves that ethylene contents the key parameter for the crystallization behavior of "random" propylene-ethylene copolymers.

3.4 Summary of Results

Wide angle X-ray diffractograms show the γ-phase content increases with crystallization temperature and ethylene content. Pure γ-form sample can be obtained by controlling the crystallization temperature and ethylene content. Melting behavior study by DSC indicates that the γ-phase melting is characterized by a broad and lower temperature endotherm than the α-phase. The area under this endotherm increases with ethylene content and crystallization temperature, consistent with findings from the WAXD study. By comparing the results of the bulk samples (the P-series) and that of the fractions obtained by solution crystallization, it is shown that the ethylene content is the utmost important factor in determining the polymorphic behavior of this copolymer. However, a distribution of ethylene content always exists in bulk propylene-ethylene copolymers, as demonstrated from the fractions obtained in this study. Equilibrium melting temperature of the propylene-ethylene copolymer decreases as the ethylene content increases. By assuming an uniform inclusion model, the excess free energy of the ethylene unit is estimated to be 30.3±2.5 cal/g.

Even though the answer as to whether the ethylene co-unit is included in the crystals is not conclusive, the inclusion model can better explain the upward curvature in the Hoffman-Weeks study of the melting behavior of α-form crystal.

Due to the co-existing α- and γ-form lamellae in the sample, lamellar thickness of these two crystal forms cannot be separated by the SAXS experiments. Further study on the dependence of lamellar thickness of ethylene content is necessary for a verdict on the inclusion and exclusion argument.

4. POLY(PROPYLENE)/POLY(1-BUTENE) BLENDS

4.1 Materials

Isotactic poly(propylene) was provided by Amoco, and isotactic poly(1-butene) was purchased from Scientific Polymer Products, Inc. (Sp^2) (catalog number #337). All atactic materials were kindly provided by Prof. J. Mays (University of Alabama, Birmingham). Atactic poly(propylene) was synthesized by anionic polymerization of (E)-2-methyl-1,3-pentadiene and subsequent hydrogenation[179]. Atactic poly(1-butene) was synthesized by anionic living polymerization of butadiene (c.a. 99% 1,2 addition), followed by hydrogenation. Both atactic materials so prepared have a very narrow molecular weight distribution ($M_w/M_n < 1.10$).

Beside the atactic materials mentioned above, another at-PP sample was used in this study. The bulk material was purchased from Sp^2 (catalog number #780). It was purified by T. H. Lee[180] by Soxhlet extraction using boiling diethyl ether. Though not measured experimentally, a broad molecular weight distribution is expected from this at-PP sample.

The molecular weights of the two isotactic materials and the atactic poly(propylene) from the purification step were determined by viscometric techniques as described in section 3.2.3 using *p*-xylene at 85 °C ($K = 9.6\times10^{-4}$ dL/g, $a = 0.63$)[157] for isotactic poly(propylene) and *n*-heptane at 35 °C ($K = 4.73\times10^{-4}$ dL/g, $a = 0.80$)[181] for isotactic poly(1-butene) and cyclohexane at 30 °C ($K = 2.09\times10^{-4}$ dL/g, $a = 0.76$)[182] for

atactic poly(propylene). Molecular weights are M_v = 111,000 g/mol for it-PP, M_v = 285,000 g/mol for it-P1B and M_v = 19,700 g/mol for at-PP. Values of the molecular weights for the atactic materials provided by Prof. J. Mays are listed in Table 4.1.

Table 4.1 Molecular weight M_w (g/mol) for at-PP and at-P1B used in this study

at-PP	at-P1B
19,700	29,600
32,000	48,500
87,000	98,000
268,000	520,000
402,000	
585,000	

4.2 Experimental Procedures

4.2.1 Sample Preparation (Melt Blending & Solution Blending)

Two different blending techniques were employed in preparing the blend samples: melt blending and solution blending. While solution blending can usually provide better mixing, melt blending is the only practical technique being used in industry for the preparation of polymer blends.

It-PP/it-P1B blend samples were prepared using melt blending by Lee[180]. A Haake Buchler Rheomix Blender operated at 190 °C with a 5-min mixing time and a rotating speed of 45 rpm was used to prepare the samples from the as-received homopolymers. The samples were taken out of the rheomixer and air-quenched to room temperature. While the following discussion on the isotactic blend will concentrate on the 30/70 (wt/wt) blend, it should be mentioned that similar results on the phase separation behavior were observed in the it-PP/it-P1B blend system at other compositions.

All the at-PP/at-P1B blend samples were obtained by solution blending. The solution blend samples were prepared by freeze drying a 1% (w/v) polymer solution in *p*-xylene. In order to maintain homogeneity within the samples, they were prepared in small amount each time (about 0.1 g) in a glass vial. The glass vial with the polymer solution was quenched into liquid nitrogen to solidify the HOT solution before being transferred to the vacuum line for removing the solvent by sublimation. The subsequent drying under vacuum was conducted at ice-water temperature.

4.2.2 Glass Transition Temperature Determination

To successfully determine the miscibility of a polymer blend system through an evaluation of the glass transition behavior by DSC, the two components should have glass transition temperatures that differ sufficiently from each other. Typical glass transition temperatures for at-PP and at-P1B are −14 °C[183] and −24 °C[184], respectively. Even though there is a small molecular weight dependence for the glass transition temperature over the molecular weight range of the samples in this study, the sufficient difference in glass transition temperatures between these two polymers enables the investigation of the miscibility behavior using differential scanning calorimetry. As mentioned in section 2.6.6, for miscible polymer blend systems, only one glass transition will be observed. The value of the glass transition temperature of a miscible blend can be sometimes described with the Fox equation. For immiscible polymer blend systems, two distinct glass transition temperatures or a very broad single glass transition (for marginal miscibility in polymers with similar T_g's) will be observed.

A Perkin Elmer differential scanning calorimeter model DSC-2 was used in this study. Benzophenone (T_m = 48.1 °C) was used as a calibration standard. The heating scan was conducted from −50 °C to 50 °C at a heating rate of 10 °C/min.

4.2.3 at-PP/at-P1B Blend Miscibility Study

The miscibility of at-PP/at-P1B blends of various molecular weights was investigated by studying the glass transitions by DSC. The DSC experiments consisted of

two parts. In the first part of the experiment, at-PP/at-P1B blends of different molecular weights were prepared at their critical compositions calculated from equations (2.27) and (2.28). The critical temperatures or a lower bound of the critical temperatures of these samples were then determined from the following procedures.

About 10 mg at-PP/at-P1B blend sample prepared by solution blending was put in a standard DSC pan. The sample was heated to 120 °C for 8 hr in order to permit a good mixing in the melt (note that this procedure assumes that the UCST of the system is below 120 °C). This step is necessary because storage at room temperature can cause phase separation in systems with UCST above room temperature even if the solution blending procedure provides the best mixing possible. (For polymer blend systems without specific interaction, the driving force for remixing is very weak and the process can take hours in the one-phase region.) After keeping the sample at 120 °C for 8 hr, the DSC temperature was reduced to a target temperature. The sample was kept at that temperature for another 6 to 8 hr. After that, it was quickly removed from the DSC and quenched into liquid nitrogen. In the mean time, the DSC was allowed to cool to −50 °C. Once the DSC chamber reached thermal equilibrium at −50°C, the blend sample was transferred back to the DSC for the scanning experiment. From the behavior of the heat capacity in the glass transition region, one can determine whether the target temperature was above or below the critical temperature. With this information, the same procedure was repeated for a new target temperature until the critical temperature or a lower bound of the critical temperature is determined.

In the second part of experiment, the phase diagram of the atactic polymer blend was determined. With the information from the first part of experiment, together with the consideration of the critical temperature and phase diagram calculation, an at-PP/at-P1B blend with suitable molecular weight was chosen. Different blend compositions were prepared and the temperature for phase separation for each of these compositions was determined from the DSC scans. To determine the phase separation temperature at a particular composition, a trial-and-error approach was used. For example, if the sample were miscible at the first target temperature, it would be tested again at a lower temperature. On the other hand, if the sample were immiscible at the first target temperature, it would be tested at a higher temperature. This procedure continued until the 'cross-over' temperature was found for that composition. Similarly, the same process was repeated for other compositions and the phase diagram for this blend was then constructed.

4.2.4 Optical Microscopy - Morphology and Growth Rate Study

The 30/70 w/w it-PP/it-P1B blend will be examined as a function of residence time in the melt state using optical microscopy, since it is believed that the indices of refraction of amorphous it-PP and it-P1B are sufficiently different. Such experiments will show that the blend is in a heterogeneous state in the liquid. One should note that such an approach can only prove the blends to be immiscible since the observation of a homogeneous morphology may result either from true molecular-level miscibility or from the lack of

spatial resolution of the microscopic technique utilized. To study the interplay between crystallization and liquid-liquid demixing, the spherulite growth behavior of the it-PP component will be observed under isothermal conditions for different residence times in the melt prior to crystallization. This study will not address the crystal growth behavior of the isotactic poly(1-butene) component.

A thin film of the 30/70 blend was melted in between two cover slips at 200 °C in a Linkam THMS 600 heating stage in which it was allowed to reside for up to 3 hr under a dry nitrogen gas purge. Optical micrographs were recorded after various residence times in the melt at 200 °C using a Carl Zeiss Axioplan light microscope. In another series of experiments, the isothermal crystallization of the it-PP component in the 30/70 blend at 145 °C after a residence time of 3 min in the melt at 180 °C is observed. These experiments enabled simultaneous observation of the macrophase separation and the crystallization of the it-PP component. The crystallization temperature was chosen such that the rates of liquid-liquid demixing and of crystallization were of about the same magnitude. In the third series of experiments, the 30/70 blend was crystallized isothermally at 130, 135 and 145 °C's after a residence time of 5 hr in the melt at 180 °C. Since the polymer sample was kept under dry nitrogen environment, the extent of degradation undergone by the sample was minimized. Isothermal crystallization of it-PP from a macroscopically phase-separated melt could be observed. These same isothermally crystallized 30/70 it-PP/it-P1B samples were subsequently heated at a rate of 5 °C/min in the microscope hot stage, and the melting of the it-PP spherulites was recorded photographically at different temperatures during the heating process. In the latter three series

of experiments, optical micrographs were recorded so as to observe simultaneously the macrophase-separated morphology and the birefringence of it-PP spherulites. Such simultaneous observations were made possible by slightly rotating the analyzer on the microscope away from the crossed-polarization condition. The temperature scale of the microscope hot stage was calibrated using the melting temperature of indium (T_m = 156.6 °C). In the crystal growth rate study, the optical micrographs were digitized and the distances of the growth fronts from the center of the spherulites in different phases as a function of time were measured with the Mocha Image Analysis software package from Jandel Scientific. Contrast enhancement was used on the digital images in all measurements during the process in order to get a better defined image of the spherulites growth front.

4.2.5 SEM (including SEM Sample Preparation)

The morphology of quenched blend samples will be investigated using the scanning electron microscopy technique. The 30/70 it-PP/it-P1B blend samples were melted at 200 °C for various periods of time and quenched directly from the melt to liquid nitrogen temperature and freeze-fractured. The fractured samples were kept in cyclohexane at room temperature for 24 hr to remove the it-P1B component at the fracture surface[185]. Samples were then washed thoroughly with fresh cyclohexane, dried, and coated with gold. Such treatment is necessary to image the surface topology as previous scanning electron microscopic (SEM) studies on untreated fractured surfaces failed to show any

distinguishable morphological features[150,180]. The morphology of the fracture surface was examined in an International Scientific Instruments SISX40 scanning electron microscope operated at 15 kV.

4.2.6 Differential Scanning Calorimetry (Melting Behavior Study)

The complex melting behavior of the it-PP component in this blend will be discussed and a correlation between the multiple melting behavior and the blend morphology resulting from competitive liquid-liquid demixing and crystallization process will be proposed.

The experiments were conducted in a Perkin-Elmer DSC-2C differential scanning calorimeter at a heating rate of 10 °C/min after isothermal crystallization in the DSC. The sample weight was kept at 4 mg in all DSC studies to minimize the effect of sample weight variation on thermal lag. In all cases, the heating scans were started from the crystallization temperature so as to prevent any crystallization of the it-P1B component.

4.3 Results and Discussion

4.3.1 Phase Diagram and χ Parameter Calculation (at-PP/at-P1B Blend)

The binodal and spinodal curves, as well as the critical temperature and critical χ parameter of the polymer blend system can be obtained by the Flory-Huggins-Hildebrand mean field theory (see section 2.6.3).

The solubility parameter difference $\Delta\delta$ for the propylene and 1-butene repeat units can be calculated by the group contribution method. Using the values given by Coleman *et al.*[186], as listed in Table 4.2, and from equation (2.29), δ_P and δ_B are calculated to be 7.43 $cal^{1/2}/cm^{3/2}$ and 7.57 $cal^{1/2}/cm^{3/2}$, respectively. This gives the solubility parameter difference between poly(propylene) and poly(1-butene) $\Delta\delta = 0.14$ $cal^{1/2}/cm^{3/2}$.

Table 4.2 Solubility parameters from the group contribution method (adapted from ref. 186)

Group	v_i^* $cm^3 \cdot mol^{-1}$	F_i^* $(cal \cdot cm^3)^{1/2} mol^{-1}$
$-CH_3$	31.8	218
$-CH_2-$	16.5	132
$>CH-$	1.9	32

Critical χ's for the PP/P1B blends with different molecular weights can be calculated from equation (2.26), with $m_i = M_{Wi}/M_i$, $v_P = 49.27$ $cm^3 \cdot mol^{-1}$, $v_B = 64.64$ $cm^3 \cdot mol^{-1}$, $M_P = 42.08$ g/mol and $M_B = 56.11$ g/mol, where M_P and M_B are the molecular weights per repeat unit. The calculated values of χ_c are shown in Table 4.3.

Moreover, from equation (2.24) with $\Delta\delta = 0.14$ $cal^{1/2}/cm^{3/2}$, the critical temperatures for each of these blends can also be calculated. The results are tabulated in Table 4.4.

As can be seen from Table 4.3 and Table 4.4, polymer blends with the lowest molecular weights for both polymers have the largest values of χ_c. For the low molecular weight blends, T_c's are all below room temperature while the T_c's for high molecular weight blends exceed 200 °C. In other words, the low molecular weight materials are more miscible while the high molecular weight counterparts are immiscible under any reasonable operating temperature.

Yet another way to show the miscibility of the polymer blend is by showing the binodal and spinodal curves of the given system. First, this is done by theoretical calculations. Using $\Delta\delta = 0.14$ $cal^{1/2}/cm^{3/2}$, the binodal curve and spinodal curves for each blend were calculated from equations (2.21), (2.22) and (2.24). The calculations were carried out in Mathcad 2.0 software. Fig. 4.1 and Fig. 4.2 show some of the calculated binodal and spinodal curves for blends with various molecular weights.

Table 4.3 Critical χ parameters $\chi_c \times 10^{+3}$ for at-PP/at-P1B blends with different molecular weights

	M_w (PP)*						
M_w(P1B)*	19,700	32,000	87,000	111,000	268,000	402,000	585,000
29,600	4.06	3.16	2.06	1.89	1.46	1.33	1.24
48,500	3.30	2.49	1.53	1.38	1.02	0.91	0.84
98,000	2.58	1.87	1.05	0.93	0.64	0.56	0.49
520,000	1.75	1.18	0.55	0.47	0.27	0.21	0.18

(*M_w in g/mol)

Table 4.4 Critical temperatures T_c (°C) for at-PP/at-P1B blends with different molecular weights

	M_w (PP)*				
M_w(P1B)*	19,700	32,000	87,000	111,000	268,000
29,600	−136	−97.0	−3.2	21.0	107
48,500	−104	−49.8	90.6	129	272
98,000	−57.3	24.4	255	324	597
520,000	44.8	200	734	920	1810

(M_w in g/mol)

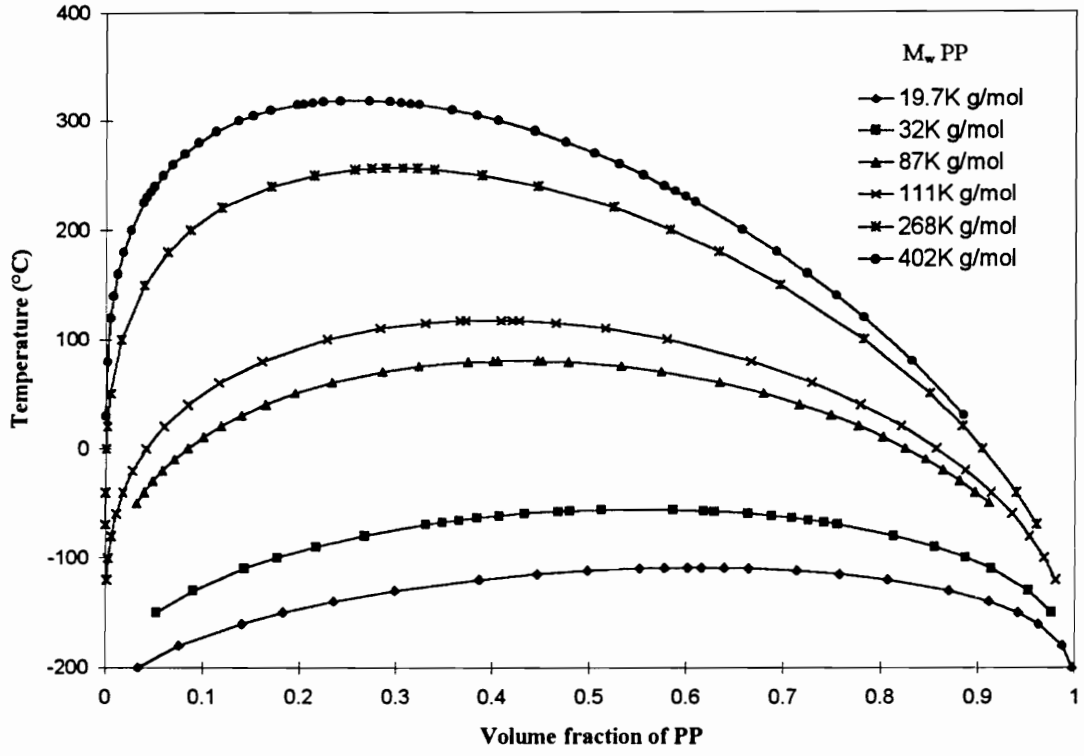

(symbols in each curve represent the data obtained from the theoretical calculations)

Fig. 4.1 Calculated binodal curves for at-PP/at-P1B blends (M_w for at-P1B = 48.5K g/mol)

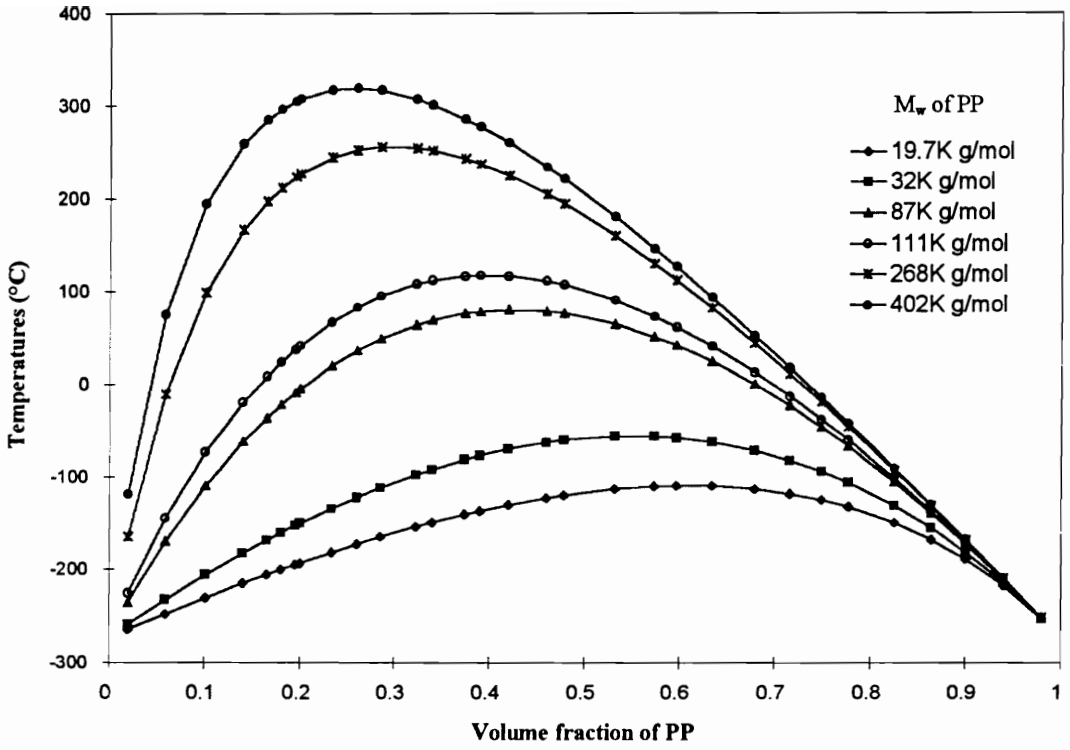

(symbols in each curve represent the data obtained from the theoretical calculations)

Fig. 4.2 Calculated spinodal curves for at-PP/at-P1B blends (M_w of at-P1B = 48.5K g/mol)

4.3.2 Error Estimation of the Solubility Parameter Difference

Since the accuracy of the critical temperature obtained from the phase diagram measurement is limited by the reliability of the phase diagram, one can question the reliability of the solubility parameter difference so obtained. Moreover, the critical temperature obtained from the phase diagram can also be compared with the one calculated from the group contribution method.

From equation (2.24), (2.27) and (2.28), the solubility parameter difference and the critical temperature are related by the relation:

$$\delta_P - \delta_B = \sqrt{\frac{RT_c}{2}}\left[\frac{1}{\sqrt{m_P v_P}} + \frac{1}{\sqrt{m_B v_B}}\right] \tag{4.1}$$

By error estimation, the above equation gives:

$$\Delta(\delta_P - \delta_B) = \sqrt{\frac{R}{8T_c}}\left[\frac{1}{\sqrt{m_P v_P}} + \frac{1}{\sqrt{m_B v_B}}\right]\Delta(T_c) \tag{4.2}$$

During DSC experiments, as the annealed temperature is getting closer to the temperature given by the binodal curve, it becomes more difficult to determine whether the system is phase separated at that temperature, because phase separation becomes slower as the annealed temperature gets closer to the binodal curve. Keeping this in mind, an uncertainty of 5 °C is assigned for the critical temperature measurement from the DSC experiment. From this, the uncertainty of the solubility parameter difference according to (4.2) is estimated to be 0.001 $cal^{1/2}/cm^{3/2}$.

4.3.3 at-PP/at-P1B Blend: DSC Miscibility Study (Effect of Molecular Weight)

Fig. 4.3 shows four DSC heating scans for the 39/61 (w/w) at-PP/at-P1B blend (87K/48.5K). As can be seen in Fig. 4.3, even at 100 °C, which is above the upper critical solution temperature of the (87K/48.5K) blend, the remixing process can take several hours. This demonstrates the necessity of keeping the samples at 120 °C for 8 hr during the DSC experiment.

In the first part of the at-PP/at-P1B blend miscibility study, the critical temperatures or a lower bound of the critical temperatures were determined from the DSC. Results of these experiments are tabulated in Table 4.5.

From Table 4.5 and from the binodal and spinodal curves in the previous section, the system with atactic poly(propylene) at molecular weight 87,000 g/mol and atactic poly(1-butene) at molecular weight 48,500 g/mol was chosen for the phase diagram study. at-PP/at-P1B blends were prepared with the following compositions: 20/80, 30/70, 39/61, 50/50 and 60/40 (w/w). The experimental results are plotted in Fig. 4.4, together with the binodal and spinodal curves providing the best fit ($\Delta\delta$ = 0.138 $cal^{1/2}/cm^{3/2}$) for the experimental data.

It can be seen that the experimental result and the value of $\Delta\delta$ obtained from group contribution calculation are in close agreement. Reliable data at extreme compositions, i.e. with concentration of at-PP lower than 20% or higher than 80%, are extremely difficult to obtain because of the small contribution of glass transition signal from one of the components.

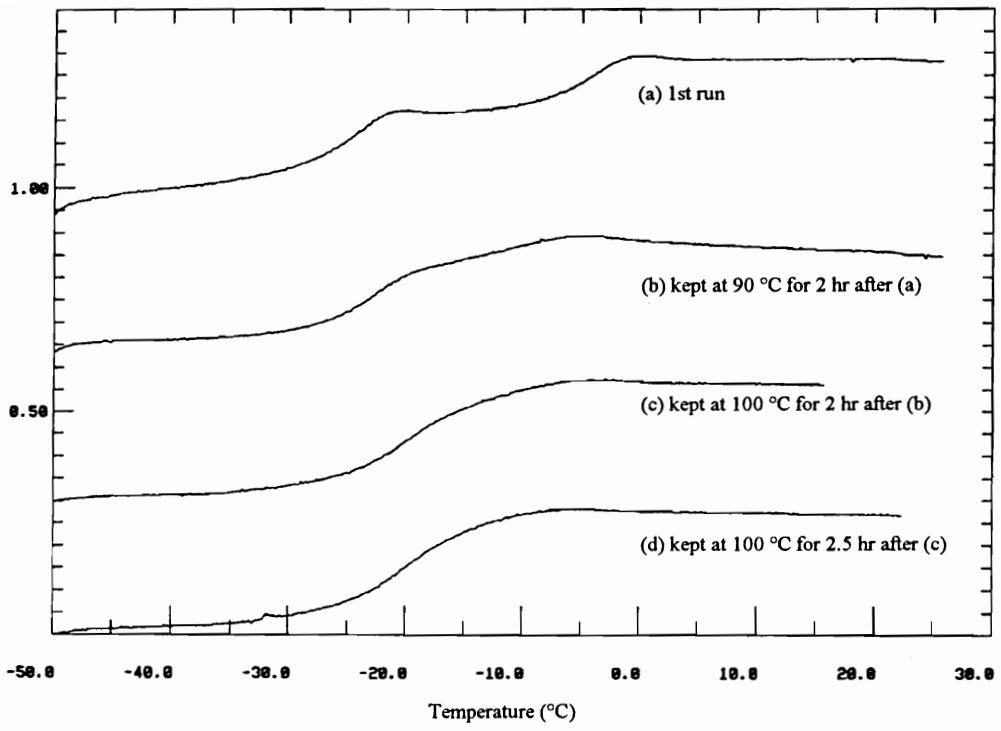

Fig. 4.3 DSC heating scan of the 39/61 (w/w) at-PP/at-P1B (87K/48.5K) blend after storing at different temperatures

Table 4.5 Summary of at-PP/at-P1B blend miscibility study

Mw* (at-P1B)	M_w* (at-PP)			
	19,700	32,000	87,000	268,000
48,500	M (25 °C)	T_c > 45 °C	T_c = 80 °C	T_c > 100 °C
98,000	M (25 °C)	T_c > 100 °C	T_c = 185 °C	T_c > 100 °C
520,000	I	I	I	T_c > 180 °C

M: miscible; I: immiscible

(* M_w in g/mol)

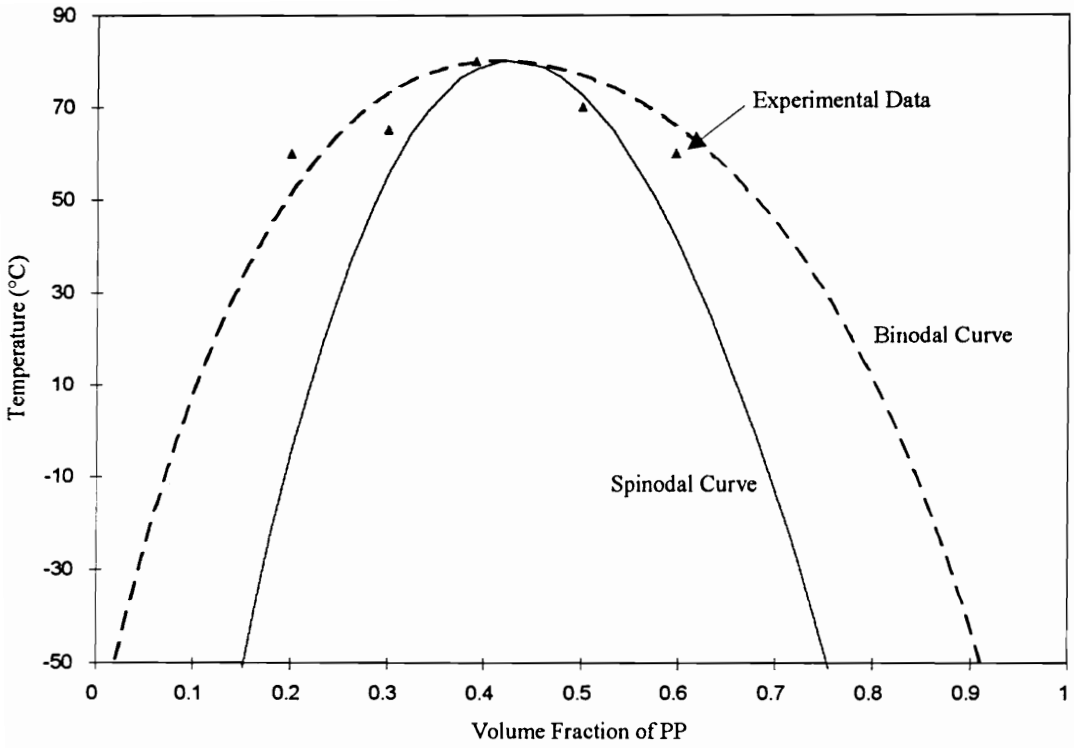

Fig. 4.4 Phase diagram of at-PP/at-P1B (87K/48.5K) blend

This study has clearly shown that miscibility on poly(propylene)/poly(1-butene) blends (at least for the atactic materials) can be directly estimated from the knowledge of the difference in solubility parameters and the molecular weights of these polymers. From the phase diagram constructed from the DSC experiments, it was shown that such materials exhibit a UCST behavior, as has been reported for mixtures of deuterated and protonated polyolefins[187,188]. If the arguments presented by Walsh and Ittel[189] is followed, that tacticity does not affect markedly the dispersive interactions and the entropy of mixing in poly(propylene)/(poly(1-butene) blends, one can predict that blends of commercial it-PP and it-P1B materials (i.e., of molecular weight above 10^5 g/mol) would be immiscible and exhibit a UCST above their respective degradation temperatures.

Finally, it should be pointed out that in order to account for the deviation from Flory-Huggins's theory, an empirical equation in the form of (4.3) is often used to relate χ_c and T_c:

$$\chi_c = \alpha/T_c + \beta \tag{4.3}$$

For a polymer blend system with known molecular weight, χ_c can be calculated from the molecular weights of the polymers according to equation (2.26). If T_c's are known for blends with different molecular weights, α and β in equation (4.3) can be obtained from the plot of χ_c vs. $1/T_c$. From this, the critical temperatures of the systems with different molecular weights can be predicted by (4.3).

This is demonstrated in Fig. 4.5. The two data points in this figure correspond to the experimental results for the 87K/48.5K and the 87K/98K blends taken from Table 4.5. The straight line corresponds to values predicted by the Flory-Huggins theory using the

$\Delta\delta$ value calculated from the group contribution method. This again shows the consistency between the results from the experiments and from the group contribution method. Critical temperatures of at-PP/at-P1B blends at other molecular weights can, in principle, be predicted from Fig. 4.5.

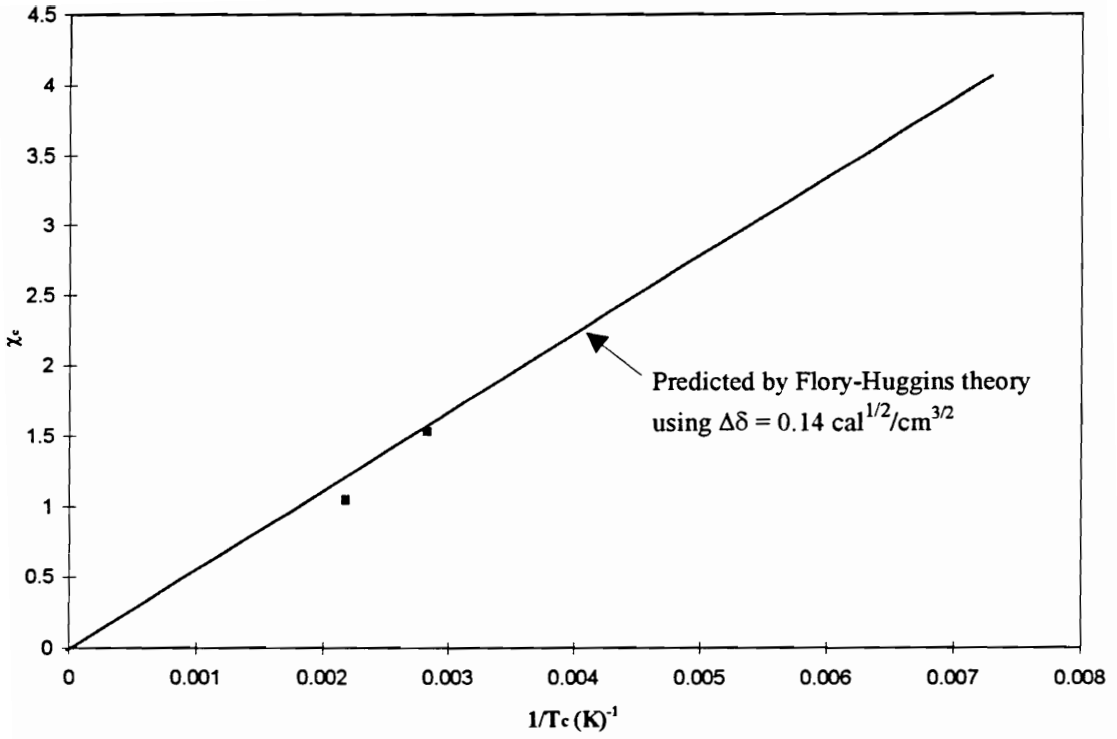

Fig. 4.5 Plot of critical χ, χ_c vs. $1/T_c$

4.3.4 it-PP/it-P1B Blend: Phase Separation and Crystallization (Morphology) Study

4.3.4.1 Optical Microscopy

Optical micrographs of the 30/70 it-PP/it-P1B blend at 200 °C are shown as a function of residence time in the melt state in Fig. 4.6(a-f). The grainy texture observed in Fig. 4.6a clearly indicates that even after a very short residence time in the liquid state, the blend is already phase separated (note that the morphological observations made here did not depend on time in the melt rheomixer for mixing times longer than 3-5 min). For longer residence times in the melt at 200 °C (Fig. 4.6b-f), coarsening of the phase-separated morphology is unambiguously observed. Identical observations were made in a 30/70 it-PP/it-P1B blend prepared by the freeze-drying process of a solution of the same it-PP and it-P1B in *p*-xylene, indicating that sample preparation had little effect on this conclusion (i.e., the freeze-drying and the melt-mixing processes yield a material that is unstable in the liquid state.) However, optical microscopy provides little information on the difference in the initial level of heterogeneity at 200 °C for samples prepared by these two methods. The morphological evolution of the blend in the liquid state undeniably implies that the 30/70 blend is undergoing a process of liquid-liquid demixing at this temperature. From the observation of interconnected domains (see Fig. 4.6a), a liquid-liquid demixing is suspected to occur by a process of spinodal decomposition followed by a breakup of the co-continuous structures and coarsening.

Similar experiments carried out on the 30/70 it-PP/it-P1B blend at other temperatures (i.e. 180, 220, and 250 °C) and on 50/50 and 80/20 it-PP/it-P1B blends at

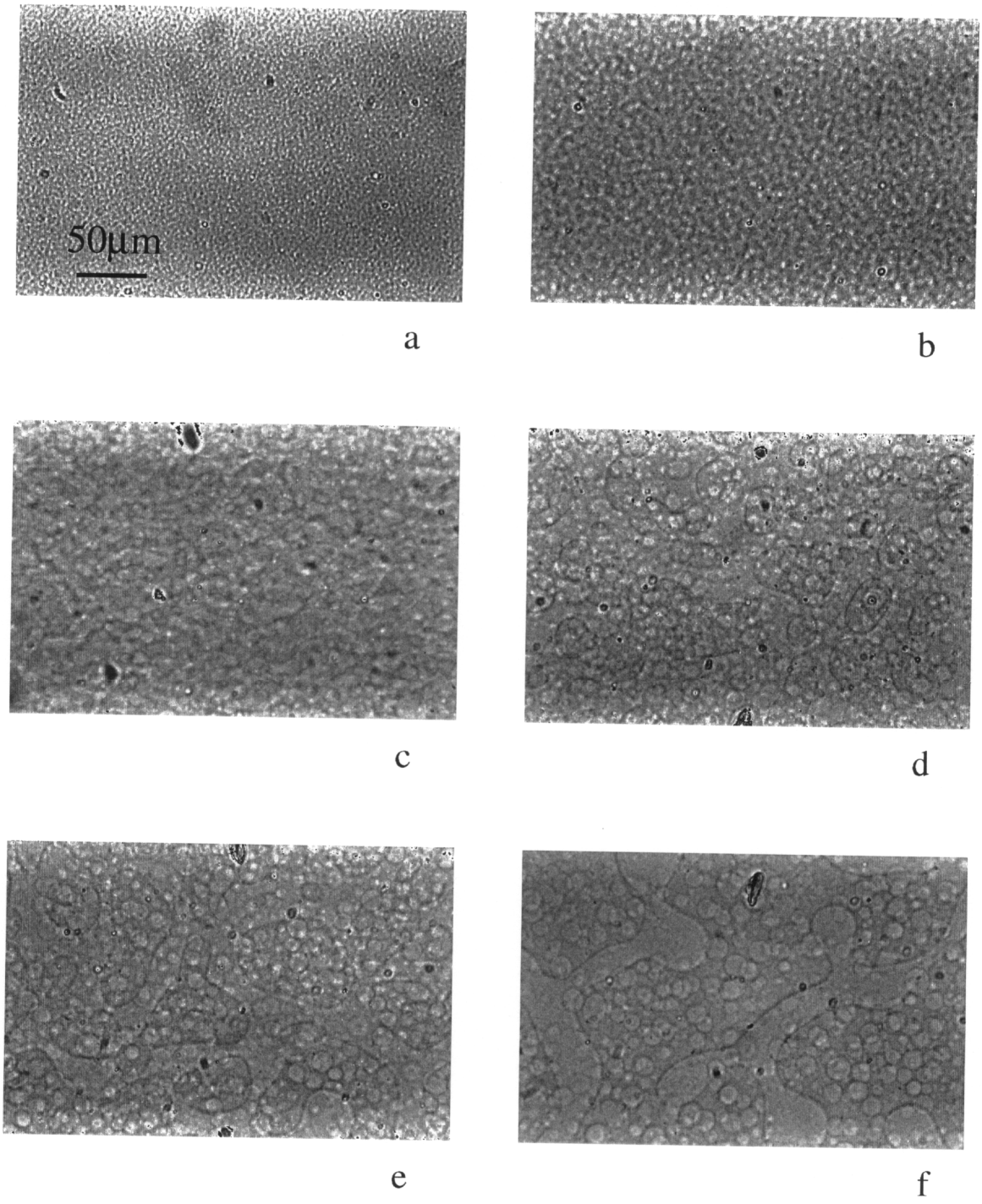

Fig. 4.6 Optical micrographs of a 30/70 it-PP/it-P1B blend at 200 °C for various residence times in the melt: (a) 5, (b) 15, (c) 35, (d) 65, (e) 90, and (f) 180 min.

180 °C yielded the same morphological evolution, suggesting that the upper critical solution temperature (UCST) is located far above the melting temperature of the it-PP component.

In the second series of experiments, the blend was first melted at 190 °C for 3 min and then cooled to 145 °C where optical micrographs were recorded as a function of time. In this temperature range, differential scanning calorimetric observations indicate that the it-PP component crystallizes to its fullest extent over a period of a few hours. Fig. 4.7a-d show the evolution of the blend morphology as a function of residence time at that temperature. Two observations can be made: first, the same grainy structure which was observed in the same blend at higher temperature (Fig. 4.6) is evident at 145 °C (the length scale of these heterogeneities is observed to increase as a function of residence time at 145 °C); second, irregularly shaped spherulites are observed to grow at this temperature in the phase-separated liquid. From these observations, one can conclude that liquid-liquid demixing occurs simultaneously to crystallization and that the patchy nature of the it-PP spherulites, which had been previously observed by Siegmann[4] and Hsu *et al.*[147], results from the crystal growth of the it-PP component through a partially phase-separated liquid.

More detailed observations of the crystal growth process of the it-PP component in the phase-separated liquid are obtained in the next two series of optical microscopy experiments. First, the blend was allowed to undergo demixing at 180 °C for 5 hr prior to quenching to 145 °C where isothermal crystallization was carried out and optical micrographs were recorded as a function of crystallization time between 130 and 210 min (Fig. 4.8b-f). The 5-hr residence time in the melt was chosen so as to obtain large enough

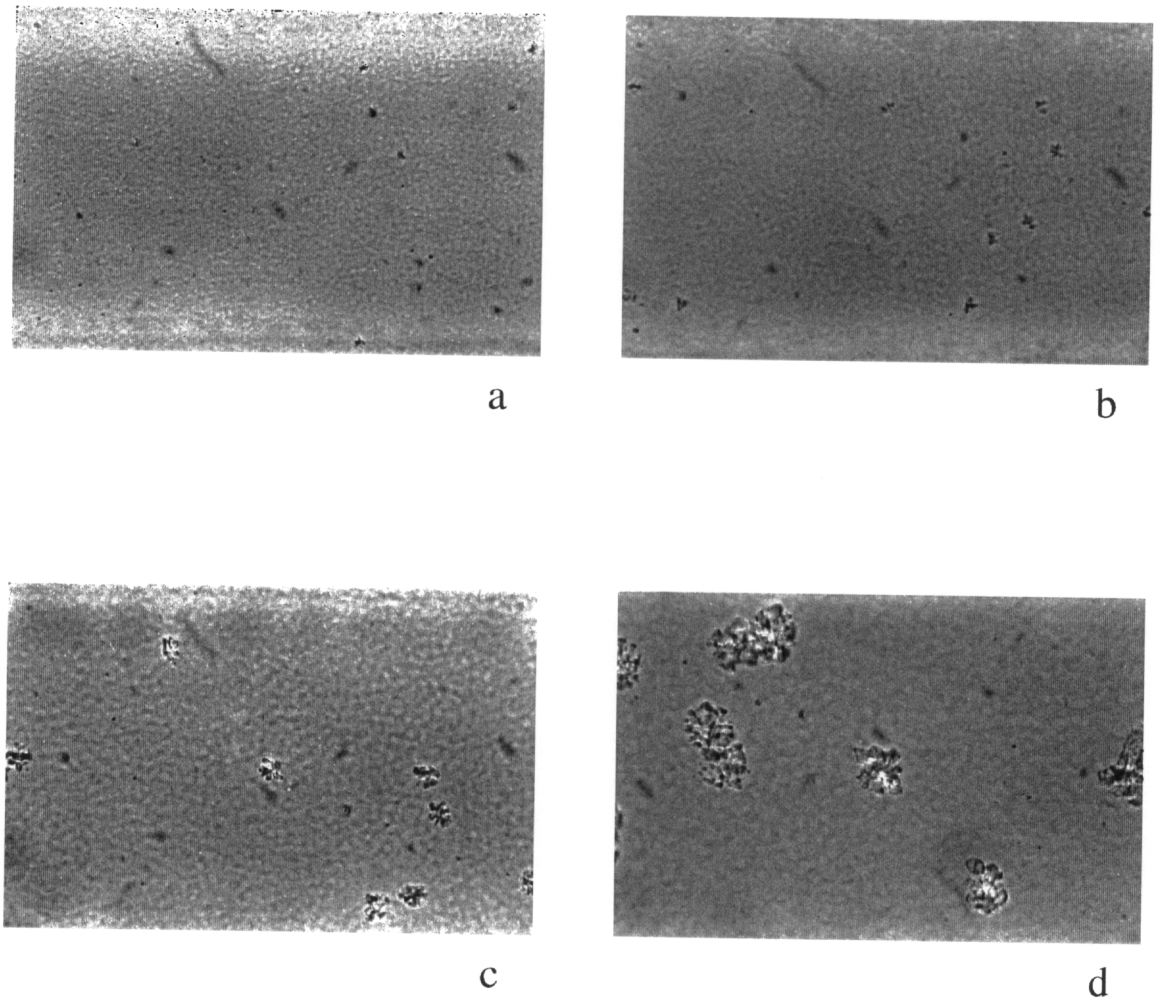

Fig. 4.7 Optical micrographs of a 30/70 it-PP/it-P1B blend at 145 °C for various crystallization times after melting at 190 °C for 3 min: (a) 10, (b) 15, (c) 30, and (d) 62 min (same magnification as in Fig. 4.6a).

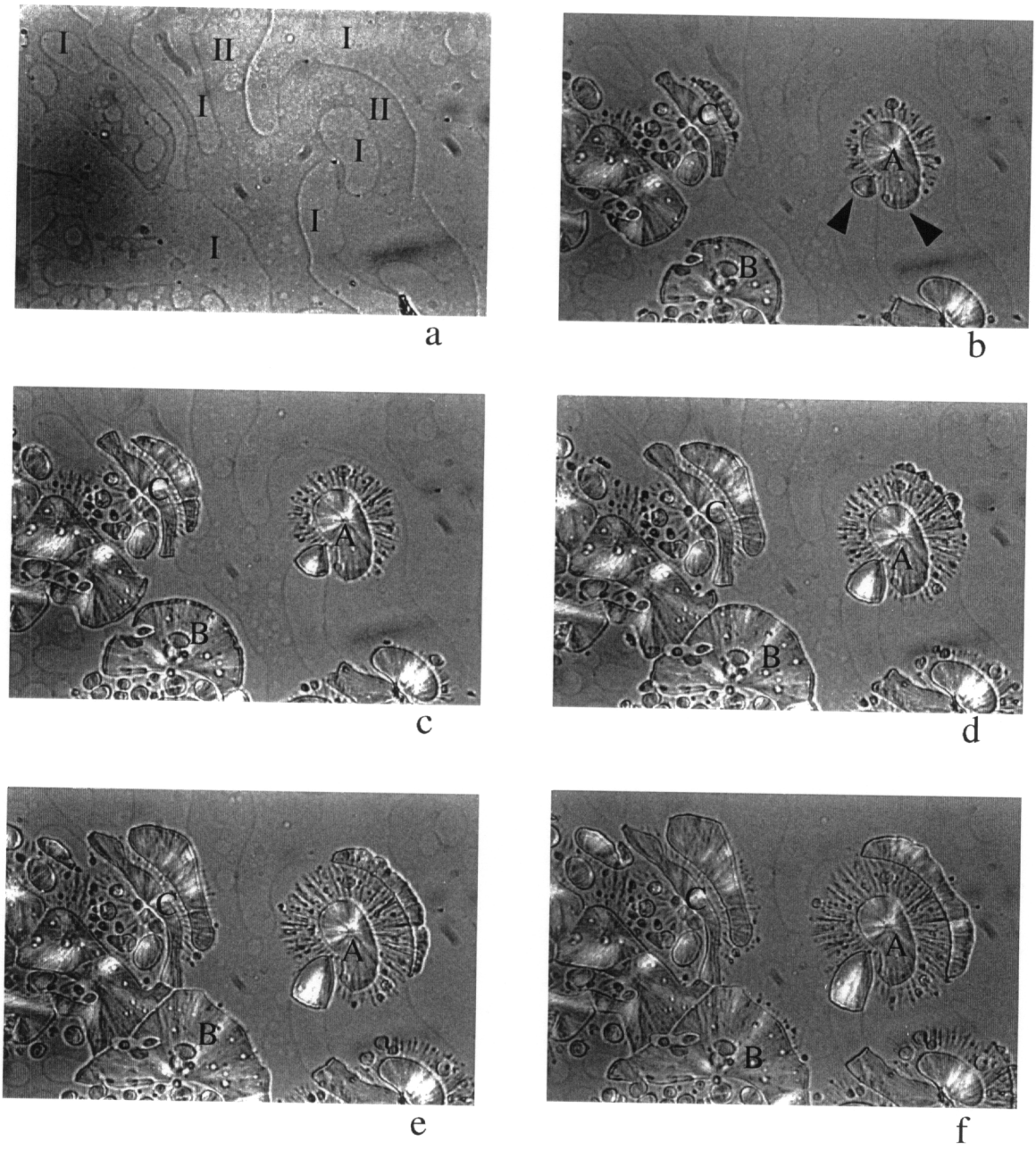

Fig. 4.8 Optical micrographs of a 30/70 it-PP/it-P1B blend (a) after melting at 180 °C for 5 hr and (b-f) for various crystallization times at 145 °C after melting at 180 °C for 5 hr: (b) 130, (c) 150, (d) 175, (e) 195, and (f) 210 min (same magnification as in Fig. 4.6a).

phase-separated domains, while a crystallization temperature of 145 °C was selected so as to minimize nucleation density and to observe the spherulitic crystal growth through multiple liquid phases. Fig. 4.8a represents the same region in the same sample as observed after cooling to 145 °C and should be fairly representative of the morphology of the phase-separated liquid prior to crystallization. To identify the phase-separated domains of similar compositions, the spatial variation in the contrast with composition in this micrograph and the observation of the resulting semicrystalline morphologies shown in the subsequent micrographs of this series were utilized. Two different liquid phases are observed and denoted by I and II (see Fig. 4.8a). Let us focus our attention on the growth process for the three spherulites marked A, B, and C on the various micrographs. Comparison of Fig. 4.8a with Fig. 4.8b-f indicates that the it-PP spherulites always nucleated in the same phase (liquid phase I on Fig. 4.8a). When crystal growth occurs within this phase (regions of spherulite A in Fig. 4.8b-f indicated by the arrows and spherulite B in Fig. 4.8b-e), the texture of the spherulite is almost identical to that observed for pure it-PP. On the other hand, when crystal growth occurs within the liquid phase II, a much more open spherulitic texture is observed and the crystal growth rate is slightly lower than that in liquid phase I (the ratio of the spherulitic growth rate in phase I to that in phase II at 145 °C is equal to 1.4 ± 0.2). In Fig. 4.8b-f, spherulites A is observed to grow successively through liquid phases I, II and I. Spherulite C is observed to cross the I $\leftrightarrow$ II liquid-liquid interfaces.

Furthermore, observation of the same region of this sample under cross polarization conditions (Fig. 4.9) indicates that crystal growth within the liquid phase I

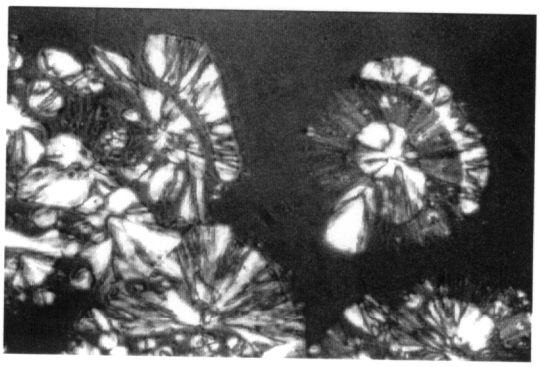

Fig. 4.9 Polarized optical micrograph of a 30/70 it-PP/it-P1B blend crystallized at 145 °C for 210 min after melting at 180 °C for 5 hr (same area as in Fig. 4.8f and same magnification as in Fig. 4.6a).

results in a morphology that produces more optical retardation than the morphology obtained by crystal growth in liquid phase II.* Examination of Fig. 4.9 also suggests that, at 145 °C, the average radial direction of crystal growth is preserved during the crossing of the various liquid-liquid interfaces. Since spherulitic growth of the it-PP component proceeds continuously through both liquid phases without a large change in the growth rate, one must conclude that both liquid phase I and liquid phase II contain a non-negligible volume fraction of the it-PP component. The observation of higher nucleation density, slightly faster crystal growth, and higher optical retardation in liquid phase I than in liquid phase II strongly suggests that liquid phase I is the it-PP-rich phase whereas liquid phase II is the it-P1B-rich phase. This statement finds further support from the observation that the overwhelming majority of the small droplets observed in Fig. 4.8a are of the liquid phase I type, as would be expected for the minor component (it-PP of a 30/70 (it-PP/it-P1B) blend. One should also note that the crystal growth rate through these phases is linear, indicating that there is no significant rejection of the it-P1B component in the interspherulitic liquid. The melting behavior of the sample crystallized at 145 °C for 210 min (Fig. 4.8f) is shown through a succession of optical micrographs taken during at a rate of 5 °C/min (Fig. 4.10a-f). This sequence of micrographs clearly indicates that the it-

* Note that the lower optical retardation of spherulitic crystals growing in liquid phase II does not arise from a shorter optical path in the liquid phase II (it-PP-rich phase) as this phase is the major phase. The lower optical retardation is due to a lower crystallinity in this phase.

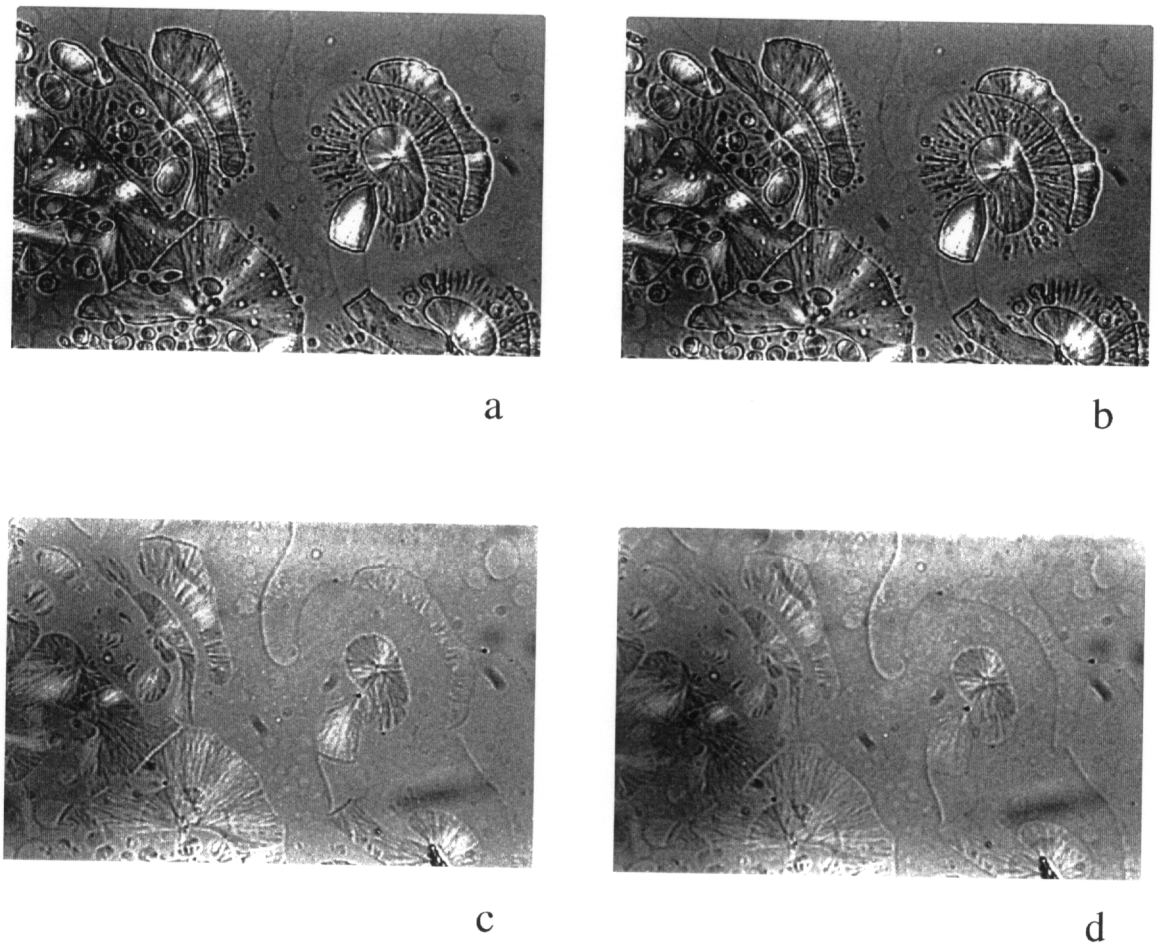

Fig. 4.10 Optical micrographs of a 30/70 it-PP/it-P1B blend at various temperatures during heating from 145 to 180 °C at a rate of 5 °C/min.
This sample was isothermally crystallized at 145 °C for 210 min after residing at 180 °C for 5 hr (same region as on Fig. 4.8 and 9): (a) 155, (b) 165, (c) 172, and (d) 173 °C (same magnification as in Fig. 4.6a).

PP crystals grown from the it-P1B-rich liquid phase melt about 8-10 °C below those formed in the it-PP-rich liquid phase. The observation will be further discussed in the context of the DSC studies.

Spherulitic growth has also been studied at a crystallization temperature of 130 °C after a 5-hr residence time in the melt at 180 °C. Optical micrographs recorded at various crystallization times are showed in Fig. 4.11a-d. The it-PP crystallization behavior is similar to that observed at higher crystallization temperature, with the difference that crystal growth rates in the two liquid phases are now of different magnitude. The spherulitic growth rate is estimated to be 4.4 ± 0.4 times faster in the it-PP-rich phase than in the it-P1B-rich phase at 130 °C. Note that for the same residence time and temperature in the melt, crystallization at 135 °C is 2.6 ± 0.6 times faster in the it-PP-rich phase than in the it-P1B-rich phase. These observations indicate that the difference in it-PP crystal growth rate between the it-PP-rich phase and the it-P1B-rich phase increases with decreasing crystallization temperature. Furthermore, at a crystallization temperature of 130 °C, the population of it-PP crystals growing in the it-P1B-rich phase is smaller than that observed at the higher crystallization temperature. This observation is consistent with reports of a lower crystallinity for the it-PP component in blends crystallized at lower temperatures or under rapid cooling conditions[4,5,147]. It is also consistent with predictions from the solidification (Erstarrung) model proposed by Fischer and co-workers[190,191] or from crystal growth processes in regime III[192,193], in which the crystallization of the it-PP component does not result in large-scale reorganization or long-range diffusion of the it-P1B molecules at the crystal growth front. Variation in the blend morphology during

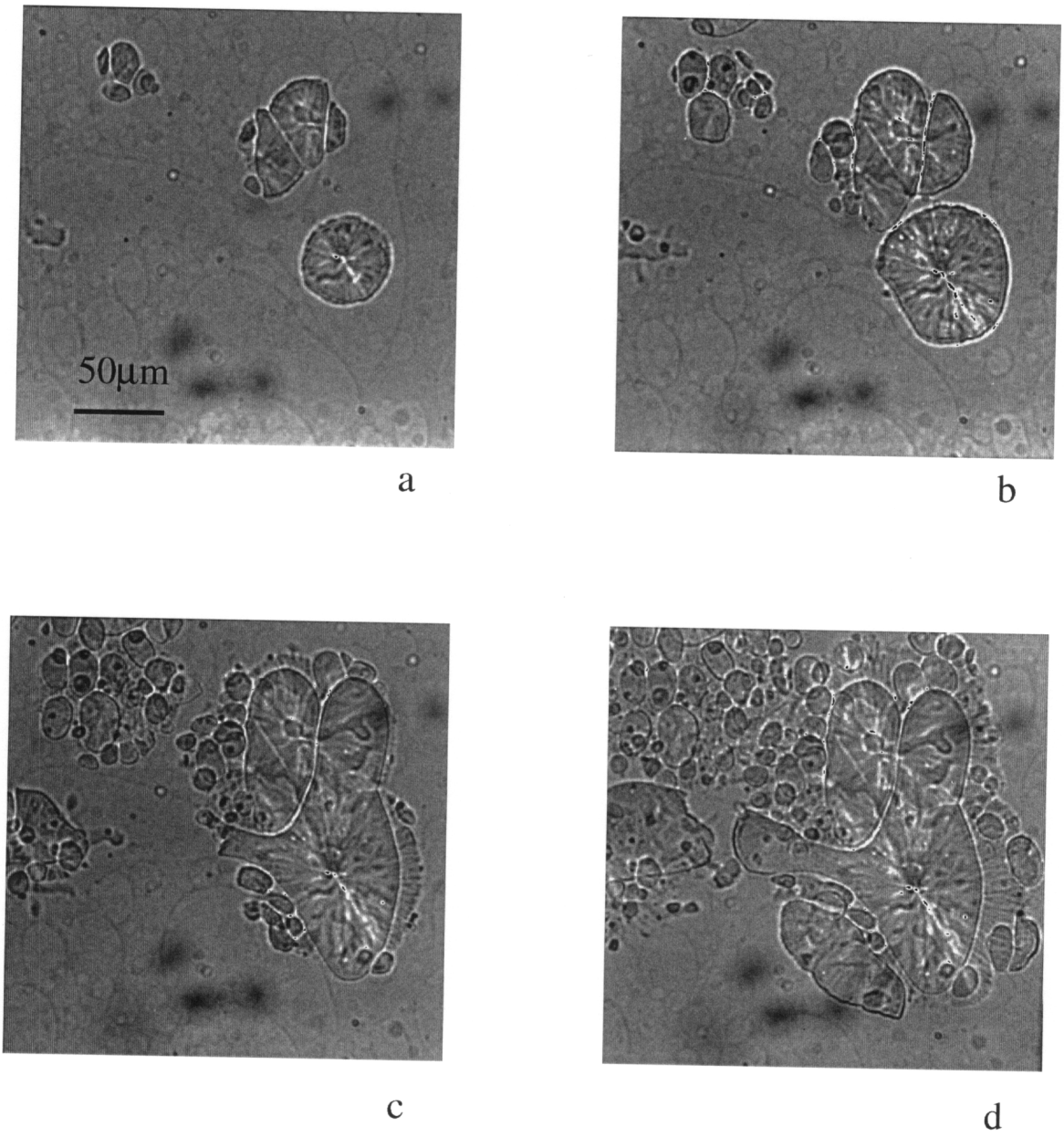

Fig. 4.11 Optical micrographs of a 30/70 it-PP/it-P1B blend as a function of crystallization time at 130 °C after a 5-hr residence time in the melt at 180 °C: (a) 3.25, (b) 5.25, (c) 8.75, and (d) 12 min.

heating of the 30/70 it-PP/it-P1B blend crystallized at 130 °C is shown in Fig. 4.12a-c for different temperatures above the crystallization temperature. As mentioned above, the population of it-PP crystals is smaller in the it-P1B-rich phase than in the it-PP-rich phase, and observation of the melting of the former crystals is thus more delicate. Inspection of Fig. 4.12a-c however suggests that crystals formed in the two liquid phases melt at approximately the same temperature.

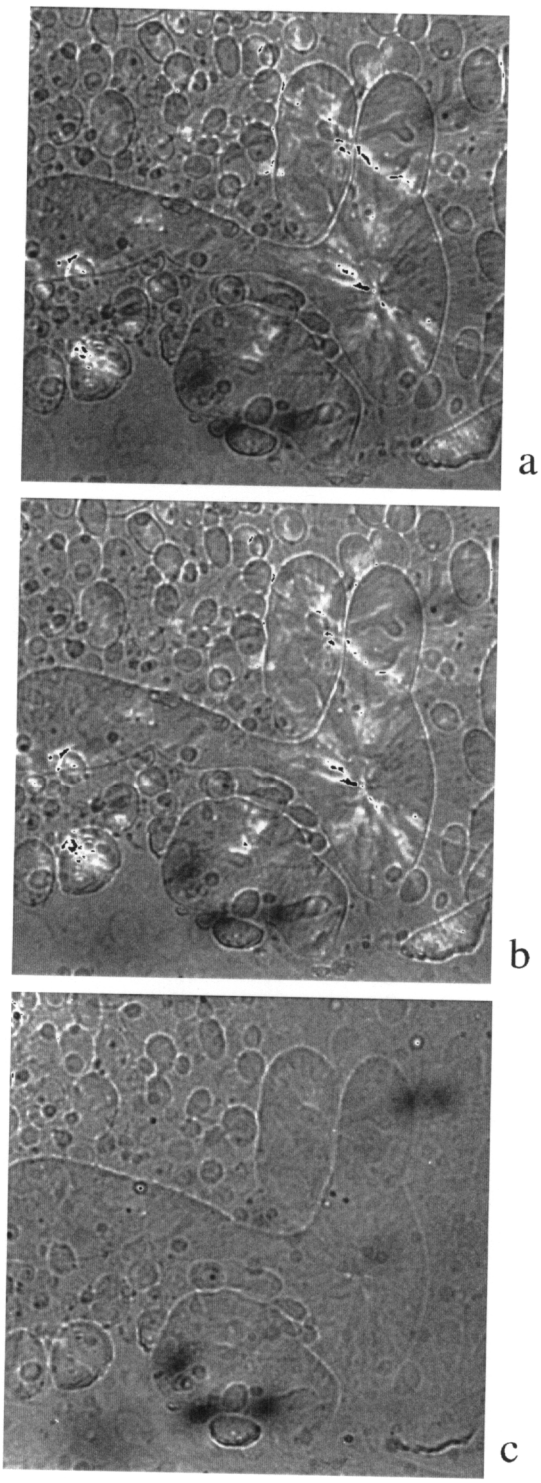

Fig. 4.12 Optical micrographs of a 30/70 it-PP/it-P1B blend during heating at 5 °C/min from a crystallization temperature of 130 °C (a) 156, (b) 159.5, and (c) 164.5 °C.

4.3.4.2 Scanning Electron Microscopy

Fig. 4.13 shows SEM micrographs of three samples that were prepared under similar conditions with the exception of increasing residence time in the melt. Comparing Fig. 4.13a-c, an increase in the coarseness of the fractured surface can clearly be seen. Such an increase in coarseness must be associated with an increase in the size of the it-P1B phase that is extracted. This observation confirms the occurrence of phase separation in the liquid state at temperatures above the melting of the it-PP component. The phase sizes determined by examination of the SEM micrographs compare very well with those observed in the optical microscopy study (Fig. 4.6a-f). This observation also suggests that under quenching conditions, no significant long-range diffusion or rejection of either component is brought about by the rapid crystallization process. It also indicates that the morphology produced by liquid-liquid demixing in a relatively thin film (ca. 50 μm thick) is similar to that observed in bulk samples, as long as the average phase size is less than the film thickness. In later stages of demixing, the phase-separated morphology observed by optical microscopy (Fig. 4.6d-f) seems to evolve more slowly, probably as a result of surface tension effects at the film/substrate interface.

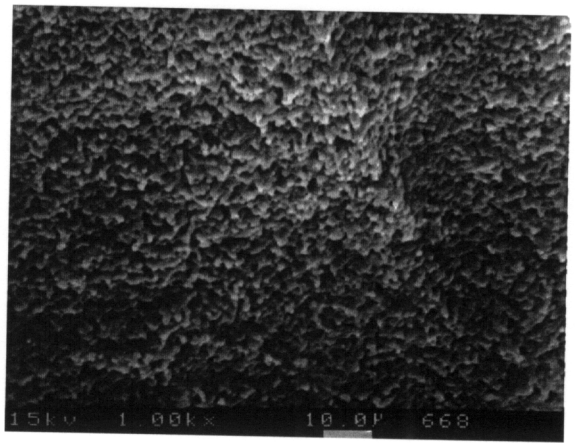

a

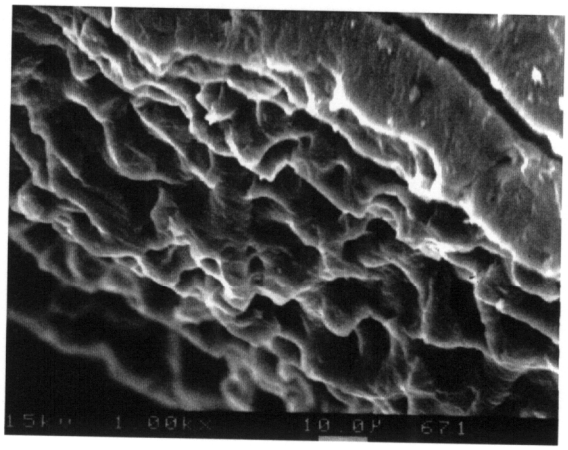

b

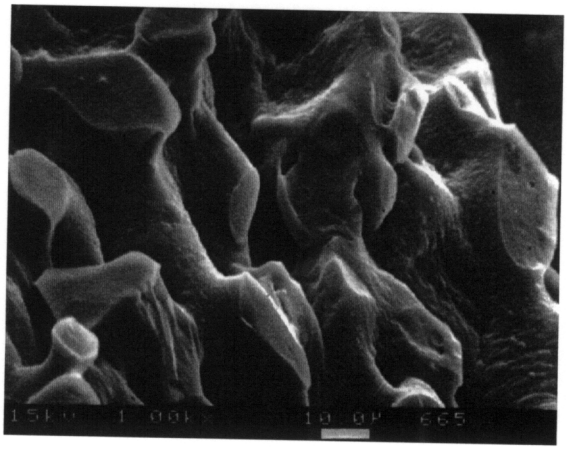

c

Fig. 4.13 Scanning electron micrographs of the freeze fracture surfaces of it-PP/it-P1B blends quenched from the melt after various residence times in the melt: (a) 1, (b) 30, and (c) 60 min.

4.3.4.3 Differential Scanning Calorimetry

Fig. 4.14 and Fig. 4.15 show the melting behavior observed by differential scanning calorimetry for the pure it-PP and for the it-PP component in the 30/70 it-PP/it-P1B blend after isothermal crystallization at 130 and 145 °C, respectively. In previous reports[150,180,194], observations of the melting behavior of it-PP in blends of various compositions were discussed but in the following the focus will be concentrated only on the 30/70 blend. Although the melting curves for the pure it-PP and the blend crystallized at 130 °C exhibit the same general shape, some slight but significant differences must be noted. Specifically, the DSC heating trace for the blend is characterized by a broader endotherm and a slightly lower melting temperature than that of the pure it-PP homopolymer. The slight depression in the observed melting temperature and the broadening in the endotherm of the blend sample may be interpreted as arising from the melting of a distribution of lamellar it-PP crystals formed from liquid phases of various compositions. Recalling the morphological findings for the 30/70 blend crystallized at 130 °C, it can be expected that (1) a smaller contribution to this endotherm form the melting of crystals formed within the it-P1B-rich phase and (2) crystals formed in these two liquid phases to melt at about the same temperature.

On the other hand, heating traces of samples crystallized at 145 °C exhibit very notable differences in the shape of the melting endotherm. The multiple-melting behavior exhibited by the 30/70 blend crystallized at 145 °C is consistent with the optical micro-scope observation of clearly distinct melting temperatures for it-PP crystals formed in the

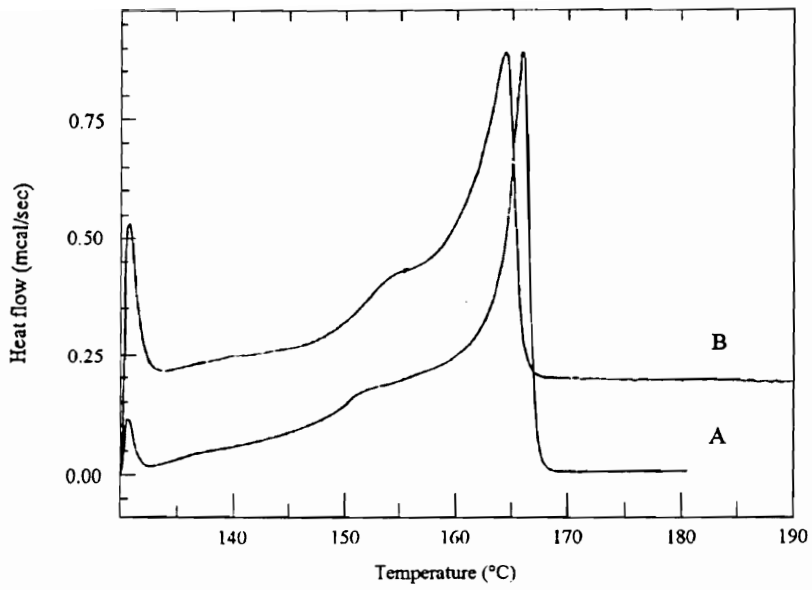

Fig. 4.14 Heating traces (A) of pure it-PP and (B) of a 30/70 it-PP/it-P1B blend isothermally crystallized at 130 °C for 30 min residing for 3 min in the melt at 180 °C.

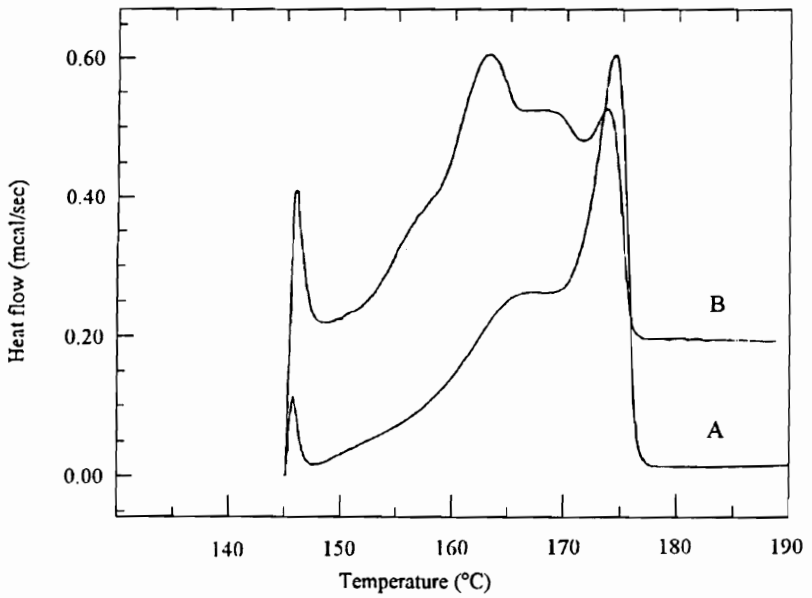

Fig. 4.15 Heating traces (A) of pure it-PP and (B) of a 30/70 it-PP/it-P1B blend isothermally crystallized at 145 °C for 4 hr after a 3-min residence in the melt at 180 °C.

it-PP-rich and it-P1B-rich liquid phases, respectively. The temperature interval between the two main endothermic peaks in the DSC thermogram is determined to be 10 °C, which is very close to that observed visually in the optical microscopy study. One should also note that the temperature interval between these two melting transitions is approximately independent of either crystallization time or residence time in the melt. Also note that the relative ratio of these two endotherms is qualitatively consistent with the volume fraction of crystals formed in the it-PP- and it-P1B-rich phases (Fig. 4.8f).

One must now attempt to explain the observed variation with crystallization temperature. First, at 145 °C the crystal growth process is slower than at 130 °C and may provide enough time for the growing front of a given it-PP lamella to extract it-PP chains from the it-P1B-rich liquid phase. The observation of a linear but different growth rate in each phase indicates that the it-P1B component is rejected into the interlamellar or interfibrillar regions of the growing spherulites and not in the interspherulitic melt. At lower crystallization temperatures, the thermodynamic driving force toward crystallization is higher and it is likely that only the it-PP chains in the direct vicinity of the lamellar crystal front are able to crystallize. This diffusion-controlled process has been previously reported for semicrystalline polymer blends exhibiting miscibility in the liquid state[195,196]. The variation in the population of it-PP crystals in the it-P1B-rich phase may also be partially accounted for by considering the UCST character of this polymer blend. Since crystallization processes are studied at temperatures well below the spinodal, one may anticipate that at the time of crystallization, the liquid phases have already reached the compositions given by the binodal points. Consequently, at 130 °C the it-P1B-rich

domains are more depleted in the poly(propylene) component than at 145 °C, and the variation in it-PP crystal growth rate with temperature in the two liquid phases reflects differences in melt composition. In mixtures of immiscible polymers such as poly(ε-caprolactone)/atactic poly(styrene)[141,142,197], phase separation results in a very low degree of phase mixing and prevents the crystallization to proceed through the liquid-liquid interfaces.

One should also point out that the difference between the observed melting temperatures or the spherulitic growth rates for the it-PP crystals grown in the it-P1B-and it-PP-rich liquid phases cannot be accounted for by the thermodynamic argument of an equilibrium melting temperature depression but must be related to different morphological features of the lamellar crystals growing in different environments. By assuming that the value of χ for the it-PP/it-P1B blends is of the same magnitude as that obtained from the solubility parameter difference between at-PP and at-P1B through determination of the critical temperature (i.e., $\Delta\delta = 0.14$ cal$^{1/2}$/cm$^{3/2}$ or $\chi = 0.0012$ at 85 °C), the Flory-Huggins theory yields a depression in the equilibrium melting temperature of it-PP crystals of much less than 1 °C, even when assuming that the it-P1B-rich phase contains only 5 wt % it-PP. It is interesting to note that in previous studies of the crystallization behavior of isotactic poly(propylene), from miscible blends of isotactic poly(propylene) with either atactic poly(1-butene) or atactic poly(propylene)[194], similar melting temperature depressions were observed for the it-PP component. Hoffman-Weeks analysis of it-PP/at-P1B blends, however, suggested that the depression was due to morphological effects since the T_m' vs. T_x curves for various blend compositions appeared to merge at the highest crystallization

temperatures. One should further point out that the multiple-melting behavior in the it-PP/it-P1B system cannot be accounted for by a melting recrystallization behavior, as rates of crystallization become exceedingly low in the temperature range where the initial melting is observed. On the basis of X-ray diffraction studies, one can also rule out the possibility for various crystal structures[180] or even co-crystallization between poly(propylene) and poly(1-butene) to be at the origin of the multiple-melting behavior[147,180].

4.3.4.4 Dynamic Mechanical Analysis

In view of the above findings and of the existing controversy in the literature, dynamic mechanical analyses for the pure it-PP and it-P1B homopolymers and for the 30/70 it-PP/it-P1B blend were conducted. Details of the experiments can be found in Lee's master thesis[180]. Quenched samples were used for this study so as to minimize the degree of crystallinity and to maximize the variation in loss modulus in the glass transition region. DMA traces for the pure it-PP, the 30/70 it-PP/it-P1B blend, and the pure it-P1B are shown in Fig. 4.16. The loss peak for the it-PP/it-P1B blend is clearly located between those of the pure polymers. The glass transition temperatures for the it-PP/it-P1B blend and the it-P1B and it-PP homopolymers are determined at the maximum of the loss modulus peak and have values of −11, −19, and +6 °C, respectively. On this basis alone, one might have concluded, in agreement with previous studies[4,5,144], that these two polymers form a miscible mixture. Since the above morphological observations prove that they are partially miscible, the DMA data must be reexamined from a different point of view. In a heterogeneous blend, each phase should exhibit an individual glass transition

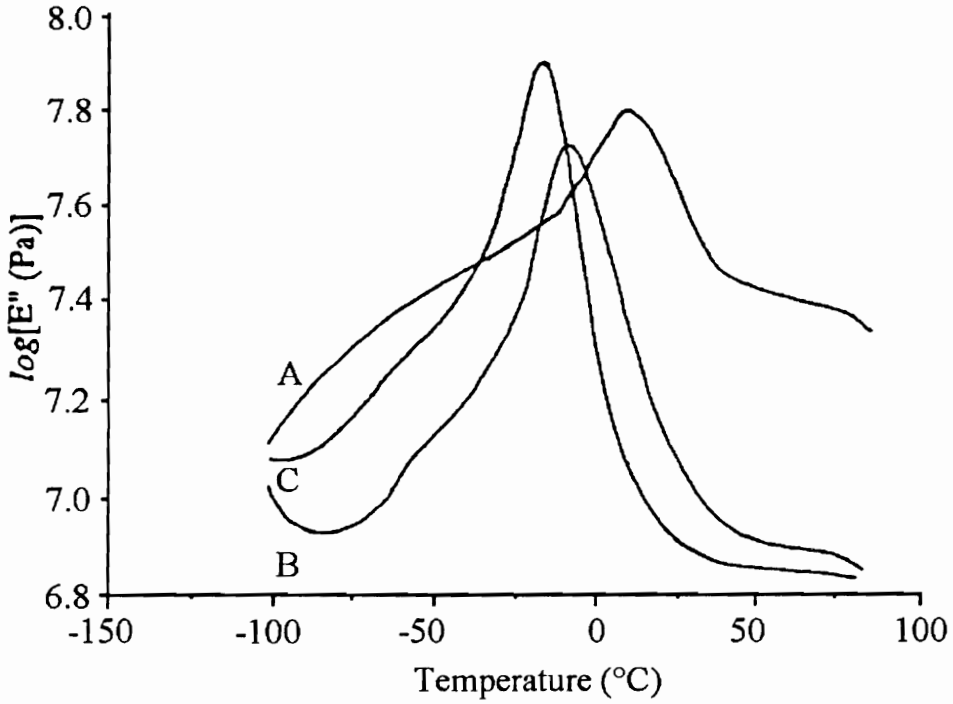

Fig. 4.16 Dynamic mechanical analysis of (A) pure it-PP, (B) a 30/70 it-PP/it-P1B blend, and (C) pure it-P1B. (adapted from ref. 180)

temperature whose value may be estimated by the Fox equation[198,199] using values for the phase composition and for the T_g of each homopolymer. The fact that a single glass transition is observed for the blend in the plot of loss modulus vs. temperature may then be interpreted as follows. Recalling that crystal growth was observed for the it-PP crystals through both liquid phases, one concluded that there must be a significant degree of molecular-level mixing within each liquid phase. The glass transition temperature of each phase may then be intermediate between those of the pure components, with a temperature slightly lower for the it-P1B-rich phase than for the it-PP-rich Phase. Noting that the glass transition temperatures of the pure homopolymers only differ by 10 °C, those of the phase-separated regions will be even less distant from one another and may not be readily resolvable by the DMA technique. One may further add that in the quenched blend used for the DMA study, liquid-liquid demixing was allowed to proceed for much shorter times than in the optical microscope study from which we inferred a significant degree of phase mixing. One may also envision that for very short residence times in the melt (5 min), the liquid-liquid demixing process produces liquid phases that may not have yet reached their equilibrium binodal concentrations. If such is the case, the liquid phases would exhibit a higher degree of phase mixing than predicted from the binodal values and their glass transition temperatures would be even closer and more difficult to resolve than in blends that would undergo a larger extent of demixing.

Finally, these observations provide an impetus to study the origin of the appealing mechanical properties of these blends. Studies of the crystal growth and melting behavior of the it-PP component in these blends and examination of the dynamic mechanical

properties suggested high degrees of molecular-level mixing within each of the two liquid phases. It would be of interest to compare the dynamic mechanical or the tensile behavior of blends crystallized at a given temperature but after different residence times in the melt. One would predict that for longer residence times in the melt, further demixing would occur and the interphase boundary would become sharper. In blends that have undergone larger extents of demixing, one may also be able to resolve two individual glass transitions by DMA as is suggested from a simple superposition of the loss modulus curves for the pure homopolymers.

4.3.4.5 Further Discussion

Having discussed the various observations made in this study of it-PP/it-P1B blends and proposed a plausible interpretation of the data, these results should be examined in the light of similar experiments carried out by Inaba *et al.*[200,201] They studied the liquid-liquid demixing in 50/50 and 70/30 w/w mixtures of it-PP and ethylene-propylene copolymers (EPR) by a combination of polarized and depolarized light scattering and optical microscopic techniques. Inaba *et al.*[200,201] showed that rapidly crystallized blends exhibit a memory of the liquid-liquid demixing process occurring before crystallization. The "structure memory" was characterized as a function of demixing time in the liquid by a time-dependent wavelength, Λ_m, for the periodic spatial concentration fluctuation resulting from the spinodal decomposition and the subsequent coarsening processes. Under conditions of rapid crystallization, the liquid-liquid phase-separated structures obtained by melt demixing are locked in by the crystallization process.

Spherulitic growth of the it-PP component after a 3-min residence time in the melt at 200 °C was observed to take place linearly as function of crystallization time at low temperature (140 °C) but nonlinearly at higher crystallization temperature (145 °C). Furthermore, identical spherulitic growth rates for the 70/30 and the 50/50 blends were measured at 140 °C and suggest that each domain in the demixing mixtures already reached the equilibrium concentration determined by the binodal points at 200 °C. The experimental observation of liquid-liquid demixing and locking in of the liquid-liquid phase-separated morphology by the crystallization process described in this paper for the 30/70 it-PP/it-P1B blend are consistent with the conclusions drawn by Inaba *et al.* on the it-PP/EPR blend.

However, differences are noted in the crystallization behavior of the it-PP component in these two different blends. Whereas the effect of crystallization temperature on the crystal growth behavior of poly(propylene) was observed in both liquid phases, Inaba *et al.* only described the crystallization of it-PP in the poly(propylene)-rich phase (the major phase in their 50/50 or 70/30 blends). In contrast with their observation of a nonlinear spherulitic growth behavior at 145 °C, the observations in this study indicate that the crystal growth behavior is linear throughout, until impingement. Furthermore, it was felt that the decrease in crystal growth rate for the it-PP component with increasing it-P1B content in a given liquid phase is not due to a depression of the it-PP equilibrium melting temperature but simply to the lower concentration of crystallizable polymer chains at the lateral melt/crystal interface. From this observation of a temperature dependence of the ratio of crystal growth rates in the two liquid phases, it is suggested that the

composition is given by the binodal curve at the crystallization temperature and not at the melting temperature. Whether these equilibrium concentrations are reached before the crystallization is initiated or at early stages during the crystallization process will certainly depend on the crystallization temperature and the associated rates of crystal nucleation and growth. This suggestion is supported by the fact that the experimental range of crystallization temperatures is located at least 100 °C below the spinodal temperature. Under such demixing conditions, the early and intermediate stages[202] of phase separation must be relatively fast[200] and should lead to a rapid establishment of the equilibrium composition within each phase. One should further note that the scaling exponent appearing in the power law between the scattering vector, q_m associated with the dominant fluctuation, Λ_m, and the demixing time is reported by Inaba *et al.* to vary between 1/3 and 2/3. Such an exponent value indicates that the demixing has already entered the transition stage[202] for residence times in the melt as short as a few seconds and has already resulted in liquid phases exhibiting equilibrium compositions.

These observations lead to the following questions about the level of phase mixing achieved during the blending process. How does the shearing process during the blending affect the UCST, and what is the time scale necessary to achieve equilibrium compositions within the phase-separated liquid? What is the time scale for the readjustment of the composition of each phase after a deep quench from the melting temperature to a crystallization temperature located at least 100 °C below the spinodal temperature? This study suggests that the composition within each liquid phase depends on the temperature reached after the deep quench, but further liquid-liquid demixing upon reaching the

various crystallization temperatures was not observed. What is the temperature dependence of this "relaxation" process?

4.4 Summary of Results

For the at-PP/at-P1B blend system, miscibility studies by DSC show a UCST behavior. Phase diagram of the 87K/48.5K at-PP/at-P1B blend is obtained with the same approach. This experimental results show a reasonable agreement with that predicted by the Flory-Huggins theory. By assuming that the χ parameter for the it-PP/it-P1B blend has the same magnitude as that obtained from the solubility parameter difference between at-PP and at-P1B through determination of the critical temperature, it can predict that the equilibrium melting temperature depression of the it-PP crystals grown from it-PP/it-P1B blends will be negligibly small.

Optical microscopic observations of a 30/70 w/w/ it-PP/it-P1B blend in its liquid state indicate that this mixture is not fully miscible at the molecular level at temperatures as high as 80 °C above the it-PP melting temperature. These observations were confirmed by SEM studies of the fracture surface of quenched blend samples. At a crystallization temperature of 145 °C, the spherulitic growth of it-PP spherulites is observed to proceed continuously, with a slightly decreasing rate (1.4 times slower), from the it-PP-rich liquid phase into the it-P1B-rich liquid phase. Crystals formed in the it-P1B-rich phase are observed to melt about 8-10 °C below the crystals formed in the it-PP-rich phase. This fact is consistent with the complex multiple-melting behavior of poly(propylene) in it-

PP/it-P1B blend observed by calorimetric measurements. For a lower crystallization temperature (130 °C), the rate of crystal growth in the it-PP-rich liquid phase is about 4.4 times greater than in the it-P1B-rich phase. A similar melting behavior for pure it-PP and the it-PP component in the blend is observed which is partially accounted for by a decrease in the population of it-PP crystals formed in the it-P1B-rich phase at lower crystallization temperatures. The observation of a single DMA loss modulus peak in quenched it-PP/it-P1B blends is explained in terms of a process of macrophase separation which results in retention of a notable degree of phase mixing and which may not have reached the stage where the composition of the liquid phases becomes invariant. This study suggests that the excellent mechanical properties of it-PP/it-P1B mixtures arise primarily from the high degree of phase mixing in the macrophase-separated blend, together with the structural connectivity provided by the continuation of crystallization between the two phases.

5. CONCLUSIONS

The roles of the ethylene co-unit on the crystallization, melting and polymorphic behavior of propylene-ethylene copolymers have been discussed in Chapter 3 based on the experimental results in this study. In summary, the ethylene co-unit has the effects of increasing γ-phase content and lowering the crystallization and melting temperatures of the propylene-ethylene copolymer system. The second and third effects mentioned above can have direct impacts during polymer processing. Adjustments will have to be made for the processing parameters in order to accommodate the changes caused by the ethylene co-unit. For example, a propylene-ethylene copolymer sample would require a processing temperature similar to that for a homopolymer sample with a similar molecular weight (in order to be processed at the similar melt viscosity). The lower crystallization temperature of the copolymers as compared with that of the it-PP homopolymer results in an increase in the production time and is therefore undesirable. The lower crystallization temperature also results in a lower melting temperature. This implies that the sample will soften at lower temperatures and therefore limits the usable temperature range above room temperature. This negative effect can sometimes be compromised by adding nucleation agents to the system to accelerate the crystallization.

As demonstrated in Chapter 3, the significance of γ-phase is negligible at fast cooling. Although this should be the case during processing in industry, the existence of γ-phase in the copolymer system should not be neglected. For example, thick components processed by injection molding exhibit higher temperatures at the inner portion of the

components for longer periods of time. Under this scenario, a significant amount of γ-phase can form at the center of the components and causes inhomogeneity within the components. On the other hand, the existence of γ-phase crystals in the products may be beneficial in certain applications. Since the γ-phase poly(propylene) crystal transforms into α-phase under deformation, this transformation may absorb some of the deformation energy and delay the fracture of the sample.

It should be emphasized that, while the suggestions above seem reasonable, all of these require verifications by further studies.

The miscibility study of poly(propylene)/poly(1-butene) blend in Chapter 4 clearly demonstrates the two phase nature of this system. The high degree phase mixing in this macrophase-separated blend and the inter-connectivity of the lamellar crystals between the two phases explain the excellent mechanical properties of the it-PP/it-P1B mixtures.

Even though the it-PP/it-P1B blend shown in this study is the first polymer blend system for which an inter-connectivity between phases to occur through lamellar crystals is reported, it suggests a new direction for designing of phase separated but highly compatible polymer blends.

6. SUGGESTED FUTURE WORK

One of the unanswered questions for the propylene-ethylene copolymers is concerned with the level of ethylene inclusion in γ-form crystals. Since it is quite clear that the ethylene co-unit content plays a critical role in the γ-phase formation, it should be even more important to learn about the location of the ethylene co-unit in order to have a better understanding of its role in the formation of the γ-phase. Does it help to form the fold surface for the γ-form crystal? Does it give better matching along the contact plane between two non-parallel chains?

This study indicates that pure γ-form samples can be obtained from propylene-ethylene copolymers for high ethylene content and at high crystallization temperatures. By measuring the crystallinity (WAXD), heat of fusion (DSC) and lamellar thickness (SAXS) for a series of pure γ-form samples with different ethylene contents, equation (2.11) and (2.12) can be used to test whether Sanchez and Eby's inclusion model is appropriate for the γ-phase.

For the lamellar thickness measurement, since there might be a broad lamellar thickness distribution for the γ-phase crystals, a more direct measure of the lamellar thickness through transmission electron microscopy (TEM) should also be used.

For poly(propylene)/poly(1-butene) blends, the phase diagram of the atactic blend was established in this study. It has also been shown that at high molecular weight, the isotactic materials are not fully miscible at molecular level. The prediction in miscibility

based on the Flory-Huggins theory was also made for it-PP/it-P1B blend at high molecular weights. This prediction was made under the assumption that the miscibility behavior is the same in the atactic and isotactic materials. As mentioned in Chapter 2, tacticity has a significant effect on miscibility for polymer blend systems with specific interactions. Even for systems without any specific interaction, tacticity effect still cannot be totally neglected. Therefore, future study to resolve this question for the poly(propylene)/poly(1-butene) blend system should be considered.

This study can be developed in two directions. First, phase behavior of it-PP/it-P1B blend with a lower molecular weight shall be investigated. As compared with the isotactic blends with high molecular weight, the phase separation and competition between crystallization and phase separation will be different. Secondly, similar experiment can be conducted with a it-PP/at-P1B blend with a similar molecular weight. By comparing the two, one should be able to tell the importance of tacticity in this system.

It has been shown in Chapter 4 the mechanical behavior of the 30/70 it-PP/it-P1B blend in DMA experiments. It would be worthwhile to perform further mechanical testing based on the dependence of phase size on residence time in the melt. Recalling that both SEM and optical micrographs showed the phase size increases with residence time in the melt, DMA experiments based on this finding should be conducted, to evaluate if there is a change in the level of phase mixing during coarsening: change that would be evidenced by an evolution in the blend's tan δ around T_g.

7. REFERENCE

1. McMillan, F. M. The chain straighteners: Fruitful innovation: the discovery of linear and stereoregular synthetic polymers. London: MacMillan, 1979.
2. Pino, P. and Moretti, G. "The impact of the discovery of the polymerization of the α-olefins on the development of the stereospecific polymerization of vinyl monomers." Polymer 28 (1987): 683.
3. Data taken from Modern Plastics Encyclopedia 72(12) (1995).
4. Siegmann, A. "Crystalline/crystalline polymer blends: Some structure-property relationships." J. Appl. Polym. Sci. 24 (1979): 2333.
5. Siegmann, A. "Crystallization of crystalline/crystalline blends: Polypropylene/poly-butene-1." J. Appl. Polym. Sci. 27 (1982): 1053.
6. Keller, A. "Polymer crystals" Rep. Prog. Phys. 31 (1968): 623.
7. Khoury, F. and Passaglia, E. "The morphology of crystalline synthetic polymers." Treatise on Solid State Chemistry. ed. Hannay, N. B. Vol. 3. New York; London: Plenum Press, 1976. 335-496.
8. Hoffman, J. D.; Davis, G. T. and Lauritzen, J. I. Jr. "The rate of crystallization of linear polymers with chain folding." Treatise on Solid State Chemistry. ed. Hannay, N. B. Vol. 3. New York; London: Plenum Press, 1976. 497-614.
9. Phillips, P. J. "Polymer crystals." Rep. Prog. Phys. 53 (1990): 549.

10. Tanaka, H. and Inoue, Y. "Effects of microtacticity on ^{1}H and ^{13}C magnetic relaxation times of isotactic polypropylene crystallized at high temperature." Eur. Polym. J. 29 (1993): 569.

11. Chai, C. K. and McCrum, N. G. "Mechanism of physical aging in crystalline polymers." Polymer 21 (1980): 706.

12. Struik, L. C. E. "The mechanical and physical ageing of semicrystalline polymers: 1." Polymer 28 (1987): 1521.

13. Read, B. E.; Dean, G. D. and Tomlins. P. E. "Effects of physical ageing on creep in polypropylene." Polymer 29 (1988): 2159.

14. Mandelkern, L.; Alamo, R. G. and Kennedy, M. A. "Interphase thickness of linear polyethylene." Macromolecules 23 (1990): 4721.

15. Keller, A. "A note on single crystals in polymers: Evidence for a folded chain conformation." Phil. Mag. 2 (1957): 1171.

16. Till, P. H. Jr. "The growth of single crystals of linear polyethylene." J. Polym. Sci. 24 (1957): 301.

17. Fischer, E. W. Z. Naturforsch. 12a (1957): 753.

18. Patil, R. and Reneker, D. H. "Molecular folds in polyethylene observed by atomic force microscopy." Polymer 35 (1994): 1909.

19. Wittmann, J. C. and Lotz, B. "Polymer decoration: The orientation of polymer folds as revealed by the crystallization of polymer vapors." J. Polym. Sci.: Polym. Phys. Ed. 23 (1985): 205.

20. Woodward, A. E. Atlas of Polymer Morphology. Munich; Vienna; New York: Hanser, 1988.

21. Marand, H.; Velikov, V.; Verma, R. K.; Cham, P. M.; Prabhu, V. and Dillard, D. "Degree of crystallinity and nature of the amorphous state in semicrystalline polymers: a somewhat controversial topic." Polym. Prep. 36 (1995): 263.

22. Keith, H. D. and Padden. F. J. Jr. "Spherulitic crystallization from the melt. I. fractionation and impurity segregation and their influence on crystalline morphology." J. Appl. Phys. 35 (1964): 1270.

23. Lauritzen, J. I. Jr. and Hoffman, J. D. "Theory of formation of polymer crystals with folded chains in dilute solution." J. Res. Natl. Bur. Std. (U.S.) 64A (1960): 73.

24. Lauritzen, J. I. Jr. and Hoffman, J. D. "Extension of theory of growth of chain-folded polymer crystals to large undercoolings." J. Appl. Phys. 44 (1973): 4340.

25. Lauritzen, J. I. Jr. "Effect of a finite substrate length upon polymer crystal lamellar growth rate." J. Appl. Phys. 44 (1973): 4353.

26. Hoffman, J. D. "Regime III crystallization in melt-crystallized polymers: The variable cluster model of chain folding." Polymer 24 (1983): 3.

27. Hoffman, J. D.; Miller, R. L.; Marand; H. and Roitman, D. B. "Relationship between the lateral surface free energy σ and the chain structure of melt-crystallized polymers." Macromolecules 25 (1992): 2221.

28. Huang, J.; Prasad, A. and Marand, H. "Study of the temperature dependence of isothermal spherulitic growth rate data for poly(pivalolactone) in blends with

poly(vinylidene fluoride): a link between coherent secondary nucleation theory and mixing thermodynamics." Polymer 35 (1994): 1896.

29. Mezghani, K.; Campbell, R. A. and Phillips, P. J. "Lamellar Thickening and the Equilibrium Melting Point of Polypropylene." Macromolecules 27 (1994): 997.
30. Flory, P. J. "Theory of crystallization in copolymers." Trans. Faraday Soc. 51 (1955): 848.
31. Sanchez, I. C. and Eby, R. K. "Crystallization of Random Copolymers." J. Res. Natl. Bur. Std.--A. Phys. & Chem. 77A (1973): 353.
32. Sanchez, I. C. and Eby, R. K. "Thermodynamics and crystallization of random copolymers." Macromolecules 8 (1975): 638.
33. Helfand, E. and Lauritzen, J. I. Jr. "Theory of copolymer crystallization." Macromolecules 6 (1973): 631.
34. Lauritzen, J. I. Jr.; DiMarzio, E. A. and Passaglia, E. "Kinetics of growth of multi-component chains." J. Chem. Phys. 45 (1966): 4444.
35. Pino, P. and Mülhaupt, R. "Stereospecific polymerization of propylene: an outlook 25 years after its discovery." Transition metal catalyzed polymerizations, Alkenes and Dienes, Pt. A. ed. Quirk, R. P. New York: Harwood Academic Publishers, 1983. 1.
36. Zambelli, A.; Sacchi, M. C. and Locatelli, P. "Stereospecific polymerization of propene: structure of the polymers and reaction mechanism." Transition metal catalyzed polymerizations, Alkenes and Dienes, Pt. A. ed. Quirk, R. P. New York: Harwood Academic Publishers, 1983. 83.

37. Doi, Y.; Suzuki, E. and Keii, T. "Regioselectivity and stereospecificity of titanium-based catalysts for propene polymerization." Transition metal catalyzed polymerizations, Alkenes and Dienes, Pt. B. ed. Quirk, R. P. New York: Harwood Academic Publishers, 1983. 737.

38. Zembelli, A.; Wolfsgruber, C.; Zannoni, G. and Bovey, F. A. "Polymerization of propylene to syndiotactic polymer. VIII. steric control forces." Macromolecules 7 (1974): 750.

39. Zembelli, A.; Wolfsgruber, C.; Zannoni, G. and Bovey, F. A. "Polymerization of propylene to syndiotactic polymer. IX. ethylene perturbation of syndiotactic propylene polymerization." Macromolecules 7 (1974): 752.

40. Hiemenz, Paul C. Polymer Chemistry: the Basic Concepts. New York, Basel: Marcel Dekker, 1984.

41. Zambelli, A.; Longo, P. and Grassi, A. "Isotactic polymerization of propene: homogeneous catalysts based on group 4 metallocenes without methylalumoxane." Macromolecules 22 (1989): 2186.

42. Resconi, L.; Bossi, S. and Abis L. "Study on the role of methylalumoxane in homogeneous olefin polymerization." Macromolecules 23 (1990): 4489.

43. Chien, J. C. W.; Rieger, B. and Herzog, H. M. "Metallocene--methyl aluminoxane catalysts for olefin polymerization. VIII. infrared spectra of anisotactic polypropylene." J. Polym. Sci.: Pt. A: Polym. Chem. 28 (1990): 2907.

44. Collins, S.; Kelly, W. M. and Holden, D. A. "Polymerization of propylene using supported, chiral, *ansa*-metallocene catalysts: production of polypropylene with narrow molecular weight distributions." Macromolecules 25 (1992): 1780.

45. Ewen, J. A.; Haspeslagh, L.; Atwood, J. L. and Zhang, H. "Crystals structures and stereospecific propylene polymerizations with chiral hafnium metallocene catalysts." J. Am. Chem. Soc. 109 (1987): 6544.

46. Ewen, J. A. "Mechanisms of stereochemical control in propylene polymerizations with soluble group 4B metallocene/methylalumoxane catalysts." J. Am. Chem. Soc. 106 (1984): 6355.

47. Ewen, J. A.; Jones, R. L.; Razavi, A. and Ferrara, J. D. "Syndiospecific propylene polymerizations with group 4 metallocenes." J. Am. Chem. Soc. 110 (1988): 6255.

48. Mallin, D. T.; Rausch, M. D.; Lin, Y.; Dong, S. and Chien, J. C. W. "*rac*-[Ethylidene (1-η^5-tetramethylcyclopentadienyl) (1-η^5-indenyl)] dichlorotitanium and its homopolymerization of propylene to crystalline-amorphous block thermoplastic elastomers." J. Am. Chem. Soc. 112 (1990): 2030.

49. Natta, G.; Pasquon, I.; Corradini, P.; Peraldo, M. and Zambelli, A. "Alti polimeri linerai del propilene aventi struttura sindiotattica." Rend. Acc. Naz. Lincei 28 (1960): 539.

50. Ogawa, T. and Elias, H. G. "On the structure of syndiotactic poly(propylene)." J. Macromol. Sci.-Chem. A17(5) (1982): 727.

51. Chatani, Y.; Maruyama, H.; Noguchi, K.; Asanuma. T. and Shiomura, T. "Crystal structure of the planar zigzag form of syndiotactic polypropylene." J. Polym. Sci., Part C 28 (1990): 393.

52. Pirozzi, B. and Napolitano, R. "Conformational analysis of the polymorphic forms of syndiotactic polypropylene in the crystalline field." Eur. Polym. J. 28 (1992): 703.

53. Lovinger, A. J.; Lotz, B.; Davis, D. D. and Padden F. J. Jr. "Structure and defects in fully syndiotactic polypropylene." Macromolecules 26 (1993): 3494.

54. De Rosa, C. and Corradini, P. "Crystal structure of syndiotactic polypropylene." Macromolecules 26 (1993): 5711.

55. Chatani, Y.; Maruyama, H.; Asanuma. T. and Shiomura, T. "Structure of a new crystalline phase of syndiotactic polypropylene." J. Polym. Sci., Polym. Phys. Ed. 29 (1991): 1649.

56. Auriemma, F.; De Rosa, C. and Corradini, P. "Analysis of the disorder occurring in the crystal structure of syndiotactic polypropylene." Macromolecules 26 (1993): 5719.

57. Sozzani, P.; Simonutti, R. and Galimberti, M. "MAS NMR characterization of syndiotactic polypropylene: crystal structure and amorphous phase conformation." Macromolecules 26 (1993): 5782.

58. Miller, R. L. and Seeley, E. G. "Crystallization kinetics of syndiotactic polypropylene" J. Polym. Sci.: Polym. Phys. Ed. 20 (1982): 2297.

59. Haftka, S. and Könnecke, K. "Properties of syndiotactic polypropylene." J. Macromol. Sci.-Phys. B30(4) (1991): 319.

60. Rodriguez-Arnold, J.; Bu, Z.; Cheng, S. Z. D.; Hsieh, E. T.; Johnson, T. W.; Geerts, R. G.; Palackal, S. J.; Hawley, G. R. and Welch, M. B. "Crystallization, melting and morphology of syndiotactic polypropylene fractions: 2. Linear crystal growth rate and crystal morphology." Polymer 35 (1994): 5194.

61. Mark, H. F.; Bikales, N. M.; Overberger, C. G.; Menges, G. and Kroschwitz, J. I. eds. Encyclopedia of Polymer Science and Engineering. New York: Wiley, 1988.

62. Turner Jones, A.; Aizlewood, J. M. and Beckett, D. R. "Crystalline forms of isotactic polypropylene." Makromol. Chem. 75 (1964): 134.

63. Brückner, S.; Meille, S. V.; Petraccone, V. and Pirozzi, B. "Polymorphism in isotactic polypropylene." Prog. Polym. Sci. 16 (1991): 361.

64. Hikosaka, M. and Seto, T. "The order of the molecular chains in isotactic polypropylene crystals." Polym. J. 5 (1973): 111.

65. De Rosa, C.; Guerra, G.; Napolitano, R.; Petraccone V. and Pirozzi, B. "Conditions for the α_1-α_2 transition in isotactic polypropylene samples." Eur. Polym. J. 20(10) (1984): 937.

66. Guerra, G.; Petraccone, V.; Corradini, P.; De Rosa, C.; Napolitano, R. and Pirozzi, B. "Crystalline order and melting behavior of isotactic polypropylene (α form)." J. Polym. Sci.: Polym. Phys. Ed. 22 (1984): 1029.

67. Khoury, F. "The spherulitic crystallization of isotactic polypropylene from solution: on the evolution of monoclinic spherulites form dendritic chain-folded crystal precursors." J. Res. Nat. Bur. Std. A. Phys. & Chem. 70A (1966): 29.

68. Binsbergen, F. L. and De Lange, B. G. M. "Morphology of polypropylene crystallized from the melt." Polymer 9 (1968): 23.

69. Lovinger, A. J. "Microstructure and unit-cell orientation in α-polypropylene." J. Polym. Sci.: Polym. Phys. Ed. 21 (1983): 97.

70. Olley, R. H. and Bassett, D. C. "On the development of polypropylene spherulites." Polymer 30 (1989): 399.

71. Norton, D. R. and Keller, A. "The spherulitic and lamellar morphology of melt-crystallized isotactic polypropylene." Polymer 26 (1985): 704.

72. Padden, F. J. Jr. and Keith, H. D. "Mechanism for lamellar branching in isotactic polypropylene." J. Appl. Phys. 44 (1973): 1217.

73. Corradini, P.; Petraccone, V. and Pirozzi, B. "The role of intermolecular interactions in determining the mode of packing of crystalline polymers." Eur. Polym. J. 19 (1983): 299.

74. Petraccone, V.; Pirozzi, B. and Meille, S. V. "Analysis of chain folding in crystalline isotactic polypropylene. The implications of tacticity and crystallographic symmetry." Polymer 27 (1986): 1665.

75. Petraccone, V.; Pirozzi, B. and Meille, S. V. "Energetic feasibility of adjacent re-entry chain folding in crystals of isotactic polypropylene." Eur. Polym. J. 25 (1989): 43.

76. Brückner, S. and Meille, S. V. "Non-parallel chains in crystalline γ-isotactic polypropylene." Nature 340 (August 1989): 455.

77. Leugering, Von H. J. and Kirsch, G. "Beeinflussung der kristallstruktur von isotaktischem polypropylen durch kristallisation aus orientierten schmelzen." Angew. Makromol. Chem. 33 (1973): 17.

78. Dragaun, H.; Hubeny, H. and Muschik, H. "Shear-induced β-form crystallization in isotactic polypropylene." J. Polym. Sci., Polym. Phys. Ed. 15 (1977): 1779.

79. Lovinger, A. J.; Chua, J. O. and Gryte, C. C. "Studies on the α and β forms of isotactic polypropylene by crystallization in a temperature gradient." J. Polym. Sci., Polym. Phys. Ed. 15 (1977): 641.

80. Fujiwara, Y. "Enhancement of βα-recrystallization in β-form isotactic polypropylene during heating after roll deformation." Polymer Bulletin 17 (1987): 539.

81. Lotz, B.; Fillon, B.; Thierry, A. and Wittmann, J. C., "Low T_c growth transitions in isotactic polypropylene: β to α and α to smectic phases." Polymer Bulletin 25 (1991): 101.

82. Rybnikár, F. "Transition of β to α phase in isotactic polypropylene." J. Macromol. Sci.-Phys. B30(3) (1991): 201.

83. Varga, J. "Melting memory effect of the β-modification of polypropylene." J. Thermal Anal. 31 (1986): 165.

84. Varga, J.; Schulek-Tóth, F. and Ille, A. "Effect of fusion conditions of β-polypropylene on the new crystallization." Colloid & Polym. Sci. 269 (1991): 655.

85. Shi, G. Y.; Zhang, X. D. and Qiu, Z. X. "Crystallization kinetics of β-phase poly(propylene)." Makromol. Chem. 193 (1992): 583.

86. Addink, E. J. and Beintema, J. "Polymorphism of crystalline polypropylene." Polymer 2 (1961): 185.

87. Morrow, D. R. and Newman, B. A. "Crystallization of low-molecular-weight polypropylene fractions." J. Appl. Phys. 39(11) (1968): 4944.

88. Kardos, J. L.; Christiansen, A. W. and Baer, E. "Structure of pressure-crystallized polypropylene." J. Polym. Sci.: Pt. A-2 4 (1966): 777.

89. Turner-Jones, A. "Development of the γ-crystal form in random copolymers of propylene and their analysis by DSC and X-ray methods." Polymer 12 (1971); 487.

90. Keith, H. D.; Padden, F. J. Jr.; Walter, N. M. and Wyckoff, H. W. "Evidence for a second crystal form of polypropylene." J. Appl. Phys. 30(10) (1959): 1485.

91. Lotz, B.; Graff, S. and Wittmann, J. C. "Crystal morphology of the γ (triclinic) phase of isotactic polypropylene and its relation to the α phase." J. Polym. Sci.: Pt. B: Polym. Phys. 24 (1986): 2017.

92. Meille, S. V.; Brückner, S. and Porzio, W. "γ-isotactic polypropylene. A structure with nonparallel chain axes." Macromolecules 23 (1990): 4114.

93. Stocker, W.; Magonov, S. N.; Cantow, H. J.; Wittmann, J. C. and Lotz, B. "Contact faces of epitaxially crystallized α- and γ-phase isotactic polypropylene observed by atomic force microscopy." Macromolecules 26 (1993): 5915.

94. Lotz, B.; Graff, S.; Straupé, C. and Wittmann, J. C. "Single crystals of γ phase isotactic polypropylene: combined diffraction and morphological support for a structure with non-parallel chains." Polymer 32 (1991): 2902.

95. Hendra, P. J.; Vile, J.; Willis, H. A.; Zichy, V. and Cudby, M. E. A. "The effect of cooling rate upon the morphology of quenched melts of isotactic polypropylenes." Polymer 25 (1984): 785.

96. Grubb, D. T. and Yoon, D. Y. "Morphology of quenched and annealed isotactic polypropylene." Polym. Commun. 27 (1986): 84.

97. Corradini, P.; Petraccone, V.; De Rosa, C. and Guerra, G. "On the structure of the quenched mesomorphic phase of isotactic polypropylene." Macromolecules 19 (1986): 2699.

98. Yan, R. J.; Li, W.; Li, G. and Jiang, B. "Structure of mesomorphic form of isotactic polypropylene." J. Macromol. Sci.-Phys. B32(1) (1993): 15.

99. Ven, Ser van der. Polypropylene and other polyolefins: polymerization and characterization. Amsterdam; Oxford; New York; Tokyo: Elsevier: 1990. Ch. 3.

100. Starkweather, H. W. Jr.; Van-Catledge, F. A. and MacDonald, R. N. "Crystalline order in copolymers of ethylene and propylene." Macromolecules 15 (1982): 1600.

101. Carman, C. J.; Harrington, R. A. and Wilkes, C. E. "Monomer sequence distribution in ethylene-propylene rubber measured by ^{13}C NMR. 3. Use of reaction probability model." Macromolecules 10 (1977): 536.

102. Abis, L. and Bacchilega, G. "Assignment of $\alpha\gamma$ and $\alpha\delta$ methylene carbons in ^{13}C NMR spectra of ethylene-propylene copolymers." Makromol. Chem. Rapid Commun. 5 (1984): 105.

103. Simonazzi, T. and Abis, L. Atti del III Convergno AIM, Gargnano, Italy (1981): 385.

104.Kanezaki, T.; Kume, K.; Sato, K. and Asakura, T. "^{13}C n.m.r. determination of the isotacticity of the propylene homopolymer part in ethylene-propylene block copolymers." Polymer 34 (1993): 3129.

105.Ray, G. J.; Johnson, P. E. and Knox, J. R. "Carbon-13 nuclear magnetic resonance determination of monomer composition and sequence distributions in ethylene-propylene copolymers prepared with a stereoregular catalyst system." Macromolecules 10 (1977): 773.

106.Randall, J. C. and Hsieh, E. T. "^{13}C NMR tetrad assignments in ethylene-propylene copolymers." Macromolecules 15 (1982): 1584.

107.Cheng, H. N. "^{13}C NMR analysis of ethylene-propylene rubbers." Macromolecules 17 (1984): 1950.

108.Cheng, H. N. and Smith, D. A. "^{13}C NMR studies of low-molecular-weight ethylene-propylene copolymers and characterization of polymer chain ends." Macromolecules 19 (1986): 2065.

109.Randall, J. C. "A review of high resolution liquid ^{13}C nuclear magnetic resonance characterizations of ethylene-based polymers." J. Macromol. Sci.--Rev. Macromol. Chem. Phys. C29 (1989): 201.

110.Natta, G. Atti Accad. Naz. Lincei 4 (1955): 61.

111.Boor, J. Jr. and Mitchell, J. C. "Kinetics of crystallization and a crystal-crystal transition in poly-1-butene." J. Polym. Sci.: Pt. A 1 (1963): 59.

112.Powers, J.; Hoffman, J. D.; Weeks, J. J. and Quinn, F. A. Jr. "Crystallization kinetics and polymorphic transformations in polybutene-1." J. Research Nat. Bur. Std - A. Phys . and Chem. 69A (1965): 335.

113.Armeniades, C. D. and Baer, E. "Effect of pressure on the polymorphism of melt crystallized polybutene-1." J. Macromol. Sci. (Phys.) B1(2) (1967): 309.

114.Gohil, R. M. and Patel, R. D. "Polymorphic transformation and multiple melting in poly(butene-1)." Ang. Makromol. Chem. 64 (1977): 43.

115.Chau, K. W.; Yang, Y. C. and Geil, P. H. "Tetragonal → twinned hexagonal crystal phase transformation in polybutene-1" J. Mat. Sci. 21 (1986): 3002.

116.Hsu, T. C. and Geil, P. H. "Deformation and stress-induced transformation of poly-butene-1" J. Macromol. Sci. - Phys. B28(1) (1989): 69.

117.Flory, P. J. "Thermodynamics of high polymer solutions." J. Chem. Phys. 10 (1942): 51.

118.Huggins, M. L. "Some properties of solutions of long-chain compounds." J. Phys. Chem. 46 (1942): 151.

119.Scott, R. L. "The thermodynamics of high polymer solutions. V. Phase equilibria in the ternary system: polymer 1-polymer 2-solvent." J. Chem. Phys. 17 (1949): 279.

120.Hildebrand, J. H. and Scott, R. L. The Solubility of Non-Electrolytes. New York: Dover, 1964.

121.Hansen, C. M. Ind. Eng. Chem. Prod. Res. Dev. 8 (1969): 2.

122.Hayes, R. A. "The relationship between glass temperature, molar cohesion, and polymer structure." J. Appl. Polym. Sci. 5 (1961): 318.

123.Small, P. A. "Some factors affecting the solubility of polymers." J. Appl. Chem. 3 (1953): 71.

124.Van Krevelen, D. W. "Chemical structure and properties of coal XXVIII--coal constitution and solvent extraction." Fuel 44 (1965): 229.

125.Hoy, K. L. J. Paint Tech. 42 (1970): 76.

126.Hoftyzer, P. J. and Van Krevelen, D. W. Properties of polymers: their estimation and correlation with chemical structure. 2nd ed. Amsterdam; New York: Elsevier, 1976. Ch. 7, 152-155.

127.Hoy, K. L. Tables of Solubility Parameters, Solvent and Coatings Mat. Res. and Dev. Dept., Union Carbide Corp. (1985)

128.Hoy, K. L. J. Coated Fabrics, 19 (1989): 53.

129.Beaucage, G.; Stein, R. S.; Hashimoto, T. and Hasegawa, H. "Tacticity effects on polymer blend miscibility." Macromolecules 24 (1991): 3443.

130.Beaucage, G.; Stein, R. S. and Koningsveld, R. "Tacticity effects on polymer blend miscibility. 1. Flory-Huggins-Staverman analysis." Macromolecules 26 (1993): 1603.

131.Beaucage, G. and Stein, R. S. "Tacticity effects on polymer blend miscibility. 2. Rate of phase separation." Macromolecules 26 (1993): 1609.

132.Beaucage, G. and Stein, R. S. "Tacticity effects on polymer blend miscibility. 3. Neutron scattering analysis." Macromolecules 26 (1993): 1617.

133.Schurer, J. W., De Boer, A. and Challa, G. "Influence of tacticity of poly(methyl methacrylate) on the compatibility with poly(vinyl chloride)." Polymer 16 (1975): 201.

134.Roerdink, E. and Challa, G. "Computerized infra-red study of the interaction of poly(vinylidene fluoride) with stereoregular poly(methyl methacrylate)." Polymer 21 (1980): 509.

135.Trask, C. A. and Roland, C. M. "A nearly ideal mixture of high polymers." Macromolecules 22 (1989): 256.

136.Olabisi, O.; Robeson, L. M. and Shaw, M. T. Polymer-Polymer Miscibility New York: Academic Press, 1979.

137.Kwei, T. K. and Frisch. H. L. "Interaction parameter in polymer mixtures." Macromolecules 11 (1978): 1267.

138.Rim, P. B. and Runt, J. P. "Melting point depression in crystalline/compatible polymer blends." Macromolecules 17 (1984): 1520.

139.Nishi, T. and Wang, T. T. "Melting point depression and kinetic effects of cooling on crystallization in poly(vinylidene fluoride)-poly(methyl methacrylate) mixtures." Macromolecules 8 (1975): 909.

140.Jorda, R. and Wilkes, G. L. "A novel use of physical aging to distinguish immiscibility in polymer blends." Polymer Bulletin 20 (1988): 479.

141.Tanaka, H. and Nishi, T. "Local phase separation at the growth front of a polymer spherulite during crystallization and nonlinear spherulitic growth in a polymer mixture with a phase diagram." Phys. Rev. A39 (1989): 783.

142.Tanaka, H. and Nishi, T. "New types of phase separation behavior during the crystallization process in polymer blends with phase diagram." Phys. Rev. Lett. 55 (1985): 1102.

143.Boor, J., Jr. and Mitchell, J. C. "Apparent nucleation of a crystal-crystal transition in poly-1-butene." J. Polym. Sci. 62 (1962): S70.

144.Piloz, A. and Decroix, J. -Y. et J. -F. May. "Etude des propriétés viscoélastiques de quelques mélanges polybutène-1 -- polypropène." Angew. Makromol. Chem. 54 (1976): 77.

145.Berticat, Ph.; Boiteux, G.; Dallox, J. C.; Douillard, A.; Guillet, J. and Seytre, G. "Quelques caracteristiques morphologiques de melanges de polymeres a base de propene et de butene." Eur. Polym. J. 16 (1980): 479.

146.Gohil, R. M. and Petermann, J. "Mixed crystals in polymer blends: Polypropylene-polybutene-1 system." J. Macromol. Sci., Phys. B18(2) (1980): 217.

147.Hsu, C. C. and Geil, P. H. "Structure-property-processing relationships of polypropylene-polybutylene blends." Polym. Eng. Sci. 27 (1987): 1542.

148.Lee, M. S. and Chen, S. A. "The enhancement of polybutene-1 crystallinity in polybutene-1/polypropylene blends." J. Polym. Sci.: Pt. C: Polym. Lett. 25 (1987): 37.

149.Trafara, G. Kautsch. + Gummi, Kunst. 41 (1988): 334.

150.Lee, T. H. and Marand, H. "On the miscibility and cocrystallization in blends of poly(propylene) and poly(butene-1)." Polym. Prepr. (Am. Chem. Soc., Div. Polym. Chem.) 32(3) (1991): 316.

151.Foglia, A. "Polybutylene, its chemistry, properties, and applications." J. Appl. Polym. Symp. 11 (1969): 1.

152.Alamo, R.; Domszy, R. and Mandelkern, L. "Thermodynamic and structural properties of copolymers of ethylene." J. Phys. Chem. 88 (1984): 6587.

153.Nandi, A. K. and Mandelkern, L. "The influence of chain structure on the equilibrium melting temperature of poly(vinylidene fluoride)." J. Polym. Sci.: Pt. B: Polym. Phys. 29 (1991): 1287.

154.Inoue, Y.; Nishioka, A. and Chûjô, R. "^{13}C nuclear magnetic resonance spectroscopy of polypropylene, 2. ^{13}C spin-lattice relaxation study in solution." Makromol. Chem. 168 (1973): 163.

155.Randall, J. C. "Carbon-13 NMR spin-lattice relaxation times of isotactic and syndiotactic sequences in amorphous polypropylene." J. Polym. Sci. Polym. Phys. Ed. 14 (1976): 1693.

156.Bovey, F. A. High Resolution NMR of Macromolecules New York: Academic Press, 1972. p 80.

157.Ang, F. and Mark, H. Monsatsh. Chem. 88 (1957): 427.

158.Ferro, D. R.; Brückner, S.; Meille, S. V. and Ragazzi, M. "Energy calculations for isotactic polypropylene: a comparison between models of the α and γ crystalline structures." Macromolecules 25 (1992): 5231.

159.Monasse, B. and Haudin, J. M. "Growth transition and morphology change in polypropylene." Colloid & Polym. Sci. 263 (1985): 822.

160.Fatou, J. G. "Melting temperature and enthalpy of isotactic polypropylene." Eur. Polym. J. 7 (1971): 1057.

161.Vonk, C. G. "Synthetic polymers in the solid state" in Small angle X-ray scattering. eds. Glatter, O. and Kratky, O. London: Academic Press, 1982. 433.

162.Alexander, L. E. X-ray diffraction methods in polymer science. 1969. Malabar, Florida: Krieger, 1985. 68-69.

163.Glatter, O. "A new iterative method for collimation correction in small-angle scattering." J. Appl. Cryst. 7 (1974): 147.

164.Randall, J. C. Polymer Sequence Determination: Carbon-13 NMR Method. New York: Academic Press, 1977. 53-58.

165.Koenig, J. L. Chemical Microstructure of Polymer Chains. 1980. New York: Wiley, 1980. Malabar, Florida: Krieger, 1990.

166.Busico, V.; Corradini, P.; De Rosa, C. and Di Benedetto, E. "Physico-chemical and structural characterization of ethylene-propylene copolymers with low ethylene content from isotactic-specific Ziegler-Natta catalysts." Eur. Polym. J. 21 (1985): 239.

167.Marigo, A.; Marega, C. and Zannetti, R. "Crystallization of the γ-form of isotactic poly(propylene), 2: synchrotron radiation measurements." Makromol. Chem. 191 (1990): 1967.

168.Marigo, A.; Marega, C. and Zannetti, R. "Crystallization of the γ-form of isotactic poly(propylene)." Makromol. Chem. 190 (1989): 2805.

169.Greco, R.; Mancarella, C.; Martuscelli, E.; Ragosta, G. and Yin, J. "Crystallization, morphology, and thermal behaviour of ethylene/propylene copolymers." Makromol. Chem. 188 (1987): 2231.

170.Orts, W. J.; Marchessault, R. H. and Bluhm, T. L. "Thermodynamics of the melting point depression in poly(β-hydroxybutyrate-co-β-hydroxyvalerate) copolymers." Macromolecules 24 (1991): 6435.

171.Avella, M.; Martuscelli, E.; Volpe, G. D.; Segre, A.; Rossi, E. and Simonzzi, T. "Composition-properties relationships in propyene-ethene random copolymers obtained with high-yield Ziegler-Natta supported catalysts." Makromol. Chem. 187 (1986): 1927.

172.Zimmermann, H. J. "Structural analysis of random propylene-ethylene copolymers." J. Macromol. Sci.--Phys. B32(2) (1993): 141.

173.Baltá Calleja, F. J.; González Arche, A. G.; Ezquerra, T. A.; Santa Cruz, C.; Batallán, F.; Frick, B. and López Cabarcos, E. "Structure and properties of ferroelectric copolymers of poly(vinylidene fluoride)." Adv. Polym. Sci. 108 (1993): 1.

174.Cheng, S. Z. D.; Janimak, J. J.; Zhang A. and Hsieh, E. T. "Isotacticity effect on crystallization and melting in polypropylene fractions: 1. Crystalline structures and thermodynamic property changes." Polymer 32 (1991): 648.

175.Yoon, D. Y. and Flory, P. J. "Chain packing at polymer interfaces." Macromolecules 17 (1984): 868.

176.Fischer, E. W.; Sterzel, H. J. and Wegner, G. "Investigation of the structure of solution grown crystals of lactide copolymers by means of chemical reactions." Kolloid Z. Z. Polym. 251 (1973): 980.

177.Hosoda, S.; Nomura, H.; Gotoh, Y. and Kihara, H. "Degree of branch inclusion into the lamellar crystal for various ethylene/α-olefin copolymers." Polymer 31 (1990): 1999.

178.Davis, G. T.; Eby R. K. and Colson, J. P. "Thermal expansion of polyethylene unit cell: effect of lamella thickness." J. Appl. Phys. 41 (1970): 4316.

179.Xu, Z.; Mays, J.; Chen, X.; Hadjichristidis, N.; Schilling, F. C.; Bair, H. E.; Pearson, D. S. and Fetters, L. J. "Molecular characterization of poly(2-methyl-1,3-pentadiene) and its hydrogenated derivative, atactic polypropylene." Macromolecules 18 (1985): 2560.

180.Lee, T. H. A study of miscibility, morphology, crystallization and melting behavior of isotactic poly(propylene) in blends of poly(propylene) and poly(1-butene). Master's Thesis. Virginia Polytechnic Institute and State University, 1992.

181.Stivala, S. S.; Valles, R. J. and Levi, D. W. "Viscosity-molecular weight relations for an isotactic polybutene-1." J. Appl. Polym. Sci. 7 (1963): 97

182.Danusso, F. and Moraglio, G. Rend. Acad. Naz. Lincei 25 (1958): 509.

183.Passaglia, E. and Kevorkian, H. K. "Specific heat of atactic and isotactic polypropylene and the entropy of the glass." J. Appl. Phys. 34 (1963): 90.

184.Gaur, U.; Wunderlich, B. B. and Wunderlich, B. J. Phys. Chem. Ref. Data 12 (1983): 34.

185.Goizueta, G.; Chiba, T. and Inoue, T. "Phase morphology of polymer blends: scanning electron microscope observation by backscattering from a microtomed and stained surface." Polymer 33 (1992): 886.

186.Coleman, M. M.; Graf, J. F. and Painter, P. C. Specific interactions and the miscibility of polymer blends: practical guides for predicting and designing miscible polymer mixtures. Lancaster: Technomic Pub., 1991.

187.Bates, F. S.; Fetters, L. J. and Wignall, G. D. "Thermodynamics of isotopic polymer mixtures: poly(vinylethylene) and poly(ethylethylene)." Macromolecules 21 (1988): 1086.

188.Graessley, W. W.; Krishnamoorti, R.; Balsara, N. P.; Fetters, L. J.; Lohse, D. J.; Schulz, D. N. and Sissano, J. A. "Effects of deuterium substitution on thermodynamic interactions in polymer blends." Macromolecules 26 (1993): 1137.

189.Walsh, D. J. and Ittel, S. D. "Equations of state and predictions of miscibility for hydrocarbon polymers." Polym. Mater. Sci. Eng. 67 (1992): 193.

190.Fischer, E. W. "Studies of structure and dynamics of solid polymers by elastic and inelastic neutron scattering." Pure Appl. Chem. 50 (1978): 1319.

191.Stamm, M.; Fischer, E. W.; Deteenmaier, M. and Convert, P. "Chain conformation in the crystalline state by means of neutron scattering methods." Faraday Discuss. Chem. Soc. 68 (1979): 263.

192.Hoffman, J. D. "Regime III crystallization in melt-crystallized polymers: the variable cluster model of chain folding." Polymer 24 (1983): 3.

193.Clark, E. J. and Hoffman, J. D. "Regime III crystallization in polypropylene." Macromolecules 17 (1984): 878.

194.Marand, H.; Cham, P. M.; Lee, T. H. and Mays, J. "Miscibility studies in blends of poly(propylene) and poly(1-butene)." Polym. Mater. Sci. Eng. 67 (1992): 199.

195.Bernstein, R. E.; Paul, D. R. and Barlow, J. W. "Polymer blends containing poly-(vinylidene fluoride). Part II: poly(vinyl esters)." Polym. Eng. Sci. 18 (1978): 683.

196.Alfonso, G. C.; Turturro, A.; Pizzoli, M.; Scandola, M. and Ceccorulli, G. "Study of poly(vinylidene fluoride)/poly(vinyl pyrrolidone) blends. I. Thermal transitions by differential scanning calorimetry." J. Polym. Sci., Polym. Pt. B: Polym. Phys. 27 (1989): 1195.

197.Li, Y.; Stein, M. and Jungnickel, B. "Competition between crystallization and phase separation in polymer blends I. Diffusion controlled supermolecular structures and phase morphologies in poly(ε-caprolactone)/polystyrene blends." J. Colloid Polym. Sci. 269 (1991): 772.

198.Paul, D. R. and Newmann, S., eds. Polymer Blends. New York: Academic Press, 1978.

199.Fox, T. G. "Influence of diluent and of copolymer composition on the glass temperature of a polymer system." Bull. Am. Phys. Soc. 1 (1956): 123.

200.Inaba, N.; Sato, K.; Suzuki, S. and Hashimoto, T. "Morphology control of binary polymer mixtures by spinodal decomposition and crystallization. 1. Principle of method and preliminary results on PP/EPR." Macromolecules 19 (1986): 1690.

201.Inaba, N.; Yamada, T.; Suzuki, S. and Hashimoto, T. "Morphology control of binary polymer mixtures by spinodal decomposition and crystallization. 2. Further studies on polypropylene and ethylene-propylene random copolymer." Macromolecules 21 (1988): 407.

202.Bates, F. S. and Wiltzius, P. "Spinodal decomposition of a symmetrical critical mixture of deuturated and protonated polymer." J. Chem. Phys. 91 (1989): 3258.

8. APPENDIX

(Tabulation of the triad concentration of the P-series propylene-ethylene copolymer fractions)

Triad concentration of the fractions of the P1 propylene-ethylene copolymer

	Triad concentration (%)					
	[PPP]	[PPE]	[PEP]	[PEE]	[EPE]	[EEE]
Bulk	94.2	3.9	1.0	0.0	0.0	0.9
A	96.3	2.0	0.2	0.3	0.2	1.1
B	–	–	–	–	–	–
C	93.3	3.8	0.6	0.0	0.0	2.4
D	–	–	–	–	–	–

Triad concentration of the fractions of the P2 propylene-ethylene copolymer

	Triad concentration (%)					
	[PPP]	[PPE]	[PEP]	[PEE]	[EPE]	[EEE]
Bulk	88.4	7.4	2.5	0.2	0.0	1.4
A	88.9	6.9	1.8	0.5	0.1	1.9
B	79.5	11.5	5.4	1.5	0.9	1.1

Triad concentration of the fractions of the P3 propylene-ethylene copolymer

	Triad concentration (%)					
	[PPP]	[PPE]	[PEP]	[PEE]	[EPE]	[EEE]
Bulk	86.2	8.3	3.0	0.3	0.0	2.2
A	90.0	6.9	2.2	0.3	0.2	0.4
B	90.7	5.4	3.0	0.9	0.0	0.0
C	75.3	16.2	6.2	1.4	0.8	0.0

Triad concentration of the fractions of the P4 propylene-ethylene copolymer

	Triad concentration (%)					
	[PPP]	[PPE]	[PEP]	[PEE]	[EPE]	[EEE]
Bulk	86.7	5.7	2.4	0.8	1.0	1.5
A	92.9	4.5	2.1	0.4	0.2	0.0
B	88.6	6.8	3.3	1.3	0.1	0.0
C	86.4	9.8	2.6	0.8	0.4	0.0
D	74.6	14.7	5.0	1.1	1.4	3.3

Triad concentration of the fractions of the P5 propylene-ethylene copolymer

	Triad concentration (%)					
	[PPP]	[PPE]	[PEP]	[PEE]	[EPE]	[EEE]
Bulk	80.2	12.6	4.4	1.2	0.8	0.8
A	–	–	–	–	–	–
B	86.7	8.0	3.6	0.6	0.2	0.9
C	80.9	13.0	3.8	0.4	0.6	1.3
D	76.8	13.2	5.5	2.5	1.1	0.9

Triad concentration of the fractions of the P6 propylene-ethylene copolymer

	Triad concentration (%)					
	[PPP]	[PPE]	[PEP]	[PEE]	[EPE]	[EEE]
Bulk	75.7	15.5	4.9	1.9	1.2	0.8
A	85.2	9.4	3.4	0.4	0.2	1.3
B	81.0	11.6	4.5	0.5	0.3	2.1
C	75.2	12.2	6.0	1.7	1.2	3.7

9. VITA

Pak-Meng Cham was born August 2, 1965 of Pui-Chiu and Bo-Ping Cham in Macau, a city located on the southeastern coast of China under Portuguese administration at the time. After spending all his early years there, he entered the Chinese University of Hong Kong in 1983. He received his bachelor degree of science in physics (with honors, second class upper division) and master degree of philosophy in physics in 1987 and 1989, respectively. After staying at his Alma Mater as a full-time teaching and research assistant for one year, in August, 1990 he joined the Materials Engineering Science program at Virginia Polytechnic Institute and State University in pursuit of a Ph.D.

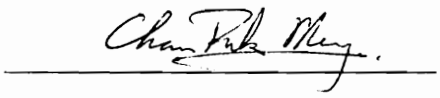

Pak-Meng Cham